Modeling Coherent Scattering Effects from a Corn Canopy at L-Band

by Avinash Sharma

B.S. in Electrical Engineering, June 1999
Rochester Institute of Technology, Rochester, NY
M.S. in Electrical Engineering, August 2012
The Johns Hopkins University, Baltimore, MD

A Dissertation submitted to

The Faculty of
The School of Engineering and Applied Science
of The George Washington University
in partial fulfillment of the requirements
for the degree of Doctor of Philosophy

January 10th, 2020

Dissertation directed by

Roger Henry Lang
Professor of Engineering and Applied Science

The School of Engineering and Applied Science of The George Washington University certifies that Avinash Sharma has passed the Final Examination for the degree of Doctor of Philosophy as of 12/09/2019. This is the final and approved form of the dissertation.

Modeling Coherent Scattering Effects from a Corn Canopy at L-Band

Avinash Sharma

Dissertation Research Committee:

Roger H. Lang, Professor of Engineering and Applied Science,
Dissertation Director

Volker J. Sorger, Associate Professor of Engineering and Applied Science,
Committee Member

Kie-Bum Eom, Professor of Engineering and Applied Science,
Committee Member

Yiwen Zhou, Adjunct Professor of Engineering and Applied Science,
Committee Member

David M. Le Vine, Research Scientist, NASA Goddard Space Flight Center,
Committee Member

© Copyright 2019 by Avinash Sharma
All rights reserved

Dedication

To my parents, Suresh and Indra

To my wife Cristina and daughter Sidney Kay

Acknowledgment

First I'd like to express my gratitude to my advisor Prof. Roger H. Lang for his consistent support and encouragement throughout my graduate studies at The George Washington University. The accomplishment of this research would not have been possible without his very patient guidance. Second, my gratitude and thanks goes out to my group supervisor at The Johns Hopkins University Applied Physics Laboratory, Mr. Chris DeBoy, for his wholehearted support throughout this process; allowing flexibility between work and school assignments, along with financial support. Finally, I'd like to thank Mary Keller of The Johns Hopkins University Applied Physics Laboratory, for all her useful technical discussions and support throughout this process.

Abstract of Dissertation

Modeling Coherent Scattering Effects from a Corn Canopy at L-Band

This research was conducted to improve the understanding between microwave backscatter and the complex dynamics of an agricultural canopy, such as corn. In particular, how important are coherent scattering effects in a corn canopy at L-Band? To study this, a coherent scattering model was developed to compute L-Band backscatter from a corn canopy over a full growing season. The model consists of a layer of random medium over a lossy dielectric half-space having a rough interface. The random medium consists of three different scatterer types used to represent the corn stalk, leaf and cob. Each scatterer has prescribed orientation statistics and dielectric properties that were taken from field measurements over a corn canopy's growing season. Concurrently, radar measurements from the same canopy was taken using a truck-mounted L-Band radar system, known as ComRad, developed and operated by George Washington University (GW) and NASA Goddard Space Flight Center (NASA/GSFC). A comparison between the measured and the modeled backscatter will show that coherent effects cannot be ignored at L-Band and highlights both the accuracy and robustness of the GW scattering model.

In addition, a careful theoretical study of the scattering mechanisms that occur in the random medium model will be presented. From this study, enhanced backscatter, which is usually presented as a multiple scattering effect will be shown to occur under single scattering in the presence of a reflecting plane. The complex scattering phenomenon will be shown to be a simple summation of a direct (or volume) scatter and direct-reflected (or

double-bounce) scatter. A graphical depiction of these scattering processes is given, which provides physical insight into a complicated problem. It will be shown that for both backscatter and specular scatter, an enhancement occurs. For like-polarization, this enhancement adds up to +3 dB additional power at backscatter, which is a well-documented phenomenon known as coherent or enhanced backscatter. A less-documented phenomenon shows up for the cross-polarized case where the enhancement can be negative, but also zero or positive, depending on the relationship of the incident angle to the Brewster angle, which is a novel contribution of this research.

Table of Contents

Dedication ..... **vi**

Acknowledgment ..... **vii**

Abstract of Dissertation ..... **viii**

List of Figures ..... **xi**

List of Tables ..... **xiv**

List of Symbols/Nomenclature ..... **xv**

Chapter 1 Introduction **1**

Chapter 2 Bistatic Scattering Coefficients from a Vegetation Layer **5**

2.1 Random media model for vegetation layer 5
2.2 Self-Consistent, Multiple Scattering Equations 8
2.3 The mean field equation 11
2.4 The Mean Field 13
2.5 The dyadic mean Green's function 16
2.6 Scattered fields 19
2.7 Bistatic Scattering Coefficient 23
2.7.1 Direct Scatter: *25*
2.7.2 Direct-Reflected Incoherent Scatter: *26*
2.7.3 Direct-Reflected Coherent Scatter: *28*
2.7.4 Reflected Scatter: *30*

Chapter 3 Scattering Amplitudes of Individual Scatterers **33**

3.1 Dipole polarizability method 33
3.2 Scattering Coefficient of an Electrically Thin Dielectric Disc and Cylinder 41
3.3 Thin-disc model reduction to the dipole model 46
3.4 Scattering from a thin dielectric cylinder 50
3.5 Numerical electromagnetic solutions 53

Chapter 4 Enhancement Effects **57**

4.1 Qualitative overview of enhanced backscatter 57
4.2 Enhanced Backscatter 58
4.2.1 Backscatter, Like-Polarization 59
4.2.2 Backscatter, Cross-Polarization 63
4.3 Enhanced Specular Scatter 67
4.4 Enhancement reduction 70
4.4.1 Surface Scatter 70
4.4.2 Antenna beamwidth 73

Chapter 5 Radar Model of Corn Canopy over the full growing season 80

5.1 Radar experiment 80
5.2 In-situ field measurements: 82
5.2.1 Leaves: 82
5.2.2 Stalks 85
5.2.3 Cobs 88
5.2.4 Soil Characteristics 89
5.2.5 Biomass 90
5.3 Radar Measurements 92
5.3.1 Radar return versus soil moisture 92
5.3.2 Radar Return versus biomass 94
5.4 Radar Model and Simulations 95
5.4.1 Scattering model for corn canopy 96
5.4.2 Two-way canopy attenuation 97
5.4.3 Leaf, Stalk and cob scatter 97
5.4.4 Direct, Direct-Reflected and Surface Scatter 98
5.4.5 Enhanced backscatter 99
5.5 Measured vs simulated total backscatter 100

Chapter 6 Conclusions and Future Work 103

References 105

Appendix A 112

A.1 Derivation of propagation constant in mean medium 112
A.2 Stationary phase integral 118
A.3 Derivation of the z-component of the propagation constant 124
A.4 Correlation of scattered field integrals 125

Appendix B 130

Relationship between the dyadic transition operator and the dyadic scattering amplitude..... 130

List of Figures

2.1 Random medium over dielectric half-space model 6

2.2 Incident and scattered field direction vectors 7

2.3 Random medium model replaced with an effective uniaxial layer 14

2.4 Geometry for determining the mean Green's function 16

2.5 Direct scatter geometry 25

2.6 Direct-reflected Type 1 scatter geometry 26

2.7 Direct-reflected Type 2 scatter geometry 27

2.8 Direct-reflected coherent scatter geoemetry 28

2.9 Reflected scatter geometry.....30

3.1 HPOL backscatter terms versus incident angle for a layer of circular discs 41

3.2 Skin depth versus incident angle for a layer of circular discs.....41

3.3 Thin disc geoemetry.....42

3.4 Comparison of HPOL backscatter versus incident angle predicted by dipole and thin disc model for a disc radius at the Raleigh limit.....45

3.5 Comparison of HPOL backscatter versus incident angle predicted by dipole and thin disc model for a disc radius less than the Raleigh limit.....46

3.6 Comparison of HPOL backscatter versus electrical size using dipole vs thin disc model.....51

3.7 Periodic dielectric cylinder 54

3.8 Simulated back and bistatic scattering coefficient.....55

3.9 Comparison of back and bistatic scattering amplitudes for periodic and approximate uniform stalk modes 55

3.10 Cross-sectional view of three-layer cylinder 56

4.1 Enhanced backscatter due to multiple scattering geometry 57

4.2 Enhanced backsatter due to single scattering in the presence of a reflecting surface geometry 57

4.3 HPOL and VPOL Fresnel reflection coefficient, magnitude and phase (lossless) 64

4.4 HPOL and VPOL Fresnel reflection coefficient, magnitude and phase (lossy) 65

4.5 Exponential coherent scattering term Ψ versus $\kappa_{s_p} - \kappa_{i_q}$ 66

4.6 SigmaHH bistatic scatter from a circular layer of discs over a dielectric half-space ..68

4.7 SigmaHV bistatic scatter from a circular layer of discs over a dielectric half-space ..69

4.8 Random medium over a dielectric half-space with a rough surface interface 70

4.9 Radar antenna geometry. 72

4.10 (a) HH-pol bistatic scattering coefficient, incident angle of -45° (b) HV-pol bistatic scattering coefficient, incident angle of -45° 77

4.11 (a) HH-pol enhanced backscatter versus antenna beamwidth (b) HV-pol enhanced backscatter versus antenna beamwidth.....78

5.1 ComRad system at OPE3 corn canopy site in Beltsville, MD.....80

5.2 Sample corn plant used for measurement 81

5.3 Monthly leaf orientation histograms 83

5.4 (a) Leaf dielectric constant measurement (b) Measured leaf dielectric constant over growing season 84

5.5 Cross-section of stalk nodes and internodes 86

5.6 Measured dielectric constant of stalk nodes and internodes taken on DoY 213 86

5.7 Effective dielectric constant for leaf, stalk and cob over growing season.....87

5.8 Cross-section of a corn cob.....88

5.9 Measured dielectric constant of the cob over the growing season 88

5.10 Measured biomass of stalk, leaf and cob 90

5.11 Stalk, leaf and cob biomass as a percent of total biomass 91

5.12 Backscatter vs soil moisture.....92

5.13 Backscatter vs soil moisture, dew data 94

5.14 Backscatter vs biomass 95

5.15 Two-way canopy attenuation over the growing season.....96

5.16 Two-way canopy attenuation over the growing season.....97

5.17 Simulated HH-pol and VV-pol for individual leaf, stalk and cob scatterers 98

5.18 Simulated direct, direct-reflected and reflected contributions over the growing season 99

5.19 Simulated enhanced backscatter over the growing season 100

5.20 Modeled vs measured backcscatter over the growing season.....101

List of Tables

3.1 Parameters describing a layer of circular discs over a dielectric half-space 40

3.2 Parameters for a layer of circular discs sized at the Raleigh limit ver a dielectric half-space 50

4.1 Comparison of predicted enhancement width using Equation 4.9 and Figure 6 from Lang and Khadr 62

4.2 Parameters for a layer of circular discs over a dielectric half-space used in [Nagi, 1991] Table 5.1 67

4.3 Parameters for a layer of thin cylinders 77

5.1 Averaged measured leaf parameters 82

5.2 Averaged measured stalk parameters 85

5.3 Averaged measured cob parameters 87

List of Symbols/Nomenclature

$\hat{i}^{\pm}$: incident wave direction vector. ± represents travel in the ±z direction

$\hat{o}^{\pm}$: scattered wave direction vector. ± represents travel in the ±z direction

$\hat{q}$: incident wave polarization vector

$\hat{p}$: scattered wave polarization vector

$\hat{h}$: horizontal polarization vector

$\hat{v}$: vertical polarization vector

$\hat{n}$: unit normal vector

θ_i : incident angle (between z-axis and $\hat{i}$) (degrees)

θ_s : scattered angle (between z-axis and $\hat{o}$) (degrees)

ϕ_i : incident azimuthal angle (degrees)

ϕ_s : incident azimuthal angle (degrees)

ε_o : free space permittivity (F/m)

ε_r : relative permittivity

ε_g : ground layer permittivity (F/m)

μ_o : free space permeability (H/m)

$\underline{E}_o$: incident electric field vector (V/m)

$\underline{E}_s$: scattered electric field vector (V/m)

k_o : propagation constant in free space (1/m)

κ_{z_q} : mean wave incident propagation constant (1/m)

κ_{z_p} : mean wave scattered propagation constant (1/m)

$\underline{x}$: position vector from origin to scatterer

$\underline{s}$: position vector from origin that spans the layer

ω : angular frequency (rad/s)

Γ_q : Fresnel reflection coefficient, $q \in \{h, v\}$

$\underline{k}$: propagation vector

k_{z_i} : z-component of $\underline{k}$

$\underline{k}_{t_i}$: transverse components of $\underline{k}$

k_{z_g} : propagation constant in the ground layer

d: layer thickness (m)

V_{pi}: volume of the i^{th} particle

$\underline{J}$: Electric current density (A/m^2)

$\underline{\underline{L}}_o^{-1}$: inverse of the dyadic Green's function

$\underline{\underline{T}}_i$: dyadic transition operator

$\underline{\underline{I}}$: unit dyadic

$\rho(\underline{s})$: density of particle as a function of a position vector

δ : small-signal parameter (fractional volume)

$\sigma^0_{pqp'q'}$: bistatic scattering coefficient (polarimetric)

$\sigma^0_{c_{pqp'q'}}$: bistatic scattering coefficient (coherent)

$\sigma^0_{i_{pqp'q'}}$: bistatic scattering coeffient (incoherent)

$\sigma^0_{d_{pqp'q'}}$: bistatic scattering coefficient due to direct scatter term

$\sigma^0_{dri1_{pqp'q'}}$: bistatic scattering coefficient due to Type-1 incoherent direct-reflected scatter term

$\sigma^0_{dri2_{pqp'q'}}$: bistatic scattering coefficient due to Type-2 incoherent direct-reflected scatter term

$\sigma^0_{drc1_{pqp'q'}}$: bistatic scattering coefficient due to Type-1 coherent direct-reflected scatter term

$\sigma^0_{drc2_{pqp'q'}}$: bistatic scattering coefficient due to Type-2 coherent direct-reflected scatter term

$\sigma^0_{r_{pqp'q'}}$: bistatic scattering coefficient due to reflected scatter term

A: area of illumination (m^2)

$I_{s_{pqp'q'}}$: Scattered intensity

$I_{i_{qq'}}$: incident intensity

N: number of scatterers

$f_{pq}(\hat{o}^{\pm}, \hat{i}^{\pm})$: bistatic scattering amplitude

$\underline{\underline{\alpha}}$: polarizability dyadic

θ_{BW} : Antenna beamwidth

θ_{HPBW} : Antenna half-power beamwidth (or 3 dB beamwidth)

Chapter 1 Introduction

Satellite radar is a valuable tool in Earth remote sensing. In particular, remote sensing of vegetation canopies to garner temporal and spatial data of biomass and underlying soil moisture at a global scale. The data acquired from satellite radar play an important role in hydrology, climate modeling, crop monitoring, famine prediction, food security and overall disaster mitigation to name a few [Lobell et al., 2008]. However, for the data to have meaningful interpretation requires an accurate scattering model for the vegetation canopy. Research in this area has been conducted over the past fifty years and a good historical review can be found in [Lang, 2016; Steele-Dunne, 2017]. A small subset of major contributing works was performed by [Fung and Ulaby, 1978; Lang 1981; Tsang and Kong, 1981; Lang and Sidhu, 1983; Karam and Fung, 1983].

In this dissertation, the development of an accurate radar scattering model for a vegetation canopy will be presented. The model's validity is checked by comparing the simulated backscatter to measured backscatter, of a corn canopy over its entire growing season. Most studies present data over a short time period in the growing season (usually the middle). This study's comparison over an entire growing season is a good check to the model's robustness due to the large variation in canopy parameters that occur over a growing season.

The model includes coherent scattering effects, which is not normally taken into consideration. The model consists of a sparse layer of discrete random medium over a dielectric half-space. The mean field for the random medium layer is then calculated. This was originally done by [Foldy, 1945] for a random medium consisting of independent isotropic point scatterers. [Lax, 1951, 1952] and later [Twersky, 1962, 1964, 1967]

extended Foldy's work to include arbitrarily shaped and correlated scatterers. Next, the mean field results in conjunction with the Distorted Born Approximation are used to calculate the scattering coefficients. Details of this approach can be found in [Lang 1981; Lang and Sidhu, 1983;] where the scattering coefficients are found at backscatter. This method is based on a wave approach which includes coherent or enhancement effects.

Another method used in modeling vegetation is based on Radiative Transfer (RT) [Tsang, 1985]. This method does not take into account coherent effects, since it is based on energy balance. A method to include the coherent effect into the RT results have been proposed by [Zuniga and Kong, 1980], but this is somewhat artificial and does not include the angular variation of the enhancement [Lang and Sharma, 2017].

In this dissertation, the bistatic scattering coefficients will be derived and shown to be a summation of distinct scattering geometries. Two of these scattering geometries will be seen to occur due to coherent effects, leading to coherent or enhanced backscatter, which has been documented by [Zuniga et al. 1980; Kravtsov and Saichev, 1982; Lang, 1981; Lang and Sidhu, 1983]. This phenomenon was demonstrated experimentally in the optical regime by [Kuga and Ishimaru, 1984; Tsang and Ishimaru, 1984], where both a peak at the backscattering angle was measured, and an angular, or enhancement width, which describes how fast the enhancement decays at angles away from backscatter. All of these cases are for like-polarization. For the cross-polarized case, [Mandt, Tsang and Ishimaru, 1990] showed that the backscatter enhancement also occurs for the cross-polarized case in the optical regime and can be either positive or negative. In [Lang and Khadr, 1992], a negative enhancement was also shown to occur for the cross-polarized case at both back and at specular scatter in the microwave regime.

This dissertation consists of four additional chapters. In Chapter 2, the bistatic scattering coefficients (polarimetric) are derived for the vegetation model. The model consists of a sparse layer of discrete random medium over a flat dielectric half-space. The random medium layer will consist of several types of dielectric scatterers, used to model vegetation plant's constituents. Scatterers such as thin discs and cylinders, will be used to model leaves and stalks.

Chapter 3 gives an overview of calculating the scattering amplitude from individual scatterers such as a dipole, a thin dielectric disc and a thin dielectric cylinder. For the dipole, the polarizability is found and used to calculate the backscattering coefficients, as developed in [Lang and Sidhu 1983]. The thin dielectric disc uses a quasi-static approximation for the internal fields in the disk, a method described by [Levine et al. 1985]. The thin dielectric cylinder uses a similar method which approximates the internal field in the cylinder with a quasi-static approximation, and is detailed in [Seker and Schneider, 1988]. Finally, the quasi-static thin disc approximation is shown to reduce to the dipole approximation for Rayleigh scatterers [Ishimaru, 1997].

In Chapter 4, a detailed study of the enhancement effects will be presented. The enhancement will be characterized by an enhancement peak and width. It will be seen that for like-polarization, a maximum limit of +3 dB will be seen to occur at both back and specular scatter. For cross-polarization, the enhancement can be either positive or negative and can be seen at both back and specular angles. The reduction in the overall enhancement will then be discussed when the other scattering mechanisms, such as direct (or volume) scatter and surface scatter (due to rough surface) is introduced. Finally, effects such as

surface roughness and antenna beamwidth on the characteristics of the enhancement will be presented.

In Chapter 5, detailed field measurements of a corn canopy taken over the full growing season will be presented. These measurements are used to model the backscattering coefficients. Concurrently, radar measurements over the same corn canopy were taken. A comparison between the model and the measurements will be discussed.

Finally in Chapter 6, a short conclusion and recommendations for future work will be given.

Chapter 2 Bistatic Scattering Coefficients from a Vegetation Layer

In this chapter, general expressions for the bistatic scattering coefficients from a layer of vegetation will be derived. The method is based on work done by [Lang, 1981] where the vegetation is modeled as a sparse layer of randomly oriented discrete scatterers. An equation for the mean field is found by using an approximation from [Foldy, 1945]. From this equation, the random layer can be replaced with an effective layer. The scatterers are then embedded in this effective medium and the correlation of the scattered field is found. This method is known as the Distorted Born Approximation (DBA). From this procedure, the scattering coefficients can finally be found. A detailed derivation of this procedure will be presented in this chapter. In addition, geometric depictions of the scattering coefficients will be presented to provide physical insight and interpretation of a complex problem.

2.1 Random media model for vegetation layer

The model for a layer of vegetation as shown in Figure 2.1 consists of a layer of random medium with a thickness of 'd', containing i-particles, each having a volume of V_{p_i}, randomly oriented and positioned over a lossy dielectric half-space. These random parameters will be collectively represented by the parameter β, having probability distribution function $p(\beta)$. This can be used to prescribe orientation statistics of the particles or any other type of random variable, such as dielectric constant or particle size. The layer is excited by an incident plane wave traveling in the $\hat{i}$ direction, with an incident polarization $\hat{q}$. The incident wave induces currents in the scatterers, resulting in a scattered wave traveling in the $\hat{o}$ direction, with a scattered polarization $\hat{p}$.

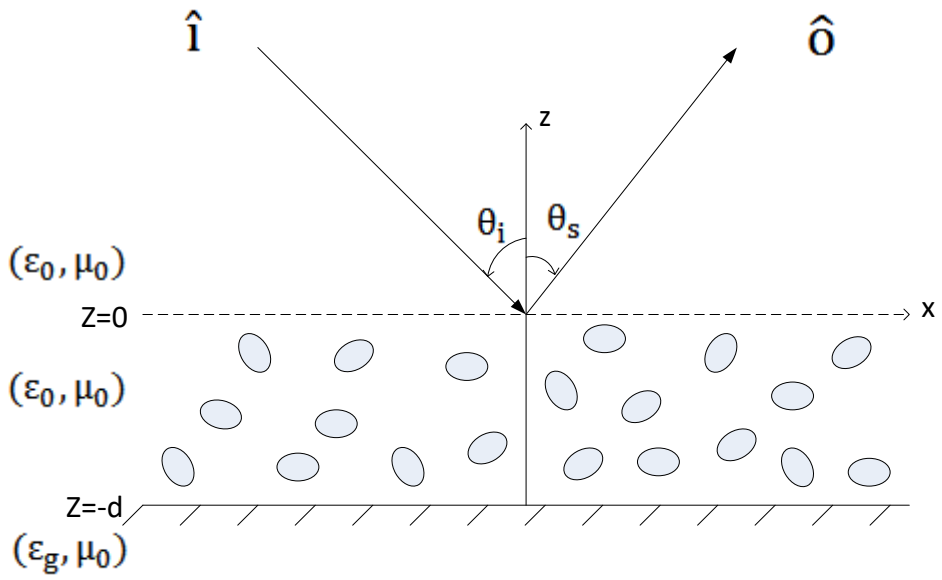

Figure 2.1 Random medium over dielectric half-space used to model a layer of vegetation

The following simplifying assumptions will be made for this model in order to realize a tractable solution for the bistatic scattering coefficients:

- particles are sparsely distributed
- particles have azimuthal symmetry
- layer is transverse homogenous
- the scatterers are independent from each other

The sparse layer allows the z=0 boundary in Figure 2.1 to be treated as diffuse (ie: zero reflection). The azimuthal symmetry assumption, results in zero average depolarization. This allows for the simplification of the propagation constant in the mean medium. The transverse homogeneity assumption allows for the density of the scatterers to be set to a

constant. Finally, statistical independence between scatterers reduces unwieldy cross-terms when computing the total scattering contribution. It is important to note that these assumptions are not only simplifying, but are valid for a layer of vegetation.

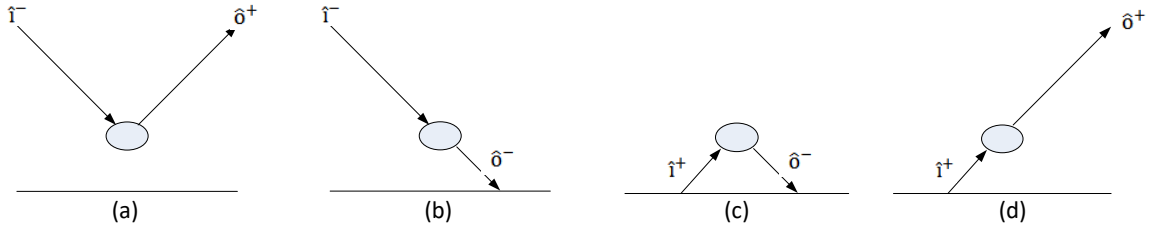

Figure 2.2 Incident and scattered field direction vectors

Within the random medium, the incident and scattered fields can be either upward or downward traveling, as shown in Figure 2.2. To represent these fields, the following direction vectors are used, $\hat{i}^-, \hat{i}^+, \hat{o}^-,$ and $\hat{o}^+$. These direction vectors can be expressed in spherical coordinates as:

$$\hat{i}^- = -\sin\theta_i \cos\phi_i \hat{x} - \sin\theta_i \sin\phi_i \hat{y} - \cos\theta_i \hat{z} \tag{2.1a}$$

$$\hat{i}^+ = \sin\theta_i \cos\phi_i \hat{x} + \sin\theta_i \sin\phi_i \hat{y} + \cos\theta_i \hat{z} \tag{2.1b}$$

$$\hat{o}^- = -\sin\theta_s \cos\phi_s \hat{x} - \sin\theta_s \sin\phi_s \hat{y} - \cos\theta_s \hat{z} \tag{2.1c}$$

$$\hat{o}^+ = \sin\theta_s \cos\phi_s \hat{x} + \sin\theta_s \sin\phi_s \hat{y} + \cos\theta_s \hat{z} \tag{2.1d}$$

The incident field will have an associated polarization, represented by its polarization vector $\hat{q}$. The polarization can either be horizontal, $\hat{h}_i$ or vertical, $\hat{v}_i$ where,

$$\hat{h}_i = \frac{\hat{i} \times \hat{z}}{\left|\hat{i} \times \hat{z}\right|} \tag{2.2a}$$

$$\hat{v}_i = \hat{h}_i \times \hat{i} \tag{2.2b}$$

Similarly, the scattered field will have an associated polarization, represented by its polarization vector $\hat{p}$. The polarization can also be either be horizontal, $\hat{h}_s$ or vertical, $\hat{v}_s$ where,

$$\hat{h}_s = \frac{\hat{o} \times \hat{z}}{\left|\hat{o} \times \hat{z}\right|} \tag{2.3a}$$

$$\hat{v}_s = \hat{h}_s \times \hat{o} \tag{2.3b}$$

Note that the $e^{-i\omega t}$ time dependence is used in this dissertation.

2.2 Self-Consistent, Multiple Scattering Equations

The self-consistent multiple scattering equations are a pair of equations that describe the scattering effects exactly. (ie: takes into account multiple scattering, diffraction etc.) However, for even simple problems, the solution of these equations is non-trivial and simplifying assumptions are needed, such as the Foldy-Lax approximation [Foldy 1945, Lax 1951]. To derive the self-consistent multiple scattering equations, we begin with the wave equation,

$$\nabla \times \nabla \times \underline{E}(\beta) - k_o^2 \underline{\underline{\varepsilon}}(\beta, \underline{x}) \cdot \underline{E}(\beta) = i\omega\mu_o \underline{J} \tag{2.4}$$

where:

$$\underline{\underline{\varepsilon}}(\beta, \underline{x}) = \underline{\underline{\varepsilon}}_d(z) + (\varepsilon_r - 1) \sum_{i=1}^{N} U_i(\beta, \underline{x})\, \underline{\underline{I}}$$

$$\underline{\underline{\varepsilon}}_d(z) = \begin{cases} \underline{\underline{I}} & z > -d \\ \varepsilon_g \underline{\underline{I}} & z < -d \end{cases}$$

$$U_i(\beta,\underline{x}) = \begin{cases} 1 & \underline{x} \in V_{pi} \\ 0 & \underline{x} \notin V_{pi} \end{cases}$$

Equation 2.4 can be expressed in operator form as follows:

$$\underline{\underline{L}}(\beta)\cdot\underline{E}(\beta) = \underline{g} \tag{2.5}$$

where:

$$\underline{\underline{L}}(\beta) = \underline{\underline{L}}_o + \underline{V}(\beta)$$
$$\underline{\underline{L}}_o = \nabla\times\nabla\times\underline{\underline{I}} - k_0^2\underline{\underline{\varepsilon}}_d(z)$$
$$\underline{V}(\beta) = \sum_{i=1}^{N} V_i(\beta) = k_0^2(\varepsilon_r - 1)\sum_{i=1}^{N} U_i(\beta,\underline{x})\,\underline{I}$$
$$\underline{g} = i\omega\mu_0\underline{J}$$

The total electric field can be expressed as the sum of incident and scattered fields:

$$\underline{E}(\beta) = \underline{E}_o + \underline{E}_s(\beta) = \underline{E}_o + \sum_{i=1}^{N}\underline{E}_s^{(i)}(\beta) \tag{2.6}$$

$\underline{E}_o$is the incident field in the absence of scatterers and is defined as

$$\underline{E}_o = \underline{\underline{L}}_o^{-1}\underline{g} \tag{2.7}$$

$\underline{E}_s^{(i)}(\beta)$ is the scattered field due to the i-th particle. Examining Equation 2.7, one can see that $\underline{\underline{L}}_o^{-1}$ is a dyadic Green's function for a source placed over the dielectric half-space.

Expanding and substituting Equation 2.6 into Equation 2.5, results in,

$$\left[\underline{\underline{L}}_o + \underline{V}(\beta)\right]\cdot\left[\underline{E}_o + \underline{E}_s(\beta)\right] = \left[\underline{\underline{L}}_o + \underline{V}(\beta)\right]\cdot\left[\underline{E}_o + \sum_{i=1}^{N}\underline{E}_s^{(i)}(\beta)\right] = \underline{g}$$

This simplifies to,

$$\underline{\underline{L}}_o\cdot\underline{E}_s^{(i)}(\beta) = -\underline{V}(\beta)\cdot\underline{E} = \underline{g}_{eq}^{(i)}(\beta) \tag{2.8}$$

The $\underline{g}_{eq}^{(i)}(\beta)$ term is an equivalent source term for the scattered electric field from the i-th particle, and exists only inside the scatterer. Since $\underline{g}_{eq}^{(i)}(\beta)$ represents the current induced

in the i-th particle by the field incident on the i-th particle, and since Maxwell's Equations are linear, the following relationship between the induced equivalent source and the incident field can be mathematically expressed as,

$$\underline{g}_{eq}^{(i)}(\beta) = \underline{\underline{T}}^{(i)}(\beta) \cdot \underline{E}^{(i)}(\beta) \tag{2.9}$$

The expression $\underline{\underline{T}}^{(i)}$ is the dyadic transition operator for the i-th particle and $\underline{E}^{(i)}(\beta)$ is the vector field incident on the i-th particle, and can be expressed as:

$$\underline{E}^{(i)}(\beta) = \underline{E}_o + \sum_{\substack{j=1 \\ j \neq i}}^{N} \underline{E}_s^{(i)}(\beta) \tag{2.10}$$

Since $\underline{\underline{T}}_j(\beta)$ is a linear and bounded operator, Equation 2.9 can be expressed in integral form as:

$$\underline{g}_{eq}^{(i)}(\beta) = \int_{-\infty}^{\infty} d\underline{x}' \, \underline{\underline{t}}_i(\beta, \underline{x}, \underline{x}') \cdot \underline{E}^{(i)}(\beta, \underline{x}') \tag{2.11}$$

Note that $\underline{\underline{T}}_j(\beta)$ is finite only within the scatterer and zero everywhere else. Substituting Equation 2.9 into Equation 2.8 and solving for $E_s^{(i)}(\beta)$ results in,

$$\underline{E}_s^{(i)}(\beta) = \underline{\underline{L}}_o^{-1} \cdot \underline{\underline{T}}_i(\beta) \cdot \underline{E}^{(i)}(\beta) \tag{2.12}$$

Note that Equation 2.12 is an expression for the scattered field in terms of the dyadic Green's function, the transition operator and the incident field on the particle. Substituting Equation 2.12 into Equations 2.6 and 2.10 results in the following pair of equations, known as the Self-Consistent, Multiple Scattering set of equations.

$$\underline{E}(\beta) = \underline{E}_o + \sum_{i=1}^{N} \underline{\underline{L}}_o^{-1} \cdot \underline{\underline{T}}_i(\beta) \cdot \underline{E}^{(i)}(\beta) \tag{2.13}$$

$$\underline{\underline{E}}^{(i)}(\beta) = \underline{\underline{E}}_o + \sum_{\substack{j=1 \\ j\neq i}}^{N} \underline{\underline{L}}_o^{-1} \cdot \underline{\underline{T}}_j(\beta) \cdot \underline{\underline{E}}^{(j)}(\beta) \tag{2.14}$$

Substituting Equation 2.14 into Equation 2.13 and expanding,

$$\underline{\underline{E}}(\beta) = \underline{\underline{E}}_o + \sum_{i=1}^{N} \underline{\underline{L}}_o^{-1} \cdot \underline{\underline{T}}_i(\beta) \cdot \underline{\underline{E}}_o + \sum_{i=1}^{N} \sum_{\substack{j=1 \\ j\neq i}}^{N} \underline{\underline{L}}_o^{-1} \cdot \underline{\underline{T}}_j(\beta) \cdot \underline{\underline{E}}_o + \ldots \tag{2.15}$$

The second term in Equation 2.15 represents single-scattering, the third term represents double-scattering and so forth. In this formulation, only single scattering term will be used. This term is known in the literature as the 1st order Born Approximation and is valid for a shallow random medium consisting of small fractional volume and low albedo, since it does not take in account attenuation of the incident and scattered waves.

2.3 The mean field equation

From Section 2.2, the 1st order Born Approximation does not account for attenuation in the random medium layer. In order to account for attenuation, an equivalent mean field method, first introduced by [Foldy, 1945], which replaces the incident field exciting each particle, $\underline{\underline{E}}^{(i)}(\beta)$, by the mean field, $\langle \underline{\underline{E}} \rangle$ will be needed. Using this method and ensemble averaging Equation 2.13, over all realizations of β,

$$\left\langle \underline{\underline{E}}(\beta) \right\rangle = \left\langle \underline{\underline{E}}_o \right\rangle + \sum_{i=1}^{N} \left\langle \underline{\underline{L}}_o^{-1} \right\rangle \cdot \left\langle \underline{\underline{T}}_i(\beta) \right\rangle \cdot \left\langle \underline{\underline{E}}^{(i)}(\beta) \right\rangle$$

Carrying through the ensemble averaging results in,

$$\left\langle \underline{\underline{E}} \right\rangle = \underline{\underline{E}}_o + \sum_{i=1}^{N} \left\langle \underline{\underline{L}}_o^{-1} \right\rangle \cdot \left\langle \underline{\underline{T}}_i(\beta) \right\rangle \cdot \left\langle \underline{\underline{E}}(\beta) \right\rangle \tag{2.16}$$

An explicit expression $\langle \underline{\underline{L}}_o^{-1} \rangle$ can be found by substituting Equation 2.7 in Equation 2.16, solving for $\underline{g}$ and comparing to Equation 2.9,

$$\left\langle \underline{\underline{L}}_o^{-1} \right\rangle = \underline{\underline{L}}_o - \sum_{i=1}^{N} \left\langle \underline{\underline{T}}_i(\beta) \right\rangle \tag{2.17}$$

Assuming identical scatterers,

$$\left\langle \underline{\underline{L}}_o^{-1} \right\rangle = \underline{\underline{L}}_o - N\left\langle \underline{\underline{T}}_i(\beta) \right\rangle = \underline{\underline{L}}_o - N\int d\underline{s}\left(p(\underline{s})\underline{\underline{T}}(\underline{s})\right)$$

where $p(\underline{s})$ is the probability distribution of the particle position variable $\underline{s}$ and N is the number of scatterers. Since the density of particles at $\underline{s}$ is $\rho(\underline{s}) = Np(\underline{s})$, then

$$\left\langle \underline{\underline{L}}_o^{-1} \right\rangle = \underline{\underline{L}}_o - \int d\underline{s}\left(\rho(\underline{s})\overline{\underline{\underline{T}}}(\underline{s})\right)$$

where $\overline{\underline{\underline{T}}}(\underline{s})$ is the dyadic transition operator of a particle located at $\underline{s}$ and the overbar denotes averaging over all particle orientations. Invoking the small fractional volume approximation, $\delta \ll 1$, where δ is the density multiplied by the volume of the scatterer. the density can be expressed as,

$$\rho(\underline{s}) = \delta\, \rho(\delta \underline{s})$$

$$\left\langle \underline{\underline{L}}_o^{-1} \right\rangle = \underline{\underline{L}}_o - \delta\int d\underline{s}\left(\rho(\delta\underline{s})\overline{\underline{\underline{T}}}(\underline{s})\right) \tag{2.18}$$

Finally, substituting Equation 2.18 into the operator form of the mean equation, $\langle \underline{\underline{L}}_o^{-1} \rangle \cdot \langle \underline{E} \rangle = \underline{g}$ results in,

$$\left[\underline{\underline{L}}_o - \delta\int d\underline{s}\left(\rho(\delta\underline{s})\overline{\underline{\underline{T}}}(\underline{s})\right)\right]\cdot\langle \underline{E}\rangle = \underline{g}$$

Note that $\underline{\underline{\overline{T}}}(\underline{s})$ operates on a vector explicitly as:

$$\underline{\underline{\overline{T}}}(s)\cdot\underline{\Psi}=\int d\underline{x}'\left[\underline{\underline{\overline{t}}}(\underline{x}-\underline{s},\underline{x}'-\underline{s})\right]\cdot\Psi(\underline{x}')$$

A final expression for the mean field in operator form is:

$$\underline{\underline{L}}_o\cdot\langle\underline{E}\rangle-\delta\int d\underline{s}\left[\rho(\delta\underline{s})\underline{\underline{\overline{T}}}(\underline{s})\cdot\langle\underline{E}\rangle\right]=\underline{g}$$

Explicitly writing out, the mean field equation becomes,

$$\nabla\times\nabla\times\langle\underline{E}(\underline{x}')\rangle-k_o^2\langle\underline{E}(\underline{x}')\rangle-\delta\iint d\underline{s}d\underline{x}'\left[\rho(\delta\underline{s})\underline{\underline{\overline{t}}}(\underline{x}'-\underline{s},\underline{x}''-\underline{s})\cdot\langle\underline{E}(\underline{x}'')\rangle\right]=g(\underline{x}')$$

(2.19)

2.4 The Mean Field

A plane wave of unit amplitude, polarization, $\hat{q}$, traveling in the $\hat{i}$ direction is incident on the effective layer, as shown in Figure 2.3. The incident wave can be expressed as:

$$\underline{E}_{o_q}=\hat{q}e^{+i\left(\underline{k}_{t_i}\cdot\underline{x}_t-k_{z_i}\hat{z}\right)} \tag{2.20}$$

Where, $\underline{k}_{t_i}$ is the transverse components of the free space propagation constant and $k_{z_i}=\sqrt{k_0^2-\left|k_{t_i}\right|^2}$

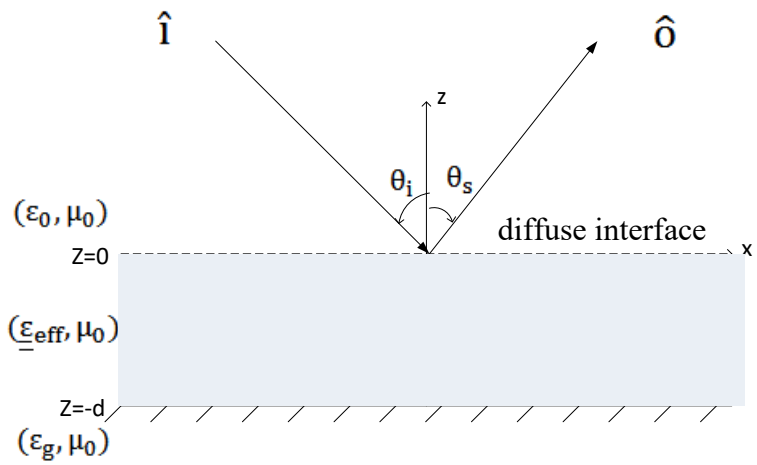

Figure 2.3 Random medium model replaced with an effective uniaxial layer

This incident wave will excite two waves in the –d < z < 0 region, one down-going and one up-going wave due to reflection from the ground interface at z=-d, and can be expressed as:

$$\left\langle \underline{E}_q(\underline{x}) \right\rangle = \left(A_q e^{-i\kappa_{z_q} z} + B_q e^{+i\kappa_{z_q} z} \right) e^{+i\underline{k}_{t_i} \cdot \underline{x}_t} \tag{2.21}$$

where $\kappa_{z_q} = k_{z_i} + \dfrac{\delta 2\pi\rho}{k_{z_i}} \bar{f}_{qq}$

This expression for κ_{z_q} (propagation constant in the mean medium) was obtained using a rigorous two-variable method in [Lang and Sidhu, 1983]. A less rigorous approach deriving the same results can be found in Appendix A.1

Additionally, a down-going wave is also excited at the z=-d interface into the z < -d region and can be expressed as,

$$\underline{E}_q\left(\underline{x}\right)=\left(C_q e^{-ik_{z_g}z}\right)e^{+i\underline{k}_{t_i}\cdot\underline{x}_t}$$

where

$$k_{z_g}=\sqrt{k_g^2-\left|k_{t_i}\right|^2}$$

Applying boundary conditions at the z=0 (a diffuse interface) and z=-d, the coefficients can be computed as:

$$A_q=1$$
$$B_q=A_q\Gamma_{g_q}e^{+i2\kappa_{z_q}d}$$
$$C_q=T_{g_q}$$

where Γ_{g_q} and T_{g_q} are the Fresnel reflection and transmission coefficients, respectively. Substituting these coefficients into the Equation 2.21, results in the mean field in the -d < z < 0 region:

$$\left\langle\underline{E}_q\left(\underline{x}\right)\right\rangle=\left(e^{-i\kappa_{z_q}z}+\Gamma_{s_q}e^{+i\kappa_{z_q}z}\right)e^{+i\underline{k}_{t_i}\cdot\underline{x}_t} \tag{2.22}$$

Where,

$$\kappa_{z_q}=k_{z_i}+\frac{2\pi\rho\delta}{k_{z_i}}\overline{f}_{qq}\left(\hat{i},\hat{i}\right)$$
$$\Gamma_{s_q}=\Gamma_{g_q}e^{+i2\kappa_{z_q}d}$$
$$\Gamma_{g_h}=\frac{k_{z_i}-k_{z_g}}{k_{z_i}+k_{z_g}}$$
$$\Gamma_{g_v}=\frac{\varepsilon_g k_{z_i}-k_{z_g}}{\varepsilon_g k_{z_i}+k_{z_g}}$$

2.5 The dyadic mean Green's function

The plane waves within the mean layer will induce currents in the scatterers, which in turn act as sources generating scattered fields. A Green's function approach for a point source within the mean layer, called the dyadic mean Green's function, will be useful analytically. The geometry is shown in Figure 2.4.

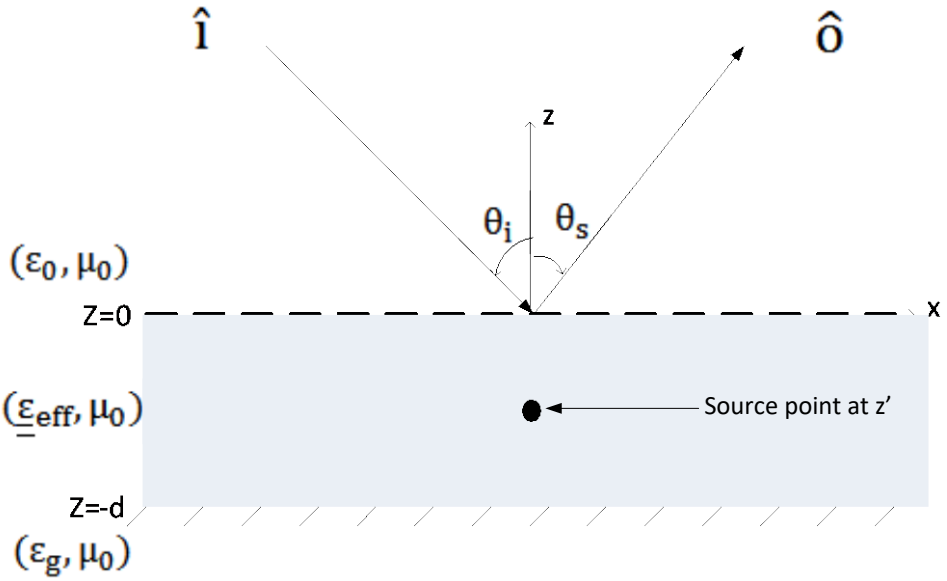

Figure 2.4 Geometry for determining the mean Green's function

An equation describing the dyadic mean Green's function $\underline{\underline{G}}(\underline{x},\underline{x}')$ is given in Equation 2.23.

$$\nabla\times\left(\nabla\times\underline{\underline{I}}\right)-k_0^2\underline{\underline{\varepsilon}}(\underline{x})\cdot\underline{\underline{G}}(\underline{x},\underline{x}')=\underline{\underline{I}}\delta(z') \tag{2.23}$$

Using a Fourier Transform approach, $\underline{\underline{G}}(\underline{x},\underline{x}')$ can be decomposed into waves traveling in the ±z directions. This is explicitly shown in Equation 2.24, which is recognized as a transverse Fourier Transform pair.

$$\underline{\underline{G}}(\underline{x},\underline{x}') = \frac{1}{(2\pi)^2}\int_{-\infty}^{\infty} d\underline{k}_t \left[\underline{\underline{\tilde{G}}}(\underline{k}_t, z, z')\, e^{+i\underline{k}_t\cdot(\underline{x}_t - \underline{x}_t')}\right] \tag{2.24}$$

The tilde denotes the transverse Fourier Transform operation. Note that $\underline{\underline{\tilde{G}}}(\underline{x},\underline{x}')$ can be expressed as a dyadic,

$$\underline{\underline{\tilde{G}}}(\underline{x},\underline{x}') = \tilde{G}_v(\underline{k}_t', z, z')\hat{v}\hat{v} + \tilde{G}_h(\underline{k}_t', z, z')\hat{h}\hat{h} \tag{2.25}$$

In order to find the dyadic Green's function the solution to a one-dimensional Fourier Transform, $\tilde{G}_p(\underline{k}_t, z, z')$, where p ∈ {h,v} is all that is needed. From Figure 2.4, $\tilde{G}_p(\underline{k}_t, z, z')$ expressed as:

$$\tilde{G}_p(k_t, z, z') = \begin{cases} T_p^+ e^{+ik_z z} & z > 0 \\ A_p e^{+i\kappa_{z_p} z} & z' < z < 0 \\ B_p e^{+i\kappa_{z_p} z} + C_p e^{-i\kappa_{z_p} z} & -d < z < z' \\ B_p e^{-ik_{z_g} z} & z < -d \end{cases}$$

Applying the continuity and jump conditions at the source point z=z' and noting that $B_p = \Gamma_p C_p$, the values for the coefficients can be determined. The continuity condition can be expressed as,

$$A_p e^{+i\kappa_{z_p} z'} = B_p e^{+i\kappa_{z_p} z'} + C_p e^{-i\kappa_{z_p} z'}$$

And the jump condition can be expressed as,

$$\lim_{\delta\to\infty}\left\{\frac{d}{dz}\tilde{G}_p\left(\underline{k}_t,z,z'\right)\Big|_{z=z'+\delta}-\frac{d}{dz}\tilde{G}_p\left(\underline{k}_t,z,z'\right)\Big|_{z=z'-\delta}\right\}=1$$

Carrying through the operations, the coefficients of interest corresponding to the mean region, are determined to be,

$$A_p=\frac{e^{-i\kappa_{z_p}z'}+\Gamma_p e^{+i\kappa_{z_p}z'}}{i2\kappa_{z_p}}$$

$$C_p=\frac{e^{+i\kappa_{z_p}z'}}{i2\kappa_{z_p}}$$

$$B_p=\Gamma_p C_p=\Gamma_p\frac{e^{+i\kappa_{z_p}z'}}{i2\kappa_{z_p}}$$

Substituting these values into $\tilde{G}_p\left(\underline{k}_t,z,z'\right)$ for the z > 0 region, due to a source located in the 0 < z' < -d region, results in,

$$\tilde{G}_p\left(\underline{k}_t,z,z'\right)=\left(\frac{e^{-i\kappa_{z_p}z'}+\Gamma_p e^{+i\kappa_{z_p}z'}}{i2\kappa_{z_p}}\right)e^{+ik_z z} \tag{2.26}$$

Substituting Equation 2.26 into Equation 2.24, the expression for the mean Green's function becomes,

$$\underline{\underline{G}}(\underline{x},\underline{x}')=\frac{1}{(2\pi)^2}\int_{-\infty}^{\infty}d\underline{k}_t\left[\left(\frac{e^{-i\kappa_{z_p}z'}+\Gamma_p e^{+i\kappa_{z_p}z'}}{i2\kappa_{z_p}}\right)e^{+ik_z z}e^{+i\underline{k}_t\cdot\left(\underline{x}_t-\underline{x}_t'\right)}\right] \tag{2.27}$$

Where $\underline{k}=\underline{k}_t+k_z$ and $\underline{x}=\underline{x}_t+\hat{z}$

The solution of this Equation 2.27 can be found by using the Method of Stationary Phase [Colin and Zucker, 1969]. The final result for the mean Green's function is,

$$G_p\left(\underline{x},\underline{x}'\right)=\frac{1}{4\pi}\frac{e^{+ik_o r}}{r}\left[e^{-i\kappa_{z_p}z'}+\Gamma_p e^{+i\kappa_{z_p}z'}\right]e^{-i\underline{k}_{t_s}\cdot\underline{x}_t'} \tag{2.28}$$

The interested reader can find a detailed solution to Equation 2.27 in the Appendix A.2.

A expression for the dyadic Green's function can now be written as,

$$\underline{\underline{G}}\left(\underline{x},\underline{x}'\right)=\frac{1}{4\pi}\frac{e^{+ik_o r}}{r}\left[\left[e^{-i\kappa_{z_v}z'}+\Gamma_v e^{+i\kappa_{z_v}z'}\right]\hat{v}\hat{v}+\left[e^{-i\kappa_{z_h}z'}+\Gamma_h e^{+i\kappa_{z_h}z'}\right]\hat{h}\hat{h}\right]e^{-i\underline{k}_{t_s}\cdot\underline{x}_t'}e^{+ik_z z}$$

A final more compact form for the dyadic Green's function is given in Equation 2.29.

$$\underline{\underline{G}}\left(\underline{x},\underline{x}'\right)=\frac{1}{4\pi}\frac{e^{+ik_o r}}{r}\left[\left(e^{-i\underline{\underline{\kappa}}_s z'}+\underline{\underline{\Gamma}}_p e^{+i\underline{\underline{\kappa}}_s z'}\right)\right]e^{-i\underline{k}_{t_s}\cdot\underline{x}_t'}e^{+ik_z z} \tag{2.29}$$

2.6 Scattered fields

From Equation 2.16, the scattered field in operator form is given by

$$\sum_{i=1}^{N}\left\langle\underline{\underline{L}}_o^{-1}\right\rangle\cdot\left\langle\underline{\underline{T}}_i\left(\beta\right)\right\rangle\cdot\left\langle\underline{E}\right\rangle$$

Converting to an integral representation, the scattered field can be expressed in terms of the dyadic mean Green's function, dyadic transition operator and the mean field as,

$$\underline{E}_s\left(\underline{x},\underline{s}\right)=\int d\underline{x}'\left[\underline{\underline{G}}\left(\underline{x},\underline{x}'\right)\right]\int d\underline{x}''\left[\underline{\underline{t}}\left(x'-s,x''-s\right)\cdot\left\langle\underline{E}\left(\underline{x}''\right)\right\rangle\right] \tag{2.30}$$

Substituting expressions for the dyadic mean Green's function given in Equation 2.27 and the mean field given by Equation 2.22, into Equation 2.30,

$$\underline{E}_s\left(\underline{x},\underline{s}\right)=\int d\underline{x}'\left[\frac{1}{4\pi}\frac{e^{+ik_o r}}{r}e^{-i\underline{k}_{t_s}\cdot\underline{x}_t'}\left(e^{-i\underline{\underline{\kappa}}_s z'}+\underline{\underline{\Gamma}}_p e^{+i\underline{\underline{\kappa}}_s z'}\right)\right]\int d\underline{x}''\left[\underline{\underline{t}}\left(\underline{x}'-\underline{s},\underline{x}''-\underline{s}\right)\cdot\left[e^{-i\underline{\underline{\kappa}}_z z''}+\underline{\underline{\Gamma}}_q e^{+i\underline{\underline{\kappa}}_z z''}\right]e^{+i\underline{k}_{t_i}\cdot\underline{x}_t''}\right]$$

This expression can be expanded as the sum of the following four terms,

$$\underline{E}_s^{(1)}\left(\underline{x},\underline{s}\right)=\int d\underline{x}'\left[\frac{1}{4\pi}e^{-i\underline{\underline{\kappa}}_s z'}e^{-i\underline{k}_{t_s}\cdot\underline{x}_t'}\right]\int d\underline{x}''\left[\underline{\underline{t}}\left(\underline{x}'-\underline{s},\underline{x}''-\underline{s}\right)\cdot e^{-i\underline{\underline{\kappa}}_z z''}e^{+i\underline{k}_{t_i}\cdot\underline{x}_t''}\right]\frac{e^{+ik_o r}}{r}$$

$$\underline{E}_s^{(2)}\left(\underline{x},\underline{s}\right)=\int d\underline{x}'\left[\frac{1}{4\pi}e^{-i\underline{\underline{\kappa}}_s z'}e^{-i\underline{k}_{t_s}\cdot\underline{x}_t'}\right]\int d\underline{x}''\left[\underline{\underline{t}}\left(\underline{x}'-\underline{s},\underline{x}''-\underline{s}\right)\cdot\underline{\Gamma}_q e^{+i\underline{\underline{\kappa}}_z z''}e^{+i\underline{k}_{t_i}\cdot\underline{x}_t''}\right]\frac{e^{+ik_o r}}{r}$$

$$\underline{E}_s^{(3)}\left(\underline{x},\underline{s}\right)=\int d\underline{x}'\left[\frac{1}{4\pi}\underline{\Gamma}_p e^{+i\underline{\underline{\kappa}}_s z'}e^{-i\underline{k}_{t_s}\cdot\underline{x}_t'}\right]\int d\underline{x}''\left[\underline{\underline{t}}\left(\underline{x}'-\underline{s},\underline{x}''-\underline{s}\right)\cdot e^{-i\underline{\underline{\kappa}}_z z''}e^{+i\underline{k}_{t_i}\cdot\underline{x}_t''}\right]\frac{e^{+ik_o r}}{r}$$

$$\underline{E}_s^{(4)}\left(\underline{x},\underline{s}\right)=\int d\underline{x}'\left[\frac{1}{4\pi}\underline{\Gamma}_p e^{+i\underline{\underline{\kappa}}_s z'}e^{-i\underline{k}_{t_s}\cdot\underline{x}_t'}\right]\int d\underline{x}''\left[\underline{\underline{t}}\left(\underline{x}'-\underline{s},\underline{x}''-\underline{s}\right)\cdot\underline{\Gamma}_q e^{+i\underline{\underline{\kappa}}_z z''}e^{+i\underline{k}_{t_i}\cdot\underline{x}_t''}\right]\frac{e^{+ik_o r}}{r}$$

These expressions will be simplified by applying assumptions about the behavior of the Green's function and mean field over the particle. In addition, the transition operator will be replaced by using its relationship with the scattering amplitude. This will be shown in detail for $\underline{E}_s^{(1)}\left(\underline{x},\underline{s}\right)$.

The $e^{-i\underline{\underline{\kappa}}_s z'}$ term can be recast as,

$$e^{-i\underline{\underline{\kappa}}_s z'}=e^{-i\underline{\underline{\kappa}}_{s_0} z'}e^{-i\underline{\underline{\kappa}}_{s_1} z'}=e^{-ik_{z_s} z'\left[\hat{h}_s\hat{h}_s+\hat{v}_s\hat{v}_s\right]}e^{-i\underline{\underline{\kappa}}_{s_1} z'}=e^{-ik_{z_s} z'}\left[\underline{\underline{I}}-\hat{o}\hat{o}\right]e^{-i\underline{\underline{\kappa}}_{s_1} z'}$$

Noting that the Green's function decays slowly across the size of the particle allows the $e^{-i\underline{\underline{\kappa}}_{s_1} z'}$ term to be approximated,

$$e^{-i\underline{\underline{\kappa}}_{s_1} z'}\approx e^{-i\underline{\underline{\kappa}}_{s_1} s_z}$$

Similarly, the $e^{-i\underline{\underline{\kappa}}_z z''}$ term can be recast as,

$$e^{-i\underline{\underline{\kappa}}_z z''}=e^{-i\underline{\underline{\kappa}}_{i_0} z''}e^{-i\underline{\underline{\kappa}}_{i_1} z''}=e^{-ik_{z_i} z''\left[\hat{h}_i\hat{h}i+\hat{v}_i\hat{v}_i\right]}e^{-i\underline{\underline{\kappa}}_{i_1} z''}=e^{-ik_{z_i} z''}\left[\underline{\underline{I}}-\hat{i}\hat{i}\right]e^{-i\underline{\underline{\kappa}}_{i_1} z''}$$

Note that the mean field also varies slowly across the particle, therefore

$$e^{-i\underline{\underline{\kappa}}_{i_1} z''} \approx e^{-i\underline{\underline{\kappa}}_{i_1} s_z}$$

Substituting these approximations into the scattered field expression for $\underline{E}_s^{(1)}(\underline{x},\underline{s})$ and dropping the subscript of '1' in the $\kappa-$term results in the following expression,

$$\underline{E}_s^{(1)}(\underline{x},\underline{s}) = \int d\underline{x}' \left[\frac{-1}{4\pi} e^{-ik_{z_s} z'} \left[\underline{\underline{I}} - \hat{o}\hat{o} \right] e^{-i\underline{\underline{\kappa}}_s s_z} e^{-i\underline{k}_{t_s} \cdot \underline{x}_t'} \right] \int d\underline{x}'' \left[\underline{\underline{t}}(\underline{x}' - \underline{s}, \underline{x}'' - \underline{s}) \cdot e^{-ik_{z_i} z''} \left[\underline{\underline{I}} - \hat{i}\hat{i} \right] e^{-i\underline{\underline{\kappa}}_i s_z} e^{+i\underline{k}_{t_i} \cdot \underline{x}_t''} \right] \frac{e^{+ik_o r}}{r}$$

$$= \frac{1}{4\pi} \frac{e^{+ik_o r}}{r} e^{-i\underline{\underline{\kappa}}_s s_z} \left[\underline{\underline{I}} - \hat{o}\hat{o} \right] \int d\underline{x}' \left[e^{-i\underline{k}_{t_s} \cdot \underline{x}_t'} e^{-ik_{z_s} z'} \right] \int d\underline{x}'' \left[\underline{\underline{t}}(\underline{x}' - \underline{s}, \underline{x}'' - \underline{s}) \cdot e^{+i\underline{k}_{t_i} \cdot \underline{x}_t''} e^{-ik_{z_i} z''} e^{-i\underline{\underline{\kappa}}_i s_z} \left[\underline{\underline{I}} - \hat{i}\hat{i} \right] \right]$$

$$= \frac{1}{4\pi} \frac{e^{+ik_o r}}{r} e^{-i\underline{\underline{\kappa}}_s s_z} \left[\underline{\underline{I}} - \hat{o}\hat{o} \right] \iint d\underline{x}' d\underline{x}'' \left[\underline{\underline{t}}(\underline{x}' - \underline{s}, \underline{x}'' - \underline{s}) e^{-ik_0 \hat{o}^+ \cdot \underline{x}'} e^{+ik_0 \hat{i}^- \cdot \underline{x}''} \right] e^{-i\underline{\underline{\kappa}}_i s_z} \left[\underline{\underline{I}} - \hat{i}\hat{i} \right]$$

where the following definitions was used,

$$\underline{k}_{t_s} + k_{z_s} \hat{z} \equiv k_0 \hat{o}^+$$
$$\underline{k}_{t_i} - k_{z_i} \hat{z} \equiv k_0 \hat{i}^-$$

Applying the following change of variables

$$\underline{x}' = \underline{x}' - \underline{s} \qquad \underline{x}' = \underline{x}' - \underline{s} \qquad d\underline{x}' = d\underline{x}'$$
$$\underline{x}'' = \underline{x}'' - \underline{s} \qquad \underline{x}'' = \underline{x}'' - \underline{s} \qquad d\underline{x}'' = d\underline{x}''$$

$$\underline{E}_s^{(1)}(\underline{x},\underline{s}) = \frac{1}{4\pi} \frac{e^{+ik_o r}}{r} e^{-i\underline{\underline{\kappa}}_s s_z} \left[\underline{\underline{I}} - \hat{o}\hat{o} \right] \iint d\underline{x}' d\underline{x}'' \left[\underline{\underline{t}}(\underline{x}', \underline{x}'') e^{-ik_0 \hat{o}^+ \cdot \underline{x}'} e^{+ik_0 \hat{i}^- \cdot \underline{x}''} e^{+ik_0 \left(-\hat{o}^+ + \hat{i}^- \right) \cdot \underline{s}} \right] e^{-i\underline{\underline{\kappa}}_i s_z} \left[\underline{\underline{I}} - \hat{i}\hat{i} \right]$$

Next, recognizing the double integral term is a 2-dimensional Fourier Transform, $\underline{E}_s^{(1)}(\underline{x},\underline{s})$ can be expressed as,

$$\underline{E}_s^{(1)}(\underline{x},\underline{s}) = \frac{(2\pi)^3}{4\pi} \frac{e^{+ik_o r}}{r} e^{-i\underline{\underline{\kappa}}_s s_z} \left[\underline{\underline{I}} - \hat{o}\hat{o} \right] \left[\tilde{\underline{\underline{t}}}\left(k_0 \hat{o}, k_0 \hat{i} \right) e^{+ik_0 \left(-\hat{o}^+ + \hat{i}^- \right) \cdot \underline{s}} \right] e^{-i\underline{\underline{\kappa}}_i s_z} \left[\underline{\underline{I}} - \hat{i}\hat{i} \right]$$

The relationship between the dyadic transition operator and the dyadic scattering amplitude, see B.7 in Appendix B, can now be used to get a final expression for the scattered field, $\underline{E}_s^{(1)}(\underline{x},\underline{s})$

$$\frac{1}{(2\pi)^3}\underline{\underline{f}}(\hat{o},\hat{i}) = \left[\underline{\underline{I}} - \hat{o}\hat{o}\right]\cdot\underline{\underline{\tilde{t}}}\left(k_0\hat{o},k_0\hat{i}\right)\cdot\left[\underline{\underline{I}} - \hat{i}\hat{i}\right]$$

Substituting into $\underline{E}_s^{(1)}(\underline{x},\underline{s})$, results in,

$$\underline{E}_s^{(1)}(\underline{x},\underline{s}) = \frac{e^{+ik_0 r}}{r} e^{-i\underline{\underline{\kappa}}_s s_z}\cdot\underline{\underline{\overline{f}}}\left(\hat{o}^+,\hat{i}^-\right)\cdot e^{-i\underline{\underline{\kappa}}_i s_z} e^{+ik_0\left(-\hat{o}^+ + \hat{i}^-\right)\cdot\underline{s}} \tag{2.31}$$

Similarly, expressions for the other three terms are:

$$\underline{E}_s^{(2)}(\underline{x},\underline{s}) = \frac{e^{+ik_0 r}}{r} e^{-i\underline{\underline{\kappa}}_s s_z}\cdot\underline{\underline{\overline{f}}}\left(\hat{o}^+,\hat{i}^+\right)\cdot\underline{\Gamma}_q e^{+i\underline{\underline{\kappa}}_i s_z} e^{+ik_0\left(-\hat{o}^+ + \hat{i}^+\right)\cdot\underline{s}} \tag{2.32}$$

$$\underline{E}_s^{(3)}(\underline{x},\underline{s}) = \frac{e^{+ik_0 r}}{r}\underline{\Gamma}_p e^{+i\underline{\underline{\kappa}}_s s_z}\cdot\underline{\underline{\overline{f}}}\left(\hat{o}^-,\hat{i}^-\right)\cdot e^{-i\underline{\underline{\kappa}}_i s_z} e^{-ik_0\left(\hat{o}^- + \hat{i}^-\right)\cdot\underline{s}} \tag{2.33}$$

$$\underline{E}_s^{(4)}(\underline{x},\underline{s}) = \frac{e^{+ik_0 r}}{r}\underline{\Gamma}_p e^{+i\underline{\underline{\kappa}}_s s_z}\cdot\underline{\underline{\overline{f}}}\left(\hat{o}^-,\hat{i}^+\right)\cdot\underline{\Gamma}_q e^{+i\underline{\underline{\kappa}}_i s_z} e^{-ik_0\left(\hat{o}^- - \hat{i}^+\right)\cdot\underline{s}} \tag{2.34}$$

2.7 Bistatic Scattering Coefficient

The bistatic scattering coefficient describes the scattering properties of a target and is defined as a ratio of a scattered intensity to an incident intensity, as expressed in Equation 2.35. Note that the order of the limits is important to ensure the far-field condition.

$$\sigma^0_{pqp'q'} = \lim_{A\to\infty}\lim_{|\underline{x}|\to\infty} \frac{4\pi|\underline{x}|^2}{A}\frac{I_{s_{pqp'q'}}}{I_{i_{qq'}}} \qquad (2.35)$$

$$p,q,p',q' \in \{h,v\}$$

where,

A is the area of illumination

$I_{i_{qq'}}$ is the incident intensity

$I_{s_{pqp'q'}}$ is the scattered intensity

The scattered intensity can be found by calculating the second moment, or the correlation of the fluctuating component of the scattered field. An explicit expression for this correlation can be found as follows,

$$I_{s_{pqp'q'}} = \left\langle E_{s_{pq}}(\underline{x}_1) E^*_{s_{pq}}(\underline{x}_2)\right\rangle = \sum_{i=1}^{N}\sum_{j=1}^{N}\left\langle E^{(i)}_{s_{pq}}(\underline{x}_1) E^{*(j)}_{s_{p'q'}}(\underline{x}_2)\right\rangle$$

$$= \sum_{i=1}^{N}\left\langle E^{(i)}_{s_{pq}}(\underline{x}_1) E^{*(i)}_{s_{p'q'}}(\underline{x}_2)\right\rangle + \sum_{i=1}^{N}\sum_{\substack{j=1\\ i\neq j}}^{N}\left\langle E^{(i)}_{s_{pq}}(\underline{x}_1) E^{*(j)}_{s_{p'q'}}(\underline{x}_2)\right\rangle$$

Assuming N identical and statistically independent scatterers,

$$= N\left\langle E^{(i)}_{s_{pq}}(\underline{x}_1) E^{*(i)}_{s_{p'q'}}(\underline{x}_2)\right\rangle + N(N-1)\left\langle E^{(i)}_{s_{pq}}(\underline{x}_1)\right\rangle\left\langle E^{*(j)}_{s_{p'q'}}(\underline{x}_2)\right\rangle$$

For large N,

$$= N\int_V d\underline{s}_4 \left[p(\underline{s}_4) \left\langle E^{(i)}_{s_{pq}}(\underline{x}_1, \underline{s}_4) E^{*(i)}_{s_{p'q'}}(\underline{x}_2, \underline{s}_4) \right\rangle \right] + N^2 \left\langle E^{(i)}_{s_{pq}}(\underline{x}_1) \right\rangle \left\langle E^{*(j)}_{s_{p'q'}}(\underline{x}_2) \right\rangle$$

Note that the integral is taken over the illuminated volume. Using the small fractional volume approximation ($\delta \ll 1$), $Np(\underline{s}_i) = \rho(\underline{s}_i) \sim \delta\rho$, the correlation of the scattered fields become,

$$\left\langle \underline{E}_{s_{pq}}(\underline{x}_1) \underline{E}^*_{s_{pq}}(\underline{x}_2) \right\rangle = \delta\rho \int_V d\underline{s}_4 \left\langle E^{(i)}_{s_{pq}}(\underline{x}_1, \underline{s}_4) E^{*(i)}_{s_{p'q'}}(\underline{x}_2, \underline{s}_4) \right\rangle \tag{2.36}$$

Using the result of Equation 2.36 into Equation 2.35, a general expression for the bistatic scattering coefficient can be expressed as,

$$\sigma^0_{pqp'q'} = \lim_{A\to\infty} \lim_{|x|\to\infty} \frac{4\pi|\underline{x}|^2}{A} \left\{ \delta\rho \int_A d\underline{s}_4 \int ds_z \sum_{i=1}^{4} \sum_{j=1}^{4} \left\langle E^{(i)}_{s_{pq}}(\underline{x}, \underline{s}) E^{*(j)}_{s_{p'q'}}(\underline{x}, \underline{s}) \right\rangle \right\} \tag{2.37}$$

Substituting Equations 2.31 through 2.34 into Equation 2.37 will result in sixteen terms contributing to the overall scattering coefficient. Carrying through the integrations, in particular, the integral of the exponential functions over $\underline{S}_t$ will reveal that only six terms are of $O(\delta^0)$, the other ten terms, due to phase cancellations are of $O(\delta^1)$ and since $\delta \ll 1$, their contribution to the overall scattering coefficient is negligible. More details on this is provided in Appendix A.4. The six non-negligible integrations will be explicitly carried out in the following section to derive expressions for the various scattering coefficients.

2.7.1 Direct Scatter:

The first of six terms that contribute to the overall scattering coefficient occurs when i=j=1, corresponding to a downward going incident field and an upward going scattered field. Neither incident nor scattered field comes into contact with the ground interface. This scatter term is referred to as direct (or volume) scatter and is depicted geometrically in Figure 2.5.

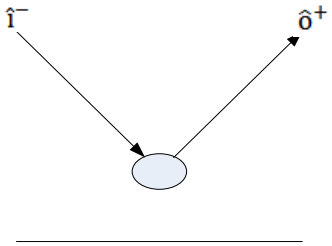

Figure 2.5 Geometry for direct-scatter (i=j=1)

Substituting Equation 2.31 into Equation 2.37, an expression for the scattering coefficient can be derived.

$$\sigma^0_{pqp'q'} = \lim_{A\to\infty}\lim_{|\underline{x}|\to\infty} \frac{4\pi|\underline{x}|^2}{A}\left\{\delta\rho\int_A d\underline{s}\int ds_z \left\langle E^{(1)}_{s_{pq}}(\underline{x},\underline{s})\, E^{*(1)}_{s_{p'q'}}(\underline{x},\underline{s})\right\rangle\right\}$$

$$\sigma^0_{d_{pqp'q'}} = 4\pi\rho\delta\left\langle f_{pq}\left(\hat{o}^+,\hat{i}^-\right) f^*_{p'q'}\left(\hat{o}^+,\hat{i}^-\right)\right\rangle \int_{-d}^{\infty} ds_z e^{-i\left[\kappa_{s_p}+\kappa_{i_q}-\kappa^*_{s_{p'}}-\kappa^*_{i_{q'}}\right]s_z}$$

Evaluating the integral, let the scaling or ordering parameter $\delta \to 1$, and using some complex number simplifications results in a final expression for the scattering coefficient due to direct scatter.

$$\sigma^0_{d_{pqp'q'}} = 4\pi\rho\left\langle f_{pq}\left(\hat{o}^+,\hat{i}^-\right)f^*_{p'q'}\left(\hat{o}^+,\hat{i}^-\right)\right\rangle\left[\frac{1-e^{-2\,Imag\left(\kappa_{s_p}+\kappa_{i_q}\right)d}}{2\,Imag\left(\kappa_{s_p}+\kappa_{i_q}\right)d}\right] \tag{2.38}$$

2.7.2 Direct-Reflected Incoherent Scatter:

There are two direct-reflected incoherent scatter terms. The first term occurs when i=j=2, corresponding to both an upward going incident and scattered field. Note that the incident field comes into contact with the ground interface and is multiplied by the appropriate Fresnel reflection coefficient. This is depicted geometrically in Figure 2.6.

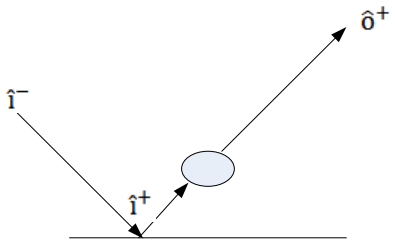

Figure 2.6 Geometry for the incoherent direct-reflected scatter (i=j=2)

Substituting Equation 2.32 into Equation 2.37, an expression for the scattering coefficient can be derived.

$$\sigma^0_{pqp'q'} = \lim_{A\to\infty}\lim_{|\underline{x}|\to\infty}\frac{4\pi|\underline{x}|^2}{A}\left\{\delta\rho\int_A d\underline{s}_t\int ds_z\left\langle E^{(2)}_{s_{pq}}\left(\underline{x},\underline{s}\right)E^{*(2)}_{s_{p'q'}}\left(\underline{x},\underline{s}\right)\right\rangle\right\}$$

$$\sigma^0_{dri1_{pqp'q'}} = 4\pi\rho\delta\left\langle f_{pq}\left(\hat{o}^+,\hat{i}^+\right)f^*_{p'q'}\left(\hat{o}^+,\hat{i}^+\right)\right\rangle\Gamma_q\Gamma^*_{q'}\int_{-d}^{\infty}ds_z e^{-i\left[\kappa_{s_p}-\kappa_{i_q}-\kappa^*_{s_{p'}}+\kappa^*_{i_{q'}}\right]s_z}$$

Evaluating the integral, let the scaling or ordering parameter $\delta \to 1$, and using some complex number simplifications results in a final expression for the scattering coefficient due to the first type of direct-reflected incoherent scatter.

$$\sigma^0_{dri1_{pqp'q'}} = 4\pi\rho\left\langle f_{pq}\left(\hat{o}^+,\hat{i}^+\right)f^*_{p'q'}\left(\hat{o}^+,\hat{i}^+\right)\right\rangle\Gamma_q\Gamma^*_{q'}\left[\frac{1-e^{2Imag\left(\kappa_{s_p}-\kappa_{i_q}\right)d}}{2Imag\left(\kappa_{s_p}-\kappa_{i_q}\right)}\right] \tag{2.39}$$

The second of the direct-reflected incoherent terms occurs when i=j=3, corresponding to a both down-going incident and scattered field. Note in this case, that the scattered field is now being reflected off the ground interface and is multiplied by its appropriate Fresnel reflection coefficient. This is depicted in Figure 2.7.

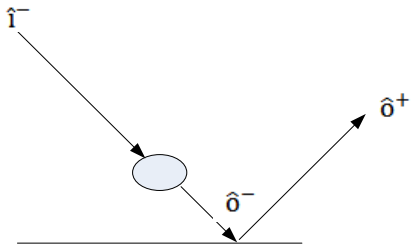

Figure 2.7 Geometry for direct-reflected incoherent scatter (i=j=3)

Substituting Equation 2.33 into Equation 2.37 results in the following expression for the scattering coefficient,

$$\sigma^0_{pqp'q'} = \lim_{A\to\infty}\lim_{|x|\to\infty}\frac{4\pi|\underline{x}|^2}{A}\left\{\delta\rho\int_A d\underline{s}\int ds_z\left\langle E^{(3)}_{s_{pq}}\left(\underline{x},\underline{s}\right)E^{*(3)}_{s_{p'q'}}\left(\underline{x},\underline{s}\right)\right\rangle\right\}$$

$$\sigma^0_{dri2_{pqp'q'}} = 4\pi\rho\delta\left\langle f_{pq}\left(\hat{o}^-,\hat{i}^-\right)f^*_{p'q'}\left(\hat{o}^-,\hat{i}^-\right)\right\rangle\Gamma_p\Gamma^*_{p'}\int_{-d}^{\infty}ds_z e^{i\left[\kappa_{s_p}-\kappa_{i_q}-\kappa^*_{s_{p'}}+\kappa^*_{i'}\right]s_z}$$

Evaluating the integral, let the scaling or ordering parameter $\delta \to 1$, and using some complex number simplifications results in a final expression for the scattering coefficient due to the second type of direct-reflected incoherent scatter.

$$\sigma^0_{dri2_{pqp'q'}} = 4\pi\rho\left\langle f_{pq}\left(\hat{o}^-,\hat{i}^-\right)f^*_{p'q'}\left(\hat{o}^-,\hat{i}^-\right)\right\rangle\Gamma_p\Gamma^*_{p'}\left[\frac{1-e^{2Imag\left(-\kappa_{s_p}+\kappa_{i_q}\right)d}}{2Imag\left(-\kappa_{s_p}+\kappa_{i_q}\right)}\right] \tag{2.40}$$

2.7.3 Direct-Reflected Coherent Scatter:

There are two direct-reflected coherent scatter terms that occur when i=2 and j=3 and when i=3 and j=2. For the first case, when i=2 and j=3, examining Equation 2.32 and 2.33, show that both incident and scattered fields are in the positive direction, with the incident field being reflected from the ground interface. Similarly, when i=3 and j=2, both incident and scattered fields are in the negative direction, with the scattered field being reflected off the ground interface. This is depicted in Figure 2.8.

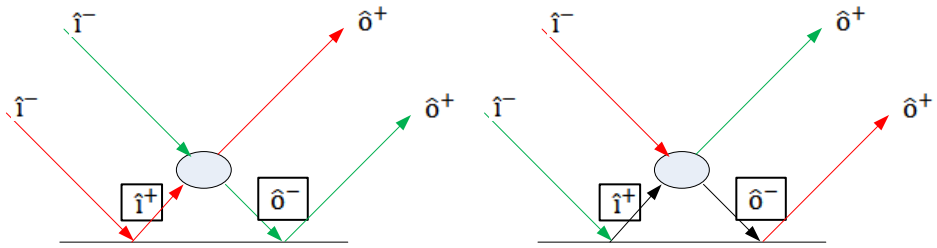

Figure 2.8 Geometry for direct-reflected coherent scatter (i=2, j=3 and i=3 and j=2)

Substituting Equation 2.32 and Equation 2.33 into Equation 2.37 results in the following expression for the scattering coefficient,

$$\sigma^0_{pqp'q'} = \lim_{A\to\infty}\lim_{|\underline{x}|\to\infty}\frac{4\pi|\underline{x}|^2}{A}\left\{\delta\rho\int_A d\underline{s}_t\int ds_z\left\langle E^{(2)}_{s_{pq}}\left(\underline{x},\underline{s}\right)E^{*(3)}_{s_{p'q'}}\left(\underline{x},\underline{s}\right)\right\rangle\right\}$$

$$\sigma^0_{drcl_{pqp'q'}} = 4\pi\rho\delta\left\langle f_{pq}\left(\hat{o}^+,\hat{i}^+\right)f^*_{p'q'}\left(\hat{o}^-,\hat{i}^-\right)\right\rangle\Gamma_q\Gamma^*_{p'}\int_{-d}^{\infty} ds_z e^{-i2\left(k_{z_s}-k_{z_i}\right)s_z}e^{-i\left[\kappa_{s_p}-\kappa_{i_q}+\kappa^*_{s_{p'}},-\kappa^*_{i'}\right]s_z}$$

Evaluating the integral, let the scaling or ordering parameter $\delta \to 1$, and using some complex number simplifications results in a final expression for the scattering coefficient due to the first component of the direct-reflected coherent scatter.

$$\sigma^0_{drc1_{pqp'q'}} = 4\pi\rho\left\langle f_{pq}\left(\hat{o}^+,\hat{i}^+\right)f^*_{p'q'}\left(\hat{o}^-,\hat{i}^-\right)\right\rangle \Gamma_q\Gamma^*_{p'}\left[\frac{1-e^{+i2\left(k_{z_s}-k_{z_i}\right)d}e^{+i2\,Real\left(\kappa_{s_p}-\kappa_{i_q}\right)d}}{i2\left[\left(k_{z_s}-k_{z_i}\right)+Real\left(\kappa_{s_p}-\kappa_{i_q}\right)\right]}\right] \tag{2.41}$$

For the second case, where i=3 and j=2, Substituting Equation 2.32 and Equation 2.33 into Equation 2.37 results in,

$$\sigma^0_{pqp'q'} = \lim_{A\to\infty}\lim_{|\underline{x}|\to\infty}\frac{4\pi|\underline{x}|^2}{A}\left\{\delta\rho\int_A d\underline{s}_t\int ds_z\left\langle E^{(3)}_{s_{pq}}\left(\underline{x},\underline{s}\right)E^{*(2)}_{s_{p'q'}}\left(\underline{x},\underline{s}\right)\right\rangle\right\}$$

$$\sigma^0_{drc2_{pqp'q'}} = 4\pi\rho\left\langle f_{pq}\left(\hat{o}^-,\hat{i}^-\right)f^*_{p'q'}\left(\hat{o}^+,\hat{i}^+\right)\right\rangle \Gamma_p\Gamma^*_{q'}\int_{-d}^{\infty} ds_z e^{+i2\left(k_{z_s}-k_{z_i}\right)s_z}e^{+i\left[\kappa_{s_p}-\kappa_{i_q}+\kappa^*_{s_{p'}}-\kappa^*_{i_{r'}}\right]s_z}$$

Evaluating the integral, let the scaling or ordering parameter $\delta \to 1$, and using some complex number simplifications results in a final expression for the scattering coefficient due to the second component of the direct-reflected coherent scatter.

$$\sigma^0_{drc2_{pqp'q'}} = 4\pi\rho\left\langle f_{pq}\left(\hat{o}^-,\hat{i}^-\right)f^*_{p'q'}\left(\hat{o}^+,\hat{i}^+\right)\right\rangle \Gamma_p\Gamma^*_{q'}\left[\frac{1-e^{-i2\left(k_{z_s}-k_{z_i}\right)d}e^{-i2\,Real\left(\kappa_{s_p}-\kappa_{i_q}\right)d}}{-i2\left[\left(k_{z_s}-k_{z_i}\right)+Real\left(\kappa_{s_p}-\kappa_{i_q}\right)\right]}\right] \tag{2.42}$$

The two direct-reflected coherent terms, contributes maximally when $k_{z_i} = k_{z_s}$, which occurs at two angles. The first angle corresponds to backscatter and the second angle corresponds to specular scatter. The contribution from these coherent terms decrease as the scattering angle goes away form the back or specular scattering angle. The

rate of decay will be shown later to be strongly dependent on the frequency and the layer depth.

2.7.4 Reflected Scatter:

The reflected term occurs when i=j=4, corresponding to a downward going scattered field and an upward going incident field. Both fields come into contact with the ground interface. This is depicted geometrically in Figure 2.9.

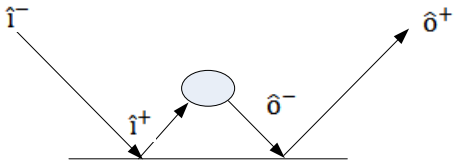

Figure 2.9 Geometry for reflected scatter (i=j=4)

Substituting Equation 2.50 into Equation 2.53 results in the following expression for the scattering coefficient,

$$\sigma^0_{pqp'q'} = \lim_{A\to\infty}\lim_{|x|\to\infty}\frac{4\pi|\underline{x}|^2}{A}\left\{\delta\rho\int_A d\underline{s}\int ds_z\left\langle E^{(4)}_{s_{pq}}(\underline{x},\underline{s})E^{*(4)}_{s_{p'q'}}(\underline{x},\underline{s})\right\rangle\right\}$$

$$\sigma^0_{r_{pqp'q'}} = 4\pi\rho\delta\left\langle f_{pq}\left(\hat{o}^-,\hat{i}^+\right)f^*_{p'q'}\left(\hat{o}^-,\hat{i}^+\right)\right\rangle\Gamma_q\Gamma^*_{q'}\Gamma_p\Gamma^*_{p'}\int_{-d}^{\infty}ds_z e^{i\left[\kappa_{s_p}+\kappa_{i_q}-\kappa^*_{s_{p'}}-\kappa^*_{i_{q'}}\right]s_z}$$

Evaluating the integral, let the scaling or ordering parameter $\delta \to 1$, and using some complex number simplifications results in a final expression for the scattering coefficient reflected scatter.

$$\sigma^0_{r_{pqp'q'}} = 4\pi\rho\left\langle f_{pq}\left(\hat{o}^-,\hat{i}^+\right)f^*_{p'q'}\left(\hat{o}^-,\hat{i}^+\right)\right\rangle\Gamma_q\Gamma^*_{q'}\Gamma_p\Gamma^*_{p'}\left[\frac{1-e^{2\,\mathrm{Imag}\left(\kappa_{s_p}+\kappa_{i_q}\right)d}}{-2\,\mathrm{Imag}\left(\kappa_{s_p}+\kappa_{i_q}\right)}\right] \qquad (2.43)$$

The equations for the various bistatic scattering coefficients are re-written below for completeness. Note that the total bistatic scattering coefficient is simply the sum of the six scattering terms shown in Equations 2.44 through 2.49.

$$\sigma^0_{d_{pqp'q'}} = 4\pi\rho\left\langle f_{pq}\left(\hat{o}^+,\hat{i}^-\right)f^*_{p'q'}\left(\hat{o}^+,\hat{i}^-\right)\right\rangle\left[\frac{1-e^{-2\,Imag\left(\kappa_{s_p}+\kappa_{i_q}\right)d}}{2\,Imag\left(\kappa_{s_p}+\kappa_{i_q}\right)}\right] \tag{2.44}$$

$$\sigma^0_{dri1_{pqp'q'}} = 4\pi\rho\left\langle f_{pq}\left(\hat{o}^+,\hat{i}^+\right)f^*_{p'q'}\left(\hat{o}^+,\hat{i}^+\right)\right\rangle\Gamma_q\Gamma^*_{q'}\left[\frac{1-e^{2\,Imag\left(\kappa_{s_p}-\kappa_{i_q}\right)d}}{2\,Imag\left(\kappa_{s_p}-\kappa_{i_q}\right)}\right] \tag{2.45}$$

$$\sigma^0_{dri2_{pqp'q'}} = 4\pi\rho\left\langle f_{pq}\left(\hat{o}^-,\hat{i}^-\right)f^*_{p'q'}\left(\hat{o}^-,\hat{i}^-\right)\right\rangle\Gamma_p\Gamma^*_{p'}\left[\frac{1-e^{2\,Imag\left(-\kappa_{s_p}+\kappa_{i_q}\right)d}}{2\,Imag\left(-\kappa_{s_p}+\kappa_{i_q}\right)}\right] \tag{2.46}$$

$$\sigma^0_{r_{pqp'q'}} = 4\pi\rho\left\langle f_{pq}\left(\hat{o}^-,\hat{i}^+\right)f^*_{p'q'}\left(\hat{o}^-,\hat{i}^+\right)\right\rangle\Gamma_q\Gamma^*_q\Gamma_p\Gamma^*_{p'}\left[\frac{1-e^{2\,Imag\left(\kappa_{s_p}+\kappa_{i_q}\right)d}}{-2\,Imag\left(\kappa_{s_p}+\kappa_{i_q}\right)}\right] \tag{2.47}$$

$$\sigma^0_{drc1_{pqp'q'}} = 4\pi\rho\left\langle f_{pq}\left(\hat{o}^+,\hat{i}^+\right)f^*_{p'q'}\left(\hat{o}^-,\hat{i}^-\right)\right\rangle\Gamma_q\Gamma^*_{p'}\left[\frac{1-e^{+i2\left(k_{z_s}-k_{z_i}\right)d}e^{+i2\,Real\left(\kappa_{s_p}-\kappa_{i_q}\right)d}}{i2\left[\left(k_{z_s}-k_{z_i}\right)+Real\left(\kappa_{s_p}-\kappa_{i_q}\right)\right]}\right] \tag{2.48}$$

$$\sigma^0_{drc2_{pqp'q'}} = 4\pi\rho\left\langle f_{pq}\left(\hat{o}^+,\hat{i}^+\right)f^*_{p'q'}\left(\hat{o}^-,\hat{i}^-\right)\right\rangle\Gamma_q\Gamma^*_{p'}\left[\frac{1-e^{-i2\left(k_{z_s}-k_{z_i}\right)d}e^{+i2\,Real\left(\kappa_{s_p}-\kappa_{i_q}\right)d}}{-i2\left[\left(k_{z_s}-k_{z_i}\right)+Real\left(\kappa_{s_p}-\kappa_{i_q}\right)\right]}\right] \tag{2.49}$$

where, $\sigma^0_{d_{pqp'q'}}$ is the direct scattering coefficient; $\sigma^0_{dri1_{pqp'q'}}$ and $\sigma^0_{dri2_{pqp'q'}}$ are the two-types of incoherent direct-reflected scattering coefficients; $\sigma^0_{r_{pqp'q'}}$ is the reflected scattering coefficient; $\sigma^0_{drc1_{pqp'q'}}$ and $\sigma^0_{drc2_{pqp'q'}}$ are the two-types of coherent direct-reflected scattering coefficients.

Note that Eq. 2.48 and Eq. 2.49 are complex conjugates and can be combined into one equation given by Eq. 2.50, which represents the total coherent scattering contribution due to direct-reflected scatter.

$$\sigma^0_{\mathrm{drc}_{\mathrm{pqp'q'}}} = 8\pi\rho\left\langle \mathrm{f}_{\mathrm{pq}}\left(\hat{\mathrm{o}}^-,\hat{\mathrm{i}}^-\right)\mathrm{f}^*_{\mathrm{p'q'}}\left(\hat{\mathrm{o}}^+,\hat{\mathrm{i}}^+\right)\right\rangle \Gamma_{\mathrm{p}}\Gamma^*_{\mathrm{q'}}\,\mathrm{Real}\left[\frac{1-\mathrm{e}^{-\mathrm{i}2\left(\mathrm{k}_{\mathrm{z_s}}-\mathrm{k}_{\mathrm{z_i}}\right)\mathrm{d}}\,\mathrm{e}^{-\mathrm{i}2\,\mathrm{Real}\left(\kappa_{\mathrm{s_p}}-\kappa_{\mathrm{i_q}}\right)\mathrm{d}}}{-\mathrm{i}2\left[\left(\mathrm{k}_{\mathrm{z_s}}-\mathrm{k}_{\mathrm{z_i}}\right)+\mathrm{Real}\left(\kappa_{\mathrm{s_p}}-\kappa_{\mathrm{i_q}}\right)\right]}\right] \tag{2.50}$$

The total coherent bistatic scattering coefficient is computed by summing all of the above scattering contributions,

$$\sigma^0_{\mathrm{c}_{\mathrm{pqp'q'}}} = \sigma^0_{\mathrm{d}_{\mathrm{pqp'q'}}} + \sigma^0_{\mathrm{dri1}_{\mathrm{pqp'q'}}} + \sigma^0_{\mathrm{dri2}_{\mathrm{pqp'q'}}} + \sigma^0_{\mathrm{drc}_{\mathrm{pqp'q'}}} + \sigma^0_{\mathrm{r}_{\mathrm{pqp'q'}}} \tag{2.51}$$

If the direct-reflected coherent term (Eq. 2.50) is not included in the summation, the result will be referred to as the incoherent bistatic scattering coefficient,

$$\sigma^0_{\mathrm{i}_{\mathrm{pqp'q'}}} = \sigma^0_{\mathrm{d}_{\mathrm{pqp'q'}}} + \sigma^0_{\mathrm{dri1}_{\mathrm{pqp'q'}}} + \sigma^0_{\mathrm{dri2}_{\mathrm{pqp'q'}}} + \sigma^0_{\mathrm{r}_{\mathrm{pqp'q'}}} \tag{2.52}$$

Chapter 3 Scattering Amplitudes of Individual Scatterers

In Chapter 2, the bistatic scattering coefficients for a layer of discrete random medium over a flat dielectric half-space was derived. One key parameter seen in these equations is the scattering amplitude $f_{pq}\left(\hat{o}^{\pm},\hat{i}^{\pm}\right)$. In this chapter, a few useful methods to calculate $f_{pq}\left(\hat{o}^{\pm},\hat{i}^{\pm}\right)$ will be presented. The first method, useful for Rayleigh-type scatterers [Ishimaru, 1997], describes $f_{pq}\left(\hat{o}^{\pm},\hat{i}^{\pm}\right)$ in terms of its dipole polarizability. The second method, valid for resonant scatterers, uses an electrostatic approximation for the internal field of the scatterer. This method will be used to calculate $f_{pq}\left(\hat{o}^{\pm},\hat{i}^{\pm}\right)$ for a thin circular dielectric disc and a thin dielectric cylinder, both of which are very useful in the radar modeling of vegetation. It will be shown that the electrostatic approximation converge to the dipole polarizability solution for Rayleigh-type scatterers.

3.1 Dipole polarizability method

A scatterer is placed in a homogenous non-magnetic medium characterized by ε_r and μ_0. If the size of the scatterer is much smaller than the surrounding wavelength, both the amplitude and phase of an incident wave are approximately constant over the whole volume of the scatterer. This incident field induces an electric charge with alternate signs on opposite sides of the scatterer, forming a dipole. The scattering from this dipole will be described in terms of a polarizability dyadic, and will be derived in this section.

First, the internal field of a small scatterer can be expressed as the sum of its transverse and normal components,

$$\underline{E}_i = \underline{E}_o^t + \frac{E_o^z}{\varepsilon_r}\hat{z}' \tag{3.1}$$

Expanding Equation 3.1 and expressing as a dyadic,

$$\left[\hat{x}' + \hat{y}' + \frac{\hat{z}'}{\varepsilon_r}\right] \cdot \left[\hat{x}' + \hat{y}' + \hat{z}'\right] \underline{E}_i$$

$$\left[\hat{x}'\hat{x}' + \hat{y}'\hat{y}' + \frac{\hat{z}'\hat{z}'}{\varepsilon_r}\right] \cdot \underline{E}_i \tag{3.2}$$

Next, the polarizability dyadic of a small scatterer, $\underline{\underline{\alpha}}$ can be represented in terms of its dipole moment $\underline{P}_m$ and the applied field, $\underline{E}_i$,

$$\underline{P}_m = \varepsilon_o \underline{\underline{\alpha}} \cdot \underline{E}_i \tag{3.3}$$

The polarization vector $\underline{P}$ of the scatterer in terms of the internal fields can be expressed as,

$$\underline{P} = \underline{D}_{int} - \varepsilon_o \underline{E}_i = \varepsilon_o \varepsilon_r \underline{E}_i - \varepsilon_o \underline{E}_i = \varepsilon_o \left(\varepsilon_r - 1\right) \underline{E}_i \tag{3.4}$$

Substituting Equation 3.2 into Equation 3.4.

$$\underline{P} = \varepsilon_o \left(\varepsilon_r - 1\right) \left[\underline{\hat{x}}'\underline{\hat{x}}' + \hat{y}'\hat{y}' + \frac{\hat{z}'\hat{z}'}{\varepsilon_r}\right] \cdot \underline{E}_i \tag{3.5}$$

The dipole moment $\underline{P}_m$, of a dielectric scatterer is equal to the electric polarization vector, $\underline{P}$, integrated over the volume of the scatterer. For an electrically small scatterer,

characterized by a constant $\underline{P}$, the integral simplifies to the multiplication of $\underline{P}$ by the volume of the scatterer.

$$\underline{P}_m = \int \underline{P} dv = \underline{P} V_p \tag{3.6}$$

Equating, Equation 3.3 and Equation 3.6,

$$\underline{P} V_p = \varepsilon_o \underline{\underline{\alpha}} \cdot \underline{E}_i$$

And then substituting Equation 3.5 into Equation 3.6, results in,

$$\varepsilon_o \left(\varepsilon_r - 1\right)\left[\hat{x}'\hat{x}' + \hat{y}'\hat{y}' + \frac{\hat{z}'\hat{z}'}{\varepsilon_r}\right] \cdot \underline{E}_i V_p = \varepsilon_o \underline{\underline{\alpha}} \cdot \underline{E}_i \tag{3.7}$$

Comparing the right and left hand side of Equation 3.7, gives an expression for the polarizability dyadic, $\underline{\underline{\alpha}}$:

$$\underline{\underline{\alpha}} = \left(\varepsilon_r - 1\right) V_p \left[\hat{x}'\hat{x}' + \hat{y}'\hat{y}' + \frac{\hat{z}'\hat{z}'}{\varepsilon_r}\right] \tag{3.8}$$

Expressing $\underline{\underline{\alpha}}$ in spherical cooridinates:

$$\underline{\underline{\alpha}} = a_r \hat{r}'\hat{r}' + a_\theta \hat{\theta}'\hat{\theta}' + a_\phi \hat{\phi}'\hat{\phi}'$$

Note that,

$$\hat{r}' = \left(\sin\theta\cos\phi\right)\hat{x}' + \left(\sin\theta\sin\phi\right)\hat{y}' + \left(\cos\theta\right)\hat{z}'$$
$$\hat{\theta}' = \left(\cos\theta\cos\phi\right)\hat{x}' + \left(\cos\theta\sin\phi\right)\hat{y}' - \left(\sin\theta\right)\hat{z}'$$
$$\hat{\phi}' = \left(-\sin\phi\right)\hat{x}' + \left(\cos\phi\right)\hat{y}'$$

Substituting these expressions into Equation 3.8,

$$\underline{\underline{\alpha}} = a_r\left[(\sin\theta\cos\phi)\hat{x}' + (\sin\theta\sin\phi)\hat{y}' + (\cos\theta)\hat{z}'\right]\left[(\sin\theta\cos\phi)\hat{x}' + (\sin\theta\sin\phi)\hat{y}' + (\cos\theta)\hat{z}'\right]$$
$$+a_\theta\left[(\cos\theta\cos\phi)\hat{x}' + (\cos\theta\sin\phi)\hat{y}' - (\sin\theta)\hat{z}'\right]\left[(\cos\theta\cos\phi)\hat{x}' + (\cos\theta\sin\phi)\hat{y}' - (\sin\theta)\hat{z}'\right]$$
$$+a_\phi\left[(-\sin\phi)\hat{x}' + (\cos\phi)\hat{y}'\right]\left[(-\sin\phi)\hat{x}' + (\cos\phi)\hat{y}'\right]$$

Expand and collect the following nine-terms of the polarizability dyadic are:

$$\alpha_{xx} = a_r\sin^2\theta\cos^2\phi + a_\theta\cos^2\theta\cos^2\phi + a_\phi\sin^2\phi \tag{3.9}$$

$$\alpha_{xy} = a_r\sin^2\theta\sin^2\phi\cos\phi + a_\theta\cos^2\theta\sin\phi\cos\phi - a_\phi\sin\phi\cos\phi \tag{3.10}$$

$$\alpha_{xz} = a_r\sin\theta\cos\theta\cos\phi - a_\theta\sin\theta\cos\theta\cos\phi \tag{3.11}$$

$$\alpha_{yx} = \alpha_{xy} \tag{3.12}$$

$$\alpha_{yy} = a_r\sin^2\theta\sin^2\phi + a_\theta\cos^2\theta\sin^2\phi + a_\phi\cos^2\phi \tag{3.13}$$

$$\alpha_{yz} = a_\theta\sin\theta\cos\theta\sin\phi - a_\phi\sin\theta\cos\theta\sin\phi \tag{3.14}$$

$$\alpha_{zx} = \alpha_{xz} \tag{3.15}$$

$$\alpha_{zy} = \alpha_{yz} \tag{3.16}$$

$$\alpha_{zz} = a_r\cos^2\theta + a_\theta\sin^2\theta \tag{3.17}$$

where,

$$a_r = \frac{(\varepsilon_r - 1)}{\varepsilon_r} = \frac{\chi}{1+\chi}$$
$$a_\theta = a_\phi = (\varepsilon_r - 1) = \chi$$

In [Lang and Sidhu, 1983], expressions for the backscatter coefficients for a layer of Rayleigh scatterers in terms of its dipole polarizability, $\underline{\underline{\alpha}}$ are derived. Expressions for σ_{hh} are reproduced below,

$$\sigma^0 = \sigma_{hhd} + \sigma_{hhdr} + \sigma_{hhr}$$

where,

$$\sigma_{hhd} = \frac{k_0^4 \delta V_p}{4\pi} \left\langle \left|\alpha_{hh}\right|^2 \right\rangle \left(\frac{1 - e^{-4\,\mathrm{Im}(\kappa_{z_h})d}}{4\,\mathrm{Im}(\kappa_{z_h})} \right)$$
$$\sigma_{hhdr} = \frac{k_0^4 \delta V_p}{4\pi} 4 \left\langle \left|\alpha_{hh}\right|^2 \right\rangle \left|\Gamma_h\right|^2 d$$
$$\sigma_{hhr} = \frac{k_0^4 \delta V_p}{4\pi} \left|\Gamma_h\right|^4 \left\langle \left|\alpha_{hh}\right|^2 \right\rangle \left(\frac{-1 + e^{-4\,\mathrm{Im}(\kappa_{z_h})d}}{4\,\mathrm{Im}(\kappa_{z_h})} \right)$$

These expressions can be obtained from the bistatic scattering coefficient equations, Equation 2.44, 2.45, 2.46, 2.47 and 2.48, derived in Chapter 2 by:

- Use reciprocity (ie: $f_{pp}\left(\hat{o}^+, \hat{i}^+\right) = f_{pp}\left(\hat{o}^-, \hat{i}^-\right)$)
- $\hat{o} = -\hat{i}$ (ie: backscatter)
- p=q
- $k_{z_i} = k_{z_s}$ ($\theta_i = \pm\theta_s$)
- $\underline{\underline{f}} = \frac{k_0^2}{4\pi} \underline{\underline{\alpha}}$

Also note that the binomial expansion of the exponential term results in the following simplification:

$$\frac{1-e^{2\,Imag\left(\kappa_{s_p}-\kappa_{i_q}\right)d}}{2\,Imag\left(\kappa_{s_p}-\kappa_{i_q}\right)} \rightarrow \frac{1-\left(1+2\,Imag\left(\kappa_{s_p}-\kappa_{i_q}\right)d\right)}{2\,Imag\left(\kappa_{s_p}-\kappa_{i_q}\right)} = d$$

Note that $\underline{\underline{\alpha}}$ is averaged over ϕ which has a uniform distribution over 2π. Substitute Equation 3.13 for α_{hh}, in the expression for σ_{hhd} ,since $\alpha_{hh} = \alpha_{yy}$ [Lang and Sidhu, 1983] to get,

$$\sigma_{hhd} = \frac{k_0^4 \delta V_p}{4\pi}\left\langle \left| a_r \sin^2\theta \sin^2\phi + a_\theta \cos^2\theta \sin^2\phi + a_\phi \cos^2\phi \right|^2 \right\rangle \left(\frac{1-e^{-4\,Imag(\kappa_{z_h})d}}{4\,Imag(\kappa_{z_h})} \right)$$

$$= \frac{k_0^4 \delta V_p}{4\pi}\left\langle \left| \frac{\chi}{1+\chi}\sin^2\theta \sin^2\phi + \chi \cos^2\theta \sin^2\phi + \chi \cos^2\phi \right|^2 \right\rangle \left(\frac{1-e^{-4\,Imag(\kappa_{z_h})d}}{4\,Imag(\kappa_{z_h})} \right)$$

Expanding,

$$= \frac{k_0^4 \delta V_p}{4\pi} \left| \begin{array}{l} \frac{\chi}{1+\chi}\frac{\chi^*}{1+\chi^*}\left\langle \sin^4\theta \sin^4\phi \right\rangle + \frac{\chi\chi^*}{1+\chi^*}\left\langle \sin^2\theta \cos^2\theta \sin^4\phi \right\rangle + \frac{\chi\chi^*}{1+\chi}\left\langle \sin^2\theta \sin^2\phi \cos^2\phi \right\rangle \\ + \frac{\chi\chi^*}{1+\chi^*}\left\langle \sin^2\theta \cos^2\theta \sin^4\phi \right\rangle + \chi\chi^*\left\langle \cos^4\theta \sin^4\phi \right\rangle + \chi\chi^*\left\langle \cos^2\theta \sin^2\phi \cos^2\phi \right\rangle \\ + \frac{\chi\chi^*}{1+\chi^*}\left\langle \sin^2\theta \sin^2\phi \cos^2\phi \right\rangle + \chi\chi^*\left\langle \cos^2\theta \sin^2\phi \cos^2\phi \right\rangle + \chi\chi^*\left\langle \cos^4\phi \right\rangle \end{array} \right|$$
$$\cdot \left(\frac{1-e^{4\,Imag(\kappa_h)d}}{4\,Imag(\kappa_h)} \right)$$

Integrating over the ϕ variable, which has a uniform distribution over 2π, and grouping terms results in,

$$\sigma_{hhd} = \frac{k_0^4 \chi \chi^* \delta V_p}{4\pi} \left| \frac{3}{8} \frac{\chi}{1+\chi} \frac{\chi^*}{1+\chi^*} \left\langle \sin^4 \theta \right\rangle - \frac{1}{2} \left\langle \sin^2 \theta \right\rangle \left[\frac{\chi + \chi^* + 2\chi\chi^*}{(1+\chi)(1+\chi^*)} \right] + 1 \right| \left(\frac{1 - e^{4\,\mathrm{Imag}(\kappa_h)d}}{4\,\mathrm{Imag}(\kappa_h)} \right) \quad (3.18)$$

Substitute Equation 3.13 for α_{hh}, in the expression for σ_{hhdr}.

$$\sigma_{hhdr} = \frac{k_0^4 \delta V_p}{4\pi} 4 \left\langle \left| \alpha_{hh} \right|^2 \right\rangle \left| \Gamma_h \right|^2 d$$

$$= \frac{k_0^4 \delta V_p}{4\pi} 4 \left\langle \left| a_r \sin^2\theta \sin^2\phi + a_\theta \cos^2\theta \sin^2\phi + a_\phi \cos^2\phi \right|^2 \right\rangle \left| \Gamma_h \right|^2 d$$

$$= \frac{k_0^4 \delta V_p}{4\pi} 4 \left\langle \left| \frac{\chi}{1+\chi} \sin^2\theta \sin^2\phi + \chi \cos^2\theta \sin^2\phi + \chi \cos^2\phi \right|^2 \right\rangle \left| \Gamma_h \right|^2 d$$

$$\sigma_{hhdr} = \frac{k_0^4 \delta V_p \chi \chi^*}{4\pi} 4 \left[\frac{3}{8} \frac{\chi}{1+\chi} \frac{\chi^*}{1+\chi^*} \left\langle \sin^4 \theta \right\rangle - \frac{1}{2} \left\langle \sin^2 \theta \right\rangle \left(\frac{\chi + \chi^* + 2\chi\chi^*}{(1+\chi)(1+\chi^*)} \right) + 1 \right] \left| \Gamma_h \right|^2 d \quad (3.19)$$

Finally, substitute Equation 3.13 for α_{hh}, in the expression for σ_{hhr}.

$$\sigma_{hhr} = \frac{k_0^4 \delta V_p}{4\pi} \left| \Gamma_h \right|^4 \left\langle \left| \alpha_{hh} \right|^2 \right\rangle \left(\frac{-1 + e^{-4\,\mathrm{Imag}(\kappa_{z_h})d}}{4\,\mathrm{Imag}(\kappa_{z_h})} \right)$$

$$= \frac{k_0^4 \delta V_p}{4\pi} \left| \Gamma_h \right|^4 \left\langle \left| a_r \sin^2\theta \sin^2\phi + a_\theta \cos^2\theta \sin^2\phi + a_\phi \cos^2\phi \right|^2 \right\rangle \left(\frac{-1 + e^{-4\,\mathrm{Imag}(\kappa_{z_h})d}}{4\,\mathrm{Imag}(\kappa_{z_h})} \right)$$

$$= \frac{k_0^4 \delta V_p}{4\pi} \left| \Gamma_h \right|^4 \left\langle \left| \frac{\chi}{1+\chi} \sin^2\theta \sin^2\phi + \chi \cos^2\theta \sin^2\phi + \chi \cos^2\phi \right|^2 \right\rangle \left(\frac{-1 + e^{-4\,\mathrm{Imag}(\kappa_{z_h})d}}{4\,\mathrm{Imag}(\kappa_{z_h})} \right)$$

$$\sigma_{hhr} = \frac{k_0^4 \delta V_p \chi \chi^*}{4\pi} \left| \Gamma_h \right|^4 \left[\frac{3}{8} \frac{\chi}{1+\chi} \frac{\chi^*}{1+\chi^*} \left\langle \sin^4 \theta \right\rangle - \frac{1}{2} \left\langle \sin^2 \theta \right\rangle \left(\frac{\chi + \chi^* + 2\chi\chi^*}{(1+\chi)(1+\chi^*)} \right) + 1 \right] \left(\frac{-1 + e^{-4\,\mathrm{Imag}(\kappa_{z_h})d}}{4\,\mathrm{Imag}(\kappa_{z_h})} \right) \quad (3.20)$$

An illustrative example, reproducing the plot from Fig. 6 in [Lang and Sidhu, 1983] is performed. This plot displays backscatter versus incident angle, as seen in Figure 3.1. The

parameters used are reproduced in Table 3.1 below. It is interesting to note that backscatter due to the reflected scatter is much less than the other scattering terms, since it is proportional to $|\Gamma_h|^4$. In general the reflected scatter term can be ignored when modeling vegetation fields, unless the ground is saturated with moisture such as mangrove or rice fields. Also, the direct-reflected and reflected backscatter is seen to increase with increasing angles of incidence. This is due to the behavior of the Fresnel reflection coefficient for horizontal polarization, which increases and approaches 1 at a 90° incidence. The direct-reflected scattering contribution is also greater than the direct scatter contribution. Finally, note that the direct scatter term is relatively flat over all incident angles. This is due to the skin depth for the layer being larger than the layer depth. A plot of the skin depth is shown in Figure 3.2. Even at an incident angle of 80°, the skin depth is 15.2 m, which is over an order of magnitude larger than the 1 m layer depth. Under this condition, the scatterers in the layer see about the same incident field, regardless of the incident angle.

Parameter	Value
Frequency	400 MHz
Layer Depth	1 m
Disc Distribution	$18/\pi$ over$[0, \pi/18]$
Disc Density	500
Disc Dielectric Constant	30.8+i0.62
Ground Dielectric Constant	12+i3
Disc Radius	7.5 cm
Disc Thickness	0.5 mm

Table 3.1 Parameters describing a layer of circular discs over a dielectric half-space

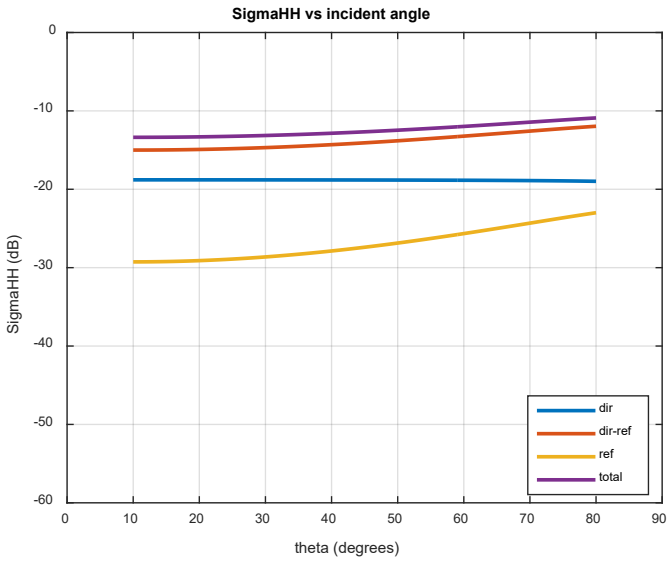

Figure 3.1 HPOL backscatter terms versus incident angle for a layer of circular discs

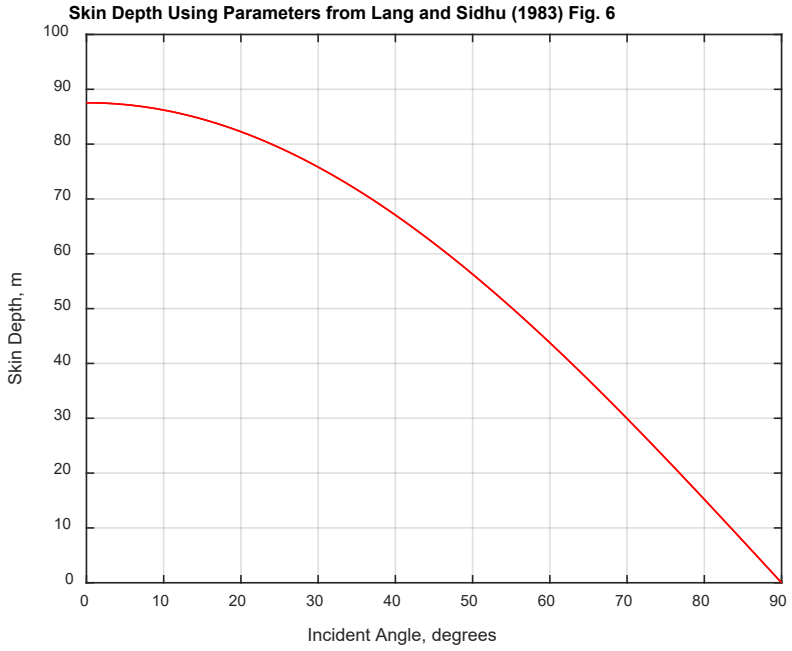

Figure 3.2 HPOL skin depth for a layer of circular discs

3.2 Scattering Coefficient of an Electrically Thin Dielectric Disc and Cylinder

In Section 3.1, the scattering coefficients for electrically small scatterers was developed using the dipole polarizability method. For larger scatterers, an approach developed by LeVine et al. (1985) will be used to derive the scattering coefficient of a thin dielectric disc.

Consider a plane wave incident on a dielectric disc having thickness, T and a complex permittivity of ε_r, as shown in Figure 3.3. An incident plane wave of unit amplitude and polarization $\hat{q}$ will excite currents that re-radiate a scattered field.

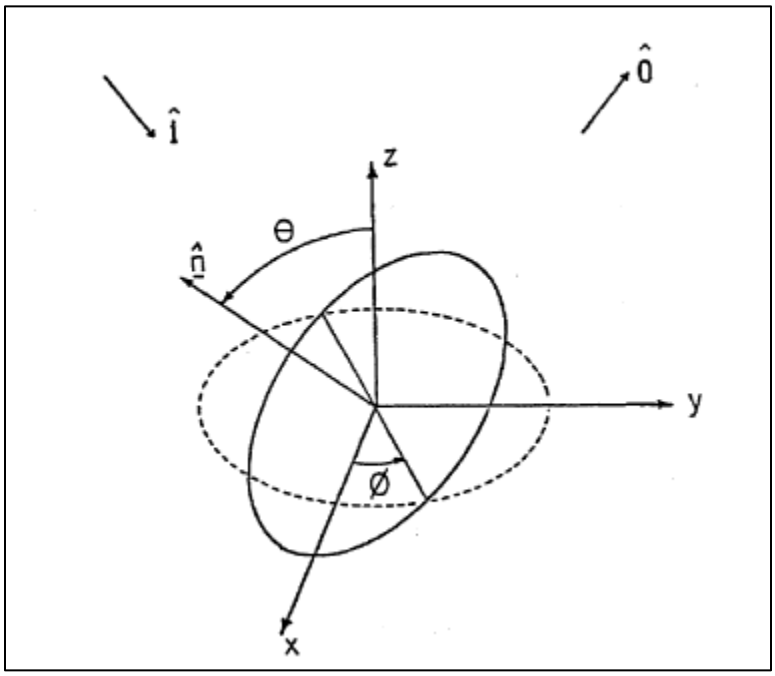

Figure 3.3 Thin disc geoemetry

If the scatterer is relatively thin (a >> t) and the radius is electrically large (a >> λ), then the induced electric field within the disc can be approximated by the electric field in an unbounded slab having the same orientation as the disc. At the disc boundary (z=t), the electric field can be expressed as a sum of the tangential and normal field components,

$$\underline{E}_i = \underline{E}_{it} + \underline{E}_{in}\hat{z} \tag{3.21}$$

Both the tangential electric field and the normal displacement field must be continuous across the boundary and the internal fields can be expressed as:

$$\underline{E}_{it} = \left(\hat{q} - \left(\hat{q}\cdot\hat{n}\right)\hat{n}\right)e^{+ik_0\hat{i}\cdot\underline{x}_t}$$
$$\underline{E}_{in} = \frac{1}{\varepsilon_r}\left(\hat{q}\cdot\hat{n}\right)\hat{n}e^{+ik_0\hat{i}\cdot\underline{x}_t}$$

The quasi-static approximation of the internal electric field within the disk is the sum of the tangential and normal components of the electric field,

$$\underline{E}_i\left(\underline{x}'\right) = \underline{E}_{it} + \underline{E}_{in} = \left[\left(\hat{q} - \left(\hat{q}\cdot\hat{n}\right)\hat{n}\right) + \frac{1}{\varepsilon_r}\left(\hat{q}\cdot\hat{n}\right)\hat{n}\right]e^{+ik_0\hat{i}\cdot\underline{x}_t} \tag{3.22}$$

From [Levine et al. 1983], the dyadic scattering amplitude can be calculated from the internal fields as,

$$f\left(\hat{o},\hat{i};\hat{q}\right) = \frac{k_0^2\left(\varepsilon_r - 1\right)}{4\pi}\left(\underline{\underline{I}} - \hat{o}\hat{o}\right)\int dv'\underline{E}_i\left(\underline{x}'\right)e^{-ik_0\left(\hat{o}\cdot\underline{x}'\right)} \tag{3.23}$$

Substituting in Equation 3.22 into 3.23,

$$= \frac{k_0^2\left(\varepsilon_r - 1\right)}{4\pi}\left(\underline{\underline{I}} - \hat{o}\hat{o}\right)\cdot\int dv'\left[\left(\hat{q} - \left(\hat{q}\cdot\hat{n}\right)\hat{n}\right) + \frac{1}{\varepsilon_r}\left(\hat{q}\cdot\hat{n}\right)\hat{n}\right]e^{+ik_0\left(\hat{i}\cdot x_t'\right)}e^{-ik_0\left(\hat{o}\cdot\underline{x}'\right)}$$

Applying the thin disc approximation:

$$e^{-ik_0\left(\hat{o}\cdot\underline{x}'\right)} = e^{-ik_0\left(\hat{o}\cdot\underline{x}_t'\right)}e^{-ik_0\left(\hat{o}\cdot\hat{z}\right)z'} = e^{-ik_0\left(\hat{o}\cdot\underline{x}_t'\right)}$$

$$= \frac{k_0^2(\varepsilon_r - 1)}{4\pi}\left(\underline{\underline{I}} - \hat{o}\hat{o}\right)\cdot\int dv'\left[\left(\hat{q} - (\hat{q}\cdot\hat{n})\hat{n}\right) + \frac{1}{\varepsilon_r}(\hat{q}\cdot\hat{n})\hat{n}\right]e^{+ik_0\left(\hat{i}\cdot\underline{x}_t'\right)}e^{-ik_0\left(\hat{o}\cdot\underline{x}_t'\right)}$$

Setting $(\epsilon_r - 1) = \chi$ and factoring out the $\hat{q}\cdot\hat{n}$ term, the final expression for the scattering amplitude of a thin planar dielectric scatterer can be expressed as,

$$\underline{\underline{f}}\left(\hat{o},\hat{i};\hat{q}\right) = \frac{k_0^2\chi}{4\pi}\left(\underline{\underline{I}} - \hat{o}\hat{o}\right)\cdot\left[\hat{q} - \frac{\chi}{1+\chi}(\hat{q}\cdot\hat{n})\hat{n}\right]\int dv' e^{+ik_0\left(\hat{i}-\hat{o}\right)\cdot\underline{x}_t'} \tag{3.24}$$

For a circular disc, the integral can be replaced with a Bessel function,

$$\underline{\underline{f}}\left(\hat{o},\hat{i};\hat{q}\right) = \frac{k_0^2\chi}{4\pi}\left(\underline{\underline{I}} - \hat{o}\hat{o}\right)\cdot\left[\hat{q} - \frac{\chi}{1+\chi}(\hat{q}\cdot\hat{n})\hat{n}\right]\left[\frac{2\pi aT}{k_s}J_1(k_s a)\right] \tag{3.25}$$

J_1 is a Bessel function of the first kind.

A comparison for HH-pol backscatter from a layer of discs versus incident angle using Equation 3.25 (thin-disc model) and the dipole model is shown in Fig. 3.4. The model parameters are detailed in Table 3.1. A plot comparing the total backscatter versus incident angle from the dipole and thin-disc methods is shown in Figure 3.4.

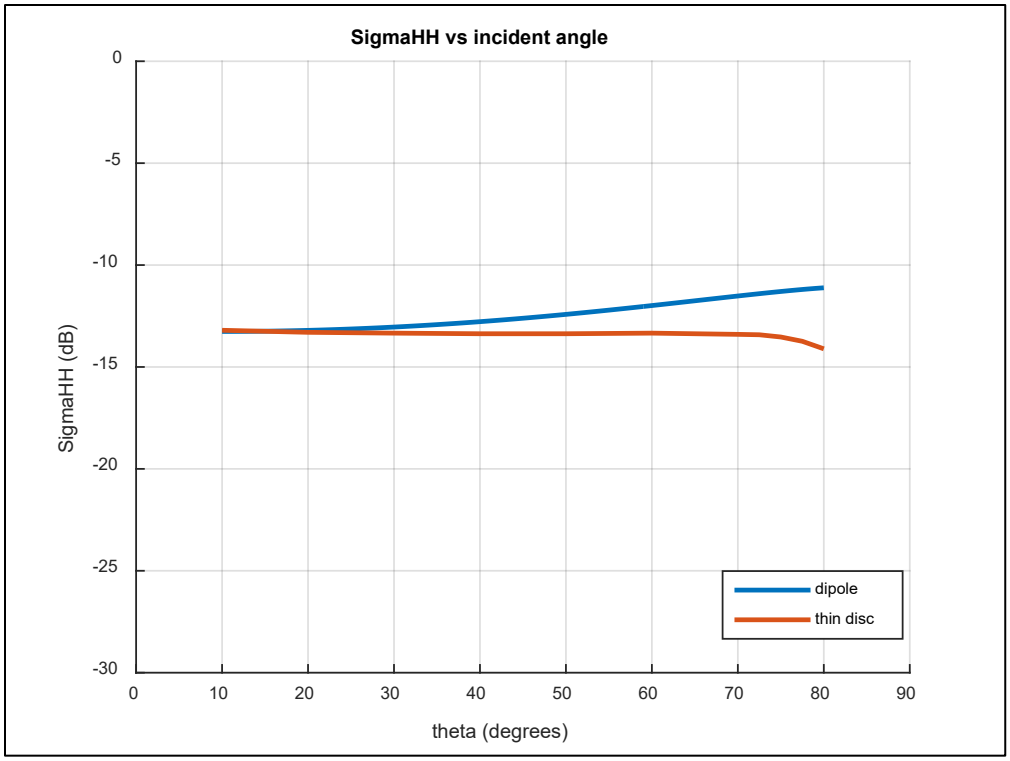

Figure 3.4 Comparison of HPOL backscatter versus incident angle predicted by dipole and thin disc model for a disc radius at the Raleigh limit

First, it is observed that both methods agree quite well for low incident angles, from 10° to about 30°. After 30° the two methods diverge. Note that the discs are at the Rayleigh limit (ie: wavelength divided by the radius of disc is equal to 0.1), where the validity of the dipole approximation becomes questionable. Reducing the size of the disc by a factor of two shows that the scattering predicted from the dipole method and the thin-disc method are much closer, as shown in Figure 3.5, where a worse case difference of 0.3 dB at 80° incident angle is seen.

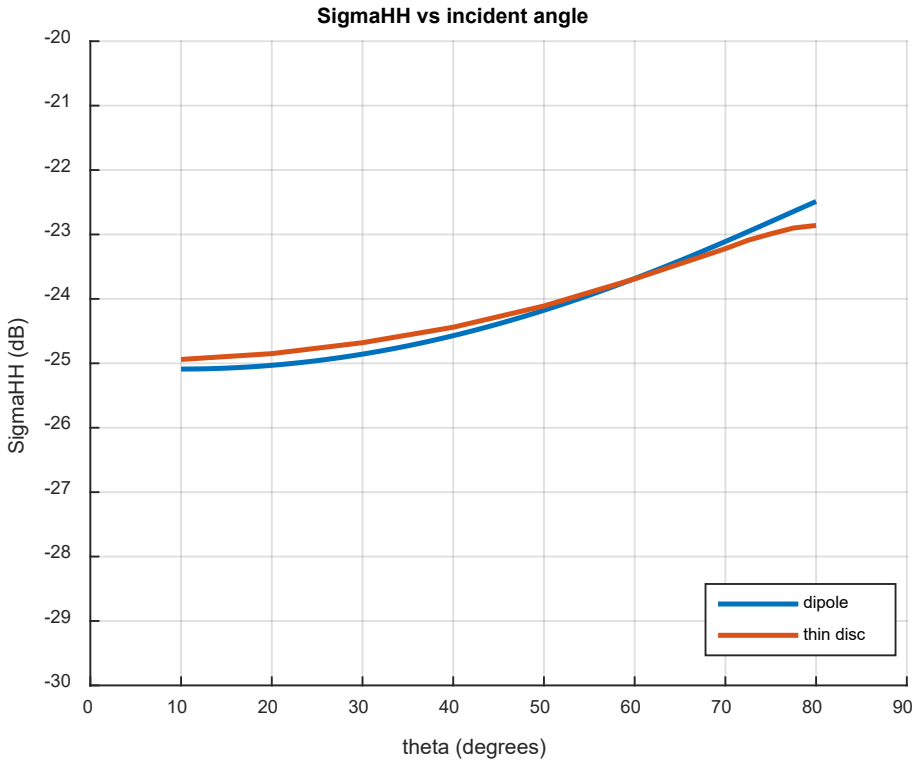

Figure 3.5 Comparison of HPOL backscatter versus incident angle predicted by dipole and thin disc model for a disc radius less than the Raleigh limit

3.3 Thin-disc model reduction to the dipole model

As seen in Section 3.2, the dipole polarizability formulation and the thin-disc formulation results appear to diverge for electrically large scatterers and converge for electrically small scatterers. It will be instructive to show analytically that the expressions derived using the thin disc model converges to the exact expressions derived via the dipole polarizability method as the disc becomes electrically small. This will be shown for the HH case and for a circular disc having a radius of ‘a’, thickness ‘t’ and a volume of ‘Vp’. First, for the thin disc model, the HH component from the scattering amplitude dyadic for the thin disc given in Equation 3.25 is extracted,

$$f_{hh}\left(-\hat{i},\hat{i}\right)=\frac{k_0^2\chi}{4\pi}\left[1-\frac{\chi}{1+\chi}\left(\hat{h}\cdot\hat{n}\right)^2\right]\left[\frac{2\pi aT}{k_s}J_1(k_s a)\right] \tag{3.26}$$

For an electrically small scatterer, set $k_s a << 1$ and use the small-argument approximation of the Bessel function,

$$f_{hh}\left(-\hat{i},\hat{i}\right)=\frac{k_0^2\chi}{4\pi}\left[1-\frac{\chi}{1+\chi}\left(\hat{h}\cdot\hat{n}\right)^2\right]\pi a^2 T \tag{3.27}$$

Noting the geometry from Figure 3.1,

$$\hat{n}=\hat{x}\sin\theta\sin\phi+\hat{y}\sin\theta\cos\phi+\hat{z}\cos\theta$$
$$\hat{h}=\hat{x}\sin\phi_i+\hat{y}\cos\phi_i$$

Substituting into Equation 3.27,

$$f_{hh}\left(-\hat{i},\hat{i}\right)=\frac{k_0^2\chi\pi a^2 T}{4\pi}\left[1-\frac{\chi}{1+\chi}\left(\sin^2\theta\cos^2\Phi\right)\right]$$
where
$$\Phi=\phi-\phi_i \tag{3.28}$$

Substituting Equation 3.28 into Equation 2.70,

$$\sigma^0_{d_{hh}}=4\pi\rho\left\langle f_{pp}\left(-\hat{i},\hat{i}\right)f^*_{pp}\left(-\hat{i},\hat{i}\right)\right\rangle\left[\frac{1-e^{-4\,\mathrm{Im}\,\kappa_{sh}d}}{4\,\mathrm{Im}\,\kappa_{sh}}\right]$$
$$=4\pi\rho\left\langle\left(\frac{k_0^2\chi\pi a^2 T}{4\pi}\left[1-\frac{\chi}{1+\chi}\left(\sin^2\theta\cos^2\Phi\right)\right]\right)\left(\frac{k_0^2\chi^*\pi a^2 T}{4\pi}\left[1-\frac{\chi^*}{1+\chi^*}\left(\sin^2\theta\cos^2\Phi\right)\right]\right)\right\rangle\left[\frac{1-e^{-4\,\mathrm{Im}\,\kappa_{sh}d}}{4\,\mathrm{Im}\,\kappa_{sh}}\right]$$
$$=\frac{4\pi\rho k_0^4|\chi|^2\left(\pi a^2\right)T^2}{(4\pi)^2}\left\langle\left[1-\frac{\chi^*}{1+\chi^*}\left(\sin^2\theta\cos^2\Phi\right)-\frac{\chi}{1+\chi}\left(\sin^2\theta\cos^2\Phi\right)+\frac{\chi}{1+\chi}\frac{\chi^*}{1+\chi^*}\left(\sin^4\theta\cos^4\Phi\right)\right]\right\rangle\left[\frac{1-e^{-4\,\mathrm{Im}\,\kappa_{sh}d}}{4\,\mathrm{Im}\,\kappa_{sh}}\right]$$

Integrating over Φ from [0,2π],

$$=\frac{4\pi\rho k_0^4|\chi|^2\left(\pi a^2\right)T^2}{(4\pi)^2}\left\langle\left[1-\frac{\chi^*}{1+\chi^*}\left(\frac{\sin^2\theta}{2}\right)-\frac{\chi}{1+\chi}\left(\frac{\sin^2\theta}{2}\right)+\frac{3}{8}\frac{\chi}{1+\chi}\frac{\chi^*}{1+\chi^*}\left(\sin^4\theta\right)\right]\right\rangle\left[\frac{1-e^{-4\,\mathrm{Im}\,\kappa_{sh}d}}{4\,\mathrm{Im}\,\kappa_{sh}}\right]$$

Finally, grouping like-terms,

$$= \frac{\rho k_0^4 |\chi|^2 \left(\pi a^2\right) T^2}{4\pi} \left[\frac{3}{8} \frac{\chi}{1+\chi} \frac{\chi^*}{1+\chi^*} \left\langle \sin^4\theta \right\rangle - \frac{1}{2} \left\langle \sin^2\theta \right\rangle \left[\frac{\chi + \chi^* + 2\chi\chi^*}{(1+\chi)(1+\chi^*)} \right] + 1 \right] \left[\frac{1 - e^{-4 \operatorname{Im} \kappa_{sh} d}}{4 \operatorname{Im} \kappa_{sh}} \right] \quad (3.29)$$

Replacing $\rho = \frac{V_p}{\delta}$ where $V_p = \pi a^2 T$ in Equation 3.29 results in,

$$\sigma^0_{d_{hh}} = \frac{k_0^4 |\chi|^2 \delta V_p}{4\pi} \left[\frac{3}{8} \frac{\chi}{1+\chi} \frac{\chi^*}{1+\chi^*} \left\langle \sin^4\theta \right\rangle - \frac{1}{2} \left\langle \sin^2\theta \right\rangle \left[\frac{\chi + \chi^* + 2\chi\chi^*}{(1+\chi)(1+\chi^*)} \right] + 1 \right] \left[\frac{1 - e^{-4 \operatorname{Im} \kappa_{sh} d}}{4 \operatorname{Im} \kappa_{sh}} \right] \quad (3.30)$$

Note that Equation 3.30, which is the HH direct-backscatter term derived using the thin-disc approximation, under the assumption that the thin-disc is electrically small, is exactly the same as Equation 3.18, which is the dipole approximation for the HH direct-backscatter term.

Similarly, if Equation 3.28 is substituted into Equation 2.71, the expression for the direct-reflected scatter terms derived via the thin-disc model will equal the expression derived using the dipole polarizability method, for an electrically small disc.

$$\sigma^0_{dr_{hh}} = 16\pi\rho \left\langle f_{hh}\left(-\hat{i}, \hat{i}\right) f^*_{hh}\left(-\hat{i}, \hat{i}\right) \right\rangle \Gamma_h \Gamma_h^* d$$

$$= 16\pi\rho \left\langle \left(\frac{k_0^2 \chi \pi a^2 T}{4\pi} \left[1 - \frac{\chi}{1+\chi} \left(\sin^2\theta \cos^2\Phi \right) \right] \right) \left(\frac{k_0^2 \chi^* \pi a^2 T}{4\pi} \left[1 - \frac{\chi^*}{1+\chi^*} \left(\sin^2\theta \cos^2\Phi \right) \right] \right) \right\rangle \Gamma_h \Gamma_h^* d$$

$$= \frac{k_0^4 \delta V_p |\chi|^2}{4\pi} 4 \left\langle \frac{3}{8} \frac{\chi}{1+\chi} \frac{\chi^*}{1+\chi^*} \left\langle \sin^4\theta \right\rangle - \frac{1}{2} \left\langle \sin^2\theta \right\rangle \left[\frac{\chi + \chi^* + 2\chi\chi^*}{(1+\chi)(1+\chi^*)} \right] + 1 \right\rangle |\Gamma_h|^2 d \quad (3.31)$$

Note that Equation 3.31, which is the HH direct-reflected backscatter term derived using the thin-disc approximation, under the assumption that the thin-disc is electrically small, is

exactly the same as Equation 3.19, which is the dipole approximation for the HH direct-reflected backscatter term.

The final scatter term is the reflected term. Substitute Equation 3.28 into Equation 2.72,

$$\sigma^0_{r_{pp}} = 4\pi\rho\left\langle f_{pq}\left(-\hat{i},\hat{i}\right)f^*_{pp}\left(\left(-\hat{i},\hat{i}\right)\right)\right\rangle\left|\Gamma^4_p\right|\left[\frac{-1+e^{4\mathrm{Im}\kappa_{s_p}d}}{4\mathrm{Im}\kappa_{s_p}d}\right]$$

$$= 4\pi\rho\left\langle\left(\frac{k_0^2\chi\pi a^2T}{4\pi}\left[1-\frac{\chi}{1+\chi}\left(\sin^2\theta\cos^2\Phi\right)\right]\right)\left(\frac{k_0^2\chi^*\pi a^2T}{4\pi}\left[1-\frac{\chi^*}{1+\chi^*}\left(\sin^2\theta\cos^2\Phi\right)\right]\right)\right\rangle\left|\Gamma^4_p\right|\left[\frac{-1+e^{4\mathrm{Im}\kappa_{s_p}d}}{4\mathrm{Im}\kappa_{s_p}d}\right]$$

$$= \frac{k_0^4\delta V_p\left|\chi\right|^2}{4\pi}\left|\Gamma^4_p\right|\left\langle\frac{3}{8}\frac{\chi}{1+\chi}\frac{\chi^*}{1+\chi^*}\left\langle\sin^4\theta\right\rangle-\frac{1}{2}\left\langle\sin^2\theta\right\rangle\left[\frac{\chi+\chi^*+2\chi\chi^*}{\left(1+\chi\right)\left(1+\chi^*\right)}\right]+1\right\rangle\left[\frac{-1+e^{4\mathrm{Im}\kappa_{s_p}d}}{4\mathrm{Im}\kappa_{s_p}d}\right]$$

(3.32)

Note that Equation 3.32, which is the HH reflected backscatter term derived using the thin-disc approximation, under the assumption that the thin-disc is electrically small, is exactly the same as Equation 3.20, which is the dipole approximation for the HH reflected backscatter term. A numerical example using parameters from Lang and Sidhu (1981) in Fig.12 is tabulated below in Table 3.2.

Parameter	Value
Frequency	1800 MHz
Layer Depth	1 m
Disc Distribution	18/π over[0, π/18]
Disc Density	4000
Disc Dielectric Constant	30.8+i0.62

Ground Dielectric Constant	12+i3
Disc Radius	7.5 cm
Disc Thickness	0.5 mm

Table 3.2 Parameters for a layer of circular discs sized at the Raleigh limit, over a dielectric half-space

The backscatter from HH is computed using the dipole approximation and the thin disc approximation as a function of the electrical size of the disc. The electrical size of the disc is taken to be the ratio of the disc radius to the wavelength. As shown in Figure 3.6, as the size of the disc decreases, the backscatter predicted from the dipole model versus the thin-disc model converges. Note that when the ratio of the disc radius to the wavelength is equal to 0.1, this is known as the Rayleigh limit [Ishimaru, 1977].

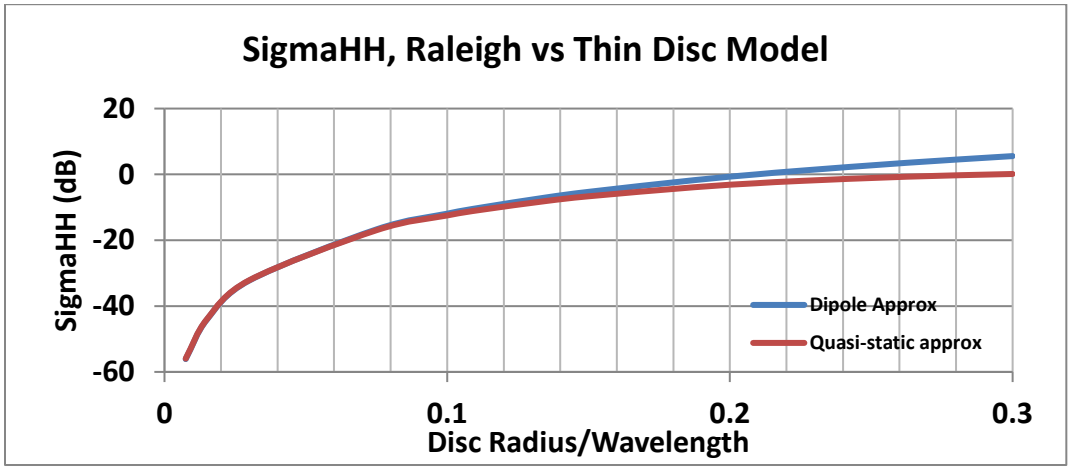

Figure 3.6 Comparison of HPOL backscatter versus electrical size using dipole vs thin disc model

3.4 Scattering from a thin dielectric cylinder

A similar electrostatic approximation, described in Seker (1988) can be used to calculate the scattering amplitude, $f\left(o^{\pm}, i^{\pm}\right)$ for a thin dielectric cylinder. The thin cylinder has a radius of a, length L, and a complex relative permittivity ε_r. At the cylinder boundary (r=a), the electric field induced in the cylinder from a plane wave source, can be expressed as a sum of the tangential and normal field components.

$$\underline{E}_i = \underline{E}_{it} + \underline{E}_{in}\hat{z} \tag{3.33}$$

Applying boundary conditions (ie: tangential electric field and the normal displacement field must be continuous across the boundary), the internal field can be expressed as,

The internal fields can be expressed as:

$$\underline{E}_t = \left(\hat{q}\cdot\hat{z}\right)\hat{z}e^{+ik_0\hat{i}\cdot\underline{x}_t} \tag{3.34}$$

$$\underline{E}_n = \frac{2}{1+\varepsilon_r}\left(\hat{q}-\hat{q}\cdot\hat{z}\right)\hat{z}e^{+ik_0\hat{i}\cdot\underline{x}_t} \tag{3.35}$$

The quasi-static approximation of the internal electric field within the disk can now be expressed as the sum of the tangential and normal components of the internal fields, given by Equation 3.34 and 3.35.

$$\underline{E}_i = \left[\left(\hat{q}\cdot\hat{z}\right)\hat{z} + \frac{2}{1+\varepsilon_r}\left(\hat{q}-\hat{q}\cdot\hat{z}\right)\hat{z}\right]e^{+ik_0\hat{i}\cdot\underline{x}_t} \tag{3.36}$$

Substituting Equation 3.36 into Equation 3.23, From Levine et al 1983, the dyadic scattering amplitude can be calculated by:

$$\underline{\underline{f}}\left(\hat{o},\hat{i}\right)=\frac{k_0^2\left(\varepsilon_r-1\right)}{4\pi}\left(\underline{\underline{I}}-\hat{o}\hat{o}\right)\int dv'\left[\left(\hat{q}\cdot\hat{z}\right)\hat{z}+\frac{2}{1+\varepsilon_r}\left(\hat{q}-\hat{q}\cdot\hat{z}\right)\hat{z}\right]e^{+ik_0\hat{i}\cdot\underline{x}_t}e^{-ik_0\left(\hat{o}\cdot\underline{x}'\right)}$$

Applying the thin cylinder approximation,

$$e^{-ik_0\left(\hat{o}\cdot x'\right)}=e^{-ik_0\hat{o}\cdot x_t'}e^{-ik_0\hat{o}\cdot\hat{z}z'}=e^{-ik_0\hat{o}\cdot x_t'}$$

$$=\frac{k_0^2\left(\varepsilon_r-1\right)}{4\pi}\left(\underline{\underline{I}}-\hat{o}\hat{o}\right)\int dv'\left[\left(\hat{q}\cdot\hat{z}\right)\hat{z}+\frac{2}{1+\varepsilon_r}\left(\hat{q}-\hat{q}\cdot\hat{z}\right)\hat{z}\right]e^{+ik_0\hat{i}\cdot\underline{x}_t}e^{-ik_0\left(\hat{o}\cdot x_t'\right)}$$

$$=\frac{k_0^2\left(\varepsilon_r-1\right)}{4\pi}\left(\underline{\underline{I}}-\hat{o}\hat{o}\right)\left[\left(\hat{q}\cdot\hat{z}\right)\hat{z}+\frac{2}{1+\varepsilon_r}\left(\hat{q}-\hat{q}\cdot\hat{z}\right)\hat{z}\right]\int dv'e^{+ik_0\left(\hat{i}-\hat{o}\right)\cdot x_t'} \tag{3.37}$$

The integral can be evaluated as follows:

$$\int dv'e^{+ik_0\left(\hat{i}-\hat{o}\right)\cdot x_t'}=\pi a^2\int_0^L dz'e^{+ik_0\left(\hat{i}-\hat{o}\right)\cdot z'\hat{z}}$$

Note that,

$$\hat{i}=-\hat{x}\sin\theta_i\cos\phi_i-\hat{y}\sin\theta_i\sin\phi_i-\hat{z}\cos\theta_i$$
$$\hat{o}=\hat{x}\sin\theta_s\cos\phi_s+\hat{y}\sin\theta_s\sin\phi_s+\hat{z}\cos\theta_s$$

Substituting into the integral expression,

$$f\left(\hat{o},\hat{i};\hat{q}\right)=\pi a^2\int_0^L dz'e^{-ik_0\left(\cos\theta_i+\cos\theta_s\right)z'}$$
$$=\pi a^2\left[\frac{1-e^{-ik_0\left(\cos\theta_i+\cos\theta_s\right)L}}{ik_0\left(\cos\theta_i+\cos\theta_s\right)L}\right]$$

Now, substitute into Equation 3.37,

$$= \frac{k_0^2(\varepsilon_r - 1)}{4\pi}\left(\underline{\underline{I}} - \hat{o}\hat{o}\right)\left[(\hat{q}\cdot\hat{z})\hat{z} + \frac{2}{1+\varepsilon_r}(\hat{q} - \hat{q}\cdot\hat{z})\hat{z}\right]\pi a^2\left[\frac{1 - e^{-ik_0(\cos\theta_i + \cos\theta_s)L}}{ik_0(\cos\theta_i + \cos\theta_s)}\right]$$

$$= \frac{k_0^2(\varepsilon_r - 1)}{4\pi}\left(\underline{\underline{I}} - \hat{o}\hat{o}\right)\left[(\hat{q}\cdot\hat{z})\hat{z} + \frac{2}{1+\varepsilon_r}\hat{q} - \frac{2}{1+\varepsilon_r}(\hat{q}\cdot\hat{z})\hat{z}\right]\pi a^2\left[\frac{1 - e^{-ik_0(\cos\theta_i + \cos\theta_s)L}}{ik_0(\cos\theta_i + \cos\theta_s)}\right]$$

$$= \frac{k_0^2(\varepsilon_r - 1)}{4\pi}\left(\underline{\underline{I}} - \hat{o}\hat{o}\right)\left[(\hat{q}\cdot\hat{z})\hat{z}\left(1 - \frac{2}{1+\varepsilon_r}\right) + \frac{2}{1+\varepsilon_r}\hat{q}\right]\pi a^2\left[\frac{1 - e^{-ik_0(\cos\theta_i + \cos\theta_s)L}}{ik_0(\cos\theta_i + \cos\theta_s)}\right]$$

The final expression for the dyadic scattering amplitude for a thin dielectric cylinder is:

$$\underline{\underline{f}}(\hat{o},\hat{i}) = \frac{k_0^2(\varepsilon_r - 1)\pi a^2}{4\pi}\left(\underline{\underline{I}} - \hat{o}\hat{o}\right)\left[(\hat{q}\cdot\hat{z})\hat{z}\left(\frac{\varepsilon_r - 1}{\varepsilon_r + 1}\right) + \frac{2}{1+\varepsilon_r}\hat{q}\right]\left[\frac{1 - e^{-ik_0(\cos\theta_i + \cos\theta_s)L}}{ik_0(\cos\theta_i + \cos\theta_s)}\right] \quad (3.38)$$

3.5 Numerical electromagnetic solutions

In this section, the use of numerical electromagnetic solvers will be discussed. For non-canonical shapes or inhomogeneous dielectric constant profiles, the use of a numerical electromagnetic field solver is required. As an example, a cylinder having a periodic dielectric constant profile will be investigated. This model will be useful in modeling a corn stalk [Lang et al. 2014]. The approximations described in the previous sections are valuable and provide insight into the scattering behavior of canonical shapes, however, cannot be used to solve this problem. Using a commercial electromagnetic solver (FEKO), which is based on the Method of Moments [Harrington, 1968], the scattering amplitude can be found.

The periodic dielectric cylinder is pictured in Figure 3.7. The cylinder has a diameter of 'd', and two sections that repeat. The first section has a length of h_1 and dielectric constant of ε_{r1} and the second section has a length of h_2 and a dielectric constant of ε_{r2}. These sections of length h1+h2 are repeated p-times.

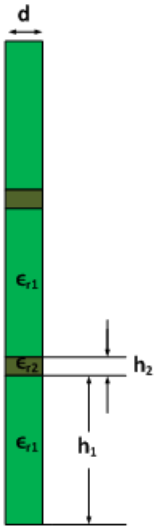

h1= 1 cm; h2= 7 cm

$\varepsilon_{r1} = 52.4 + i13.8$

$\varepsilon_{r2} = 13.4 + i13.0$

d= 1.08 cm

p= 8

Figure 3.7. Periodic dielectric constant cylinder

This cylinder with parameters shown in Fig. 3.7 is excited with a 1.25 GHz plane wave at 40° incidence. The cylinder is modeled in FEKO and the back and bistatic scattering amplitudes are computed. Recall from Ch. 2, that the back and bistatic scattering amplitudes are required in order to compute the scattering coefficients. The result is plotted in Figure 3.8 for both HH-pol and VV-pol.

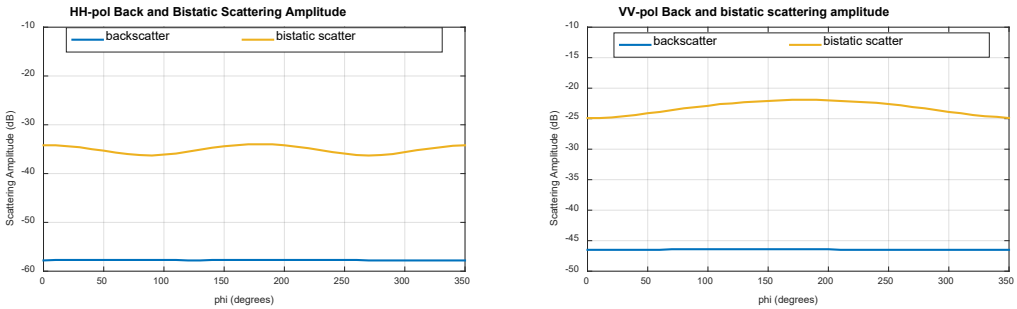

Figure 3.8 Simulated back and bistatic scattering coefficients.

It is worthwhile to consider whether there exists a uniform dielectric constant that can replace the complex periodic dielectric constant. From [Ishimaru, 1997], any periodic dielectric structure can support an infinite set of modes having varying wave numbers,

known as space harmonics. At low frequencies, the periodic dielectric structure allow only the lowest mode to propagate, so that the layer acts approximately as if it had a uniform dielectric constant equal to an average value for the periodic layer. Using a basic volumetric dielectric mixing model,

$$\varepsilon_{\text{eff}} = \frac{1}{p}\sum_{l}^{p}\frac{h_{1-p}\varepsilon_{1-p} + h_{2-p}\varepsilon_{2-p}}{h_{1-p} + h_{2-p}} \tag{3.39}$$

where h_{1-p} and h_{2-p} are the lengths of the p-th pair; ε_{1-p} and ε_{2-p} are the dielectric constant of the p-th pair, and p is the number of pairs in the cylinder. Now replacing the cylinder with a homogeneous dielectric constant using Eq. 3.39, the back and bistatic scattering amplitudes are computed and plotted in Figure 3.9, along with the results from the periodic cylinder model. Clearly, at 1.25 GHz and 40° incident angle, Eq. 3.39 is a very good approximation.

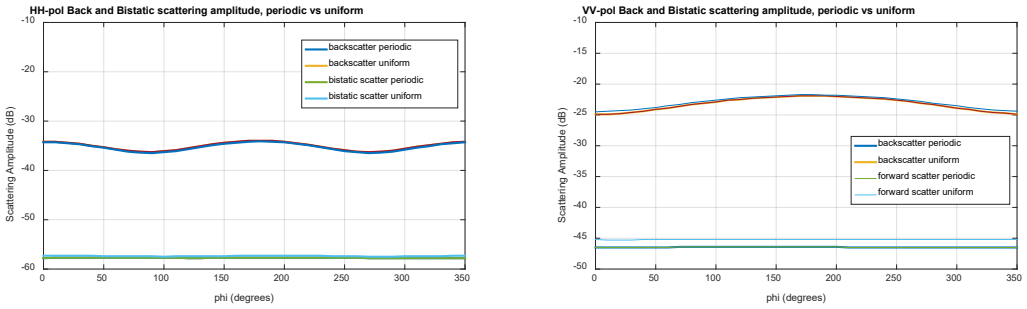

Figure 3.9 Comparison of back and bistatic scattering amplitudes for a periodic and approximate uniform stalk models

Another scattering geometry that can be simplified using dielectric mixing is a three-layer cylinder. This structure consists of three concentric layers with different dielectric constants, as picture in Fig. 3.10.

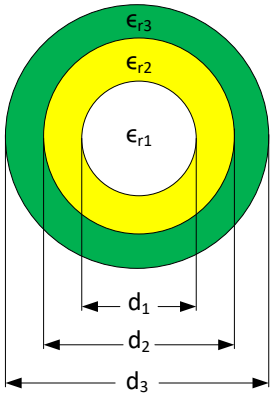

Fig. 3.10 Cross-sectional view of a three layer cylinder

The effective dielectric constant can be expressed as,

$$\varepsilon_{eff-cob} = \frac{d_1^2}{d_3^2}\varepsilon_{r1} + \frac{d_2^2 - d_1^2}{d_3^2}\varepsilon_{r2} + \frac{d_3^2 - d_2^2}{d_3^2}\varepsilon_{r3} \qquad 3.40$$

Chapter 4 Enhancement Effects

In Chapter 2 the derivation for the bistatic scattering coefficients from a layer of random medium over a dielectric half-space was presented. In this chapter, these results will be used to show that at certain angles, the waves within the layer can form conjugate paths, resulting in an increase in scattered power. Even though enhanced backscatter is a well-known phenomenon in acoustics, microwave and optical regimes, the majority of the published literature relates to the like-polarized case. In this chapter, the behavior of enhanced backscatter for both like and cross-polarized case will be studied. In addition, details of parameters that can mask coherent effects will also be discussed.

4.1 Qualitative overview of enhanced backscatter

In this section, the concept of enhanced backscatter will be presented. In optics the effect is often called coherent backscatter and is a multiple scattering event, where on average, the scattering from a discrete set of particles in a medium will tend to constructively add in the direction towards backscatter [Ishimaru, 1978]. As shown in Figure 4.1, conjugate wave pairs (or a pair of waves having the same trajectory, traveling in opposite directions) are the source of enhanced backscatter, since they add coherently in the backscatter direction, due to having the same phase. Away from backscatter, as seen in Figure 4.1b, the path lengths for the wave pairs are no longer identical (ie: the waves have different phases), resulting in a reduction in enhanced backscatter.

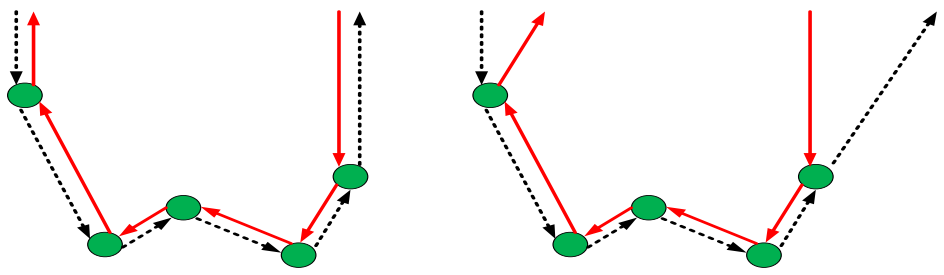

Figure 4.1 Enhanced backscatter due to multiple scattering geometry

Enhanced backscatter is not exclusive to multiple scattering in discrete random media, but can exist under single scattering in the presence of a reflecting plane, as shown in Figure 4.2. The reflecting plane mimics multiple scatter, creating the conjugate wave pairs. In figure 4.2a, each wave traverses the same path, but in opposite directions, resulting in a pair of coherent waves. Away from backscatter, as shown in Figure 4.2b, the path lengths are no longer equal; therefore the two waves are no longer fully coherent, resulting in a reduction in enhancement at this angle. The next section will present a more theoretical formulation to describe the enhanced scattering that occurs under a single scattering approximation in the presence of a reflecting plane.

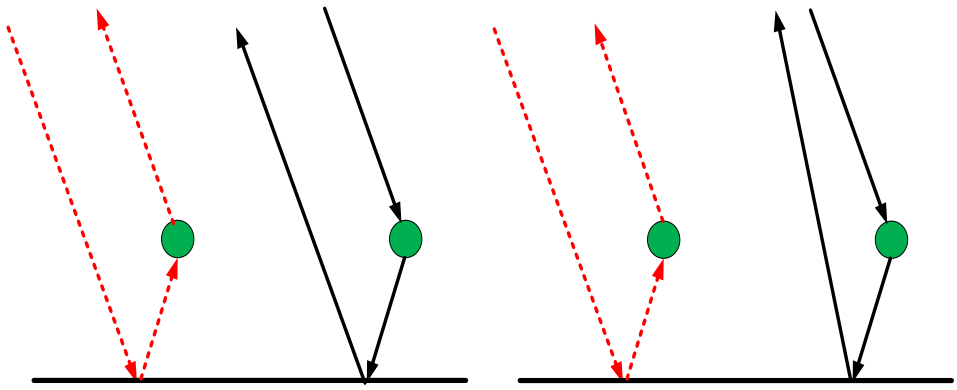

Figure 4.2 Enhanced backscatter due to single scattering in the presence of a reflecting surface geometry

4.2 Enhanced Backscatter

The presence of a reflecting ground plane, which generates a reflected wave, is the source of enhanced backscatter. From Chapter 2, recall that there are three expressions for the bistatic scattering coefficients, Equations 2.45, 2.46, and 2.49, for waves that undergo

a single reflection, known as direct-reflected scatter. This type of scattering is due to scatter paths that are either reflected from a ground plane and then scattered, or scattered and then reflected from a ground plane. These equations are reproduced below,

$$\sigma^0_{dri1_{pqp'q'}} = 4\pi\rho\left\langle f_{pq}\left(\hat{o}^+,\hat{i}^+\right) f^*_{p'q'}\left(\hat{o}^+,\hat{i}^+\right)\right\rangle \Gamma_q \Gamma^*_{q'}\left[\frac{1-e^{2Imag\left(\kappa_{s_p}-\kappa_{i_q}\right)d}}{2Imag\left(\kappa_{s_p}-\kappa_{i_q}\right)}\right] \tag{4.1}$$

$$\sigma^0_{dri2_{pqp'q'}} = 4\pi\rho\left\langle f_{pq}\left(\hat{o}^-,\hat{i}^-\right) f^*_{p'q'}\left(\hat{o}^-,\hat{i}^-\right)\right\rangle \Gamma_p \Gamma^*_{p'}\left[\frac{1-e^{2Imag\left(-\kappa_{s_p}+\kappa_{i_q}\right)d}}{2Imag\left(-\kappa_{s_p}+\kappa_{i_q}\right)}\right] \tag{4.2}$$

$$\sigma^0_{drc_{pqp'q'}} = 8\pi\rho\left\langle f_{pq}\left(\hat{o}^-,\hat{i}^-\right) f^*_{p'q'}\left(\hat{o}^+,\hat{i}^+\right)\right\rangle \Gamma_p \Gamma^*_{q'}\,Real\left[\frac{1-e^{-i2\left(k_{z_s}-k_{z_i}\right)d} e^{-i2Real\left(\kappa_{s_p}-\kappa_{i_q}\right)d}}{-i2\left[\left(k_{z_s}-k_{z_i}\right)+Real\left(\kappa_{s_p}-\kappa_{i_q}\right)\right]}\right] \tag{4.3}$$

Recall that Equations 4.1 and 4.2 are the incoherent direct-reflected terms and Equation 4.3 is the coherent direct-reflected term. The incoherent terms contribute over all angles, whereas the coherent term does not. On closer inspection of Equation 4.3, the coherent term contribute maximally when $k_{z_i} = k_{z_s}$, which occurs at two angles, backscatter and specular and is known as either enhanced backscatter or enhanced specular scatter. First, the enhanced backscatter for both like and cross-polarization cases will be discussed, followed by enhanced specular backscatter.

4.2.1 Backscatter, Like-Polarization

In order to see the effect of the direct-reflected coherent terms at backscatter, apply the following to Equations 4.1 through 4.3:

- Use reciprocity (ie: $f_{pp}\left(\hat{o}^+,\hat{i}^+\right) = f_{pp}\left(\hat{o}^-,\hat{i}^-\right)$)

- $\hat{o} = -\hat{i}$
- p=q
- $k_{z_i} = k_{z_s}\ (\theta_i = \pm\theta_s)$

Also note that the binomial expansion of the exponential term results in the following simplification:

$$\frac{1-e^{2\,\mathrm{Imag}\left(\kappa_{s_p}-\kappa_{i_q}\right)d}}{2\,\mathrm{Imag}\left(\kappa_{s_p}-\kappa_{i_q}\right)} \rightarrow \frac{1-\left(1+2\,\mathrm{Imag}\left(\kappa_{s_p}-\kappa_{i_q}\right)d\right)}{2\,\mathrm{Imag}\left(\kappa_{s_p}-\kappa_{i_q}\right)} = d$$

Applying the above, the backscattering coefficients for both the incoherent and coherent direct-reflected terms reduce to:

$$\sigma^0_{dri1_{pp'}} = 4\pi\rho\left\langle f_{pp}\left(-\hat{i}^-,\hat{i}^+\right)f^*_{p'p'}\left(-\hat{i}^-,\hat{i}^+\right)\right\rangle\Gamma_p\Gamma^*_{p'}d \tag{4.5}$$

$$\sigma^0_{dri2_{ppp'p'}} = 4\pi\rho\left\langle f_{pp}\left(-\hat{i}^-,\hat{i}^-\right)f^*_{p'p'}\left(-\hat{i}^-,\hat{i}^-\right)\right\rangle\Gamma_p\Gamma^*_{p'}d \tag{4.6}$$

$$\sigma^0_{drc1_{ppp'p'}} = 8\pi\rho\left\langle f_{pp}\left(-\hat{i}^-,\hat{i}^+\right)f^*_{p'p'}\left(-\hat{i}^-,\hat{i}^+\right)\right\rangle\Gamma_p\Gamma^*_{p'}d \tag{4.7}$$

At backscatter, the coherent direct-reflected term (Equation 4.7) equals the sum of the incoherent direct-reflected terms (Equation 4.5 and Equation 4.6), due to reciprocity in the

scattering amplitude function. In other words, the coherent term doubles the power at backscatter, or causes a 3 dB increase in power at backscatter, [Lang and Khadr, 1992]

In addition to an enhancement peak, there is also an associated enhancement width, which characterizes how quickly the peak decreases away from the backscattering angle. This enhancement width depends on the frequency, angle of incidence and layer properties. In order to characterize the enhancement width, the bistatic equations are needed. In particular, the enhancement width can be seen to be proportional to the $\frac{1-e^{-i2\left(k_{z_s}-k_{z_i}\right)d}}{i2\left(k_{z_s}-k_{z_i}\right)}$ term. To find the first null in this function, manipulate as follows,

$$\frac{1-e^{-i2\left(k_{z_s}-k_{z_i}\right)d}}{i2\left(k_{z_s}-k_{z_i}\right)}=e^{-i\left(k_{z_s}-k_{z_i}\right)d}\frac{\left(e^{+i\left(k_{z_s}-k_{z_i}\right)d}-e^{-i\left(k_{z_s}-k_{z_i}\right)d}\right)}{i2\left(k_{z_s}-k_{z_i}\right)}$$

$$=e^{-i\left(k_{z_s}-k_{z_i}\right)d}\frac{\sin\left(\left(k_{z_s}-k_{z_i}\right)d\right)}{\left(k_{z_s}-k_{z_i}\right)}$$

Multiply top and bottom by d, to get into sinc-form.

$$=de^{-i\left(k_{z_s}-k_{z_i}\right)d}\frac{\sin\left(\left(k_{z_s}-k_{z_i}\right)d\right)}{\left(k_{z_s}-k_{z_i}\right)d}$$

$$=de^{-i\left(k_{z_s}-k_{z_i}\right)d}\sin c\left(\left(k_{z_s}-k_{z_i}\right)d\right)$$

$$=d\left[\cos\left(\left(k_{z_s}-k_{z_i}\right)d\right)-i\sin\left(\left(k_{z_s}-k_{z_i}\right)d\right)\right]\sin c\left(\left(k_{z_s}-k_{z_i}\right)d\right)$$

The enhancement width is proportional to, $d\left[\cos\left(\left(k_{z_s}-k_{z_i}\right)d\right)\right]\sin c\left(\left(k_{z_s}-k_{z_i}\right)d\right)$.

The first null in this function can be found by setting,

$$\left(k_{z_s} - k_{z_i}\right) d = \frac{\pi}{2}$$

Note that $k_{z_i} = k_o \cos\theta_i$ and $k_{z_s} = k_o \cos\theta_s$

$$k_o \left(\cos\theta_s - \cos\theta_i\right) d = \frac{\pi}{2}$$

Let $\theta_s = \theta_i + \Delta\theta$ where $\Delta\theta$ is the angle from the incident angle to the first null.

$$k_o \left(\cos\left(\theta_i + \Delta\theta\right) - \cos\theta_i\right) d = \frac{\pi}{2}$$

Solving for $\Delta\theta$ and multiplying by two results in an expression for the enhancement width.

$$\Delta\theta = 2\left[\cos^{-1}\left[\frac{\pi}{2k_o d} + \cos\theta_i\right] - \theta_i\right] \tag{4.8}$$

From Equation 4.8, enhancement width is seen to be dependent on the incident angle and the layer thickness. As a check on the validity of Equation 4.8, a comparison will be made with previously published results from Figure 6 in [Lang and Khadr, 1992]. The comparison is tabulated in Table 4.1, which shows good agreement between the two, with a small error due to reading from a graph.

Frequency (GHz)	Layer Thickness (m)	Enhancement Width (degrees) from [Lang and Khadr, 1992]	Enhancement Width (degrees) from Equation 4.8
0.5	1	~ 32	32.71
1	1	~ 14	14.5
2	1	~ 7	6.94

Table 4.1 Comparison of predicted enhancement width using Equation 4.9 and Figure 6 from Lang and Khadr

4.2.2 Backscatter, Cross-Polarization

In order to see the effect of the coherent terms for the cross-polarized case, apply the following to Equations 4.1 through 4.4,

- Use reciprocity (ie: $f_{pp}\left(\hat{o}^{+},\hat{i}^{+}\right)=f_{pp}\left(\hat{o}^{-},\hat{i}^{-}\right)$)
- $\hat{o}=-\hat{i}$
- p≠q
- $k_{z_i}=k_{z_s}\ (\theta_i=\pm\theta_s)$

These are seen in Equations 4.9 through 4.11, where Equations 4.9 and 4.10 are the incoherent terms and Equation 4.11 is the coherent term. Unlike the like-polarized case, these equations cannot be simplified further, so the effect of the coherent term is not as obvious.

$$\sigma^0_{dri1_{pqp'q'}} = 4\pi\rho\left\langle f_{pq}\left(-\hat{i}^-,\hat{i}^+\right)f^*_{p'q'}\left(\hat{i}^-,\hat{i}^+\right)\right\rangle \Gamma_q\Gamma^*_{q'}\left[\frac{1-e^{2Imag\left(\kappa_{s_p}-\kappa_{i_q}\right)d}}{2Imag\left(\kappa_{s_p}-\kappa_{i_q}\right)}\right] \tag{4.9}$$

$$\sigma^0_{dri2_{pqp'q'}} = 4\pi\rho\left\langle f_{pq}\left(-\hat{i}^-,\hat{i}^-\right)f^*_{p'q'}\left(-\hat{i}^-,\hat{i}^-\right)\right\rangle \Gamma_p\Gamma^*_{p'}\left[\frac{1-e^{2Imag\left(-\kappa_{s_p}+\kappa_{i_q}\right)d}}{2Imag\left(-\kappa_{s_p}+\kappa_{i_q}\right)}\right] \tag{4.10}$$

$$\sigma^0_{drc_{pqp'q'}} = 8\pi\rho\left\langle f_{pq}\left(-\hat{i}^-,\hat{i}^+\right)f^*_{p'q'}\left(-\hat{i}^-,\hat{i}^-\right)\right\rangle \Gamma_q\Gamma^*_{p'}\left[\frac{1-e^{+i2Real\left(\kappa_{s_p}-\kappa_{i_q}\right)d}}{i2\left[Real\left(\kappa_{s_p}-\kappa_{i_q}\right)\right]}\right] \tag{4.11}$$

Examining the above equations, a major difference in particular between the coherent and the incoherent terms are the Fresnel reflection coefficients being dissimilar for the coherent terms. If p=h (for horizontal polarization) and q=v (for vertical polarization), the Fresnel reflection coefficients can be computed from Equations 4.12 and 4.13.

$$\Gamma_h = \frac{\cos\theta_i - \sqrt{\varepsilon_g - \sin^2\theta_i}}{\cos\theta_i + \sqrt{\varepsilon_g - \sin^2\theta_i}} \tag{4.12}$$

$$\Gamma_v = \frac{\varepsilon_g\cos\theta_i - \sqrt{\varepsilon_g - \sin^2\theta_i}}{\varepsilon_g\cos\theta_i + \sqrt{\varepsilon_g - \sin^2\theta_i}} \tag{4.13}$$

where θ_i is the incident angle and ε_g is the dielectric constant of the ground. An example plot of Equations 4.12 and 4.13 would be helpful in highlighting key characteristics of Γ_h and Γ_v. For an ε_g equal to 23, the magnitude of Γ_h and Γ_v is plotted versus a range of incident angles, as seen in Figure 4.3.

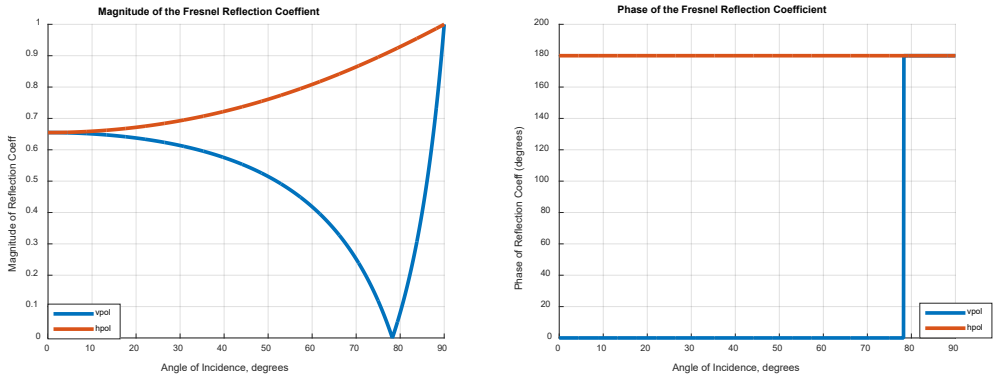

Figure 4.3 HPOL and VPOL Fresnel reflection coefficient, magnitude and phase

A couple of important observations can be made from this plot. First, the magnitude of Γ_h is always less than or equal to the magnitude of Γ_v. Second, for Γ_v, there exists an incident angle where there is zero reflection, known as the Brewster angle, θ_B [Balanis, 2012]. In this example, θ_B is about 79.5°. Note that there is no equivalent θ_B for the horizontally polarized reflection coefficient. Third, when the incident angle is less than the Brewster angle $(\theta_i < \theta_B)$, there is a 180° phase difference between the Γ_h and Γ_v. However, an abrupt change occurs when the incident angle is greater than the Brewster angle $(\theta_i > \theta_B)$, where the phase of Γ_h and Γ_v are equal.

Using these observations about the Fresnel reflection coefficients in Equations 4.12 and 4.13 reveals that when $\theta_i < \theta_B$, there is an out-of-phase condition between Γ_h and Γ_v, resulting in the coherent terms having a negative sign, which causes the scattering coefficient to decrease at the backscatter angle. When $\theta_i > \theta_B$, because the phases of Γ_h and Γ_v are equal, there is an increase at the backscatter angle. Finally, when $\theta_i = \theta_B$, the case where there is zero reflection, there is zero enhancement.

Note that the above discussion assumed a lossless dielectric half-space. If loss is included, there are some changes that occur. To see this, plots of the magnitude and phase of Γ_h and Γ_v with ε_g equal to 23+i14.1 are generated in Figure 4.4. The main difference when looking at the magnitude plot, is seen at the Brewster angle, where instead of zero reflection, there is an angle where there is minimal reflection. The main difference when looking at the phase plot, is the instantaneous 180° phase change at the Brewster angle is now more gradual.

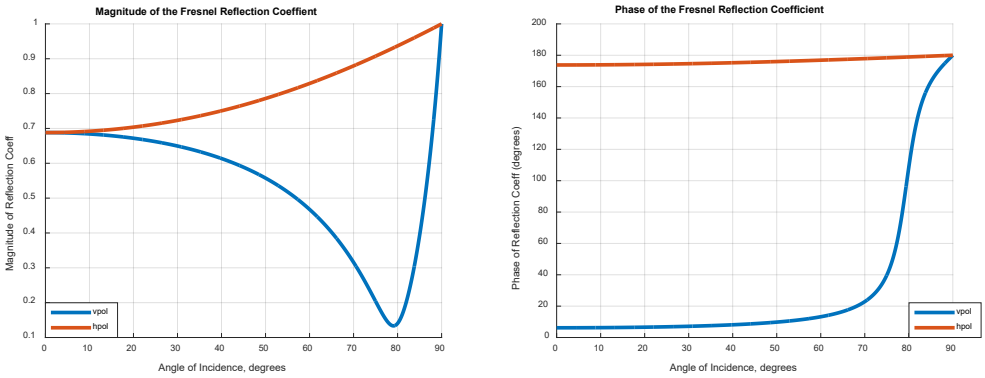

Figure 4.4 HPOL and VPOL Fresnel reflection coefficient, magnitude and phase (lossy)

The behavior of the Fresnel reflection coefficients is not the only term in Eq. 4.11causing a polarity change between positive and negative. The bracketed exponential term, in Eq 4.11, $\left[\frac{1-e^{-i2\,\mathrm{Real}\left(\kappa_{s_p}-\kappa_{i_q}\right)d}}{-i2\left[\mathrm{Real}\left(\kappa_{s_p}-\kappa_{i_q}\right)\right]}\right]$, which will be denoted by Ψ, also varies between positive and negative values as a function of $\left|\kappa_{s_p}-\kappa_{i_q}\right|$. A plot of Ψ versus $\left|\kappa_{s_p}-\kappa_{i_q}\right|$ is shown in Fig. 4.5, which shows a damped periodic oscillatory behavior, which takes on positive and negative values.

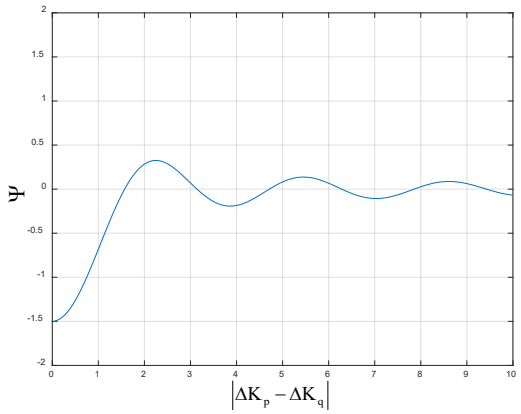

Figure 4.5 Exponential coherent scattering term Ψ vs differential propagation constant $\left|\kappa_{s_p} - \kappa_{i_q}\right|$

4.3 Enhanced Specular Scatter

To this point, enhancement effects have been exclusive to backscatter. In this section, enhancement effects will be shown to also show up at another angle, namely at the specular angle, which is not often published in the literature. Note that the coherent direct-reflected scattering coefficient expressions contribute maximally when $k_{z_i} = k_{z_s}$. This equality holds for two angles, when $\theta_i = \theta_s$ (backscatter) and when $\theta_i = -\theta_s$ (specular scatter).

At this point it would be instructive to show some plots for the bistatic scattering coefficients. Simulating a layer of thin dielectric discs, with parameters given in Table 4.2, the bistatic scattering coefficients are plotted versus the scattering angle, for an incident angle of 45°. For convenience, the scattering angles are swept to encompass both backscatter and specular scatter. It is important to note that the specular reflection of the mean field is not accounted for in these plots, since the interest is in the behavior of the enhancement.

First, in Figure 4.6, all the components of σ^0_{HH} (direct, direct-reflected incoherent, direct-reflected coherent, reflected) are plotted versus the scattering angle, in addition to the total incoherent and coherent σ^0_{HH}. First, the reflected component is much lower than the rest of the scattering terms. This is usually true for most cases since the backscatter from the reflected term is proportional to the fourth power of the Fresnel reflection coefficient, as seen in Equation 2.47. Unless the ground is saturated with moisture, like rice or mangrove fields, this term can generally be ignored. Second, a 3 dB enhancement is seen between the coherent direct-reflected and the incoherent direct-reflected terms at both backscatter angle of -45° and at the specular scattering angle of +45° and this enhancement decreases away from the back and specular scattering angles. Finally, note that the enhancement for the total σ^0_{HH} is about 1.5 dB. This is important to note that if the other scattering terms are of the same order (or dominant), the enhancement effect due to the coherent terms are reduced.

Parameter	Value
Frequency	1500 MHz
Incident Angle	45°
Layer Depth	1 m
Disc Distribution	$\cos\theta$ [0, π/2] 0 elsewhere
Disc Density	4000 per/m3
Disc Dielectric Constant	17.0+i5.55
Ground Dielectric Constant	23+i14.1

Disc Radius	3.0 cm
Disc Thickness	0.2 mm

Table 4.2 Parameters for a layer of circular discs over a dielectric half-space taken from [Nagi, 1994, (Table 5.1)]

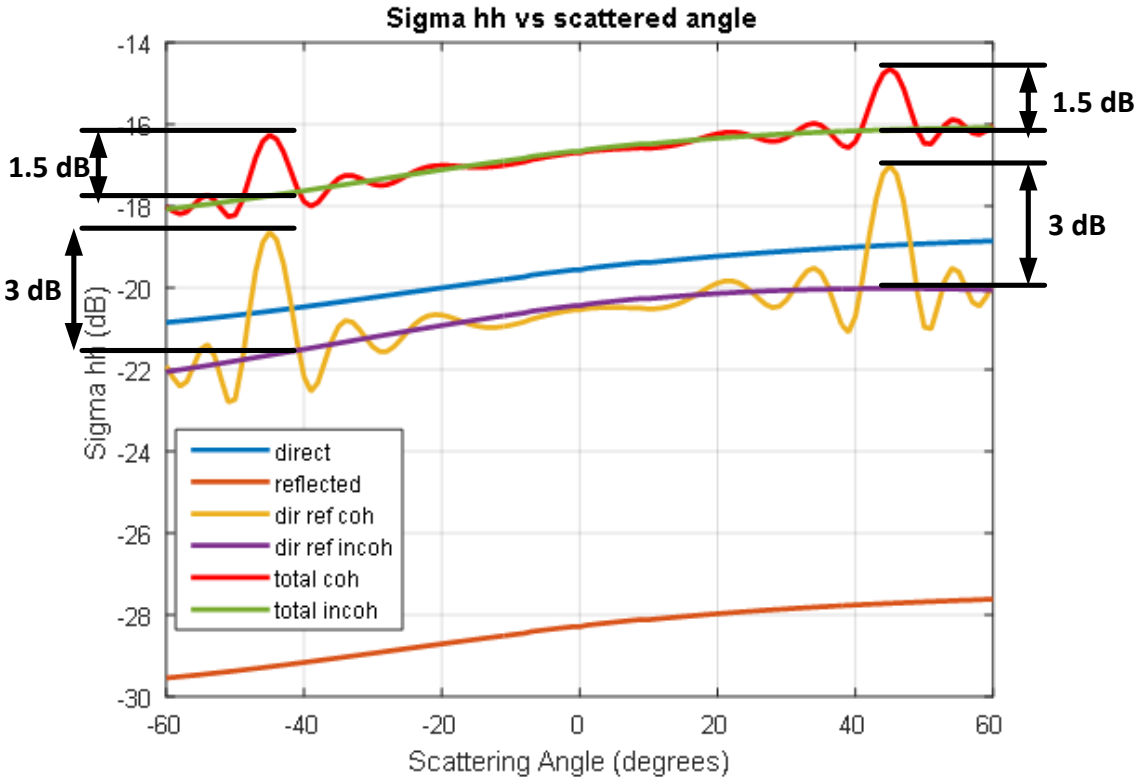

Figure 4.6 SigmaHH bistatic scatter from a circular layer of discs over a dielectric half-space

Next, as seen in Figure 4.7, the components of σ^0_{HV} is plotted versus scattering angle. Here again, enhancements at both back and specular is seen, however, they are negative. Again, the reflected scatter is much less than the other scattering components. There is roughly -2 dB of enhancement at both back and specular scattering angles for the incoherent and coherent direct-reflected terms. When all terms are combined, the enhancement is less pronounced.

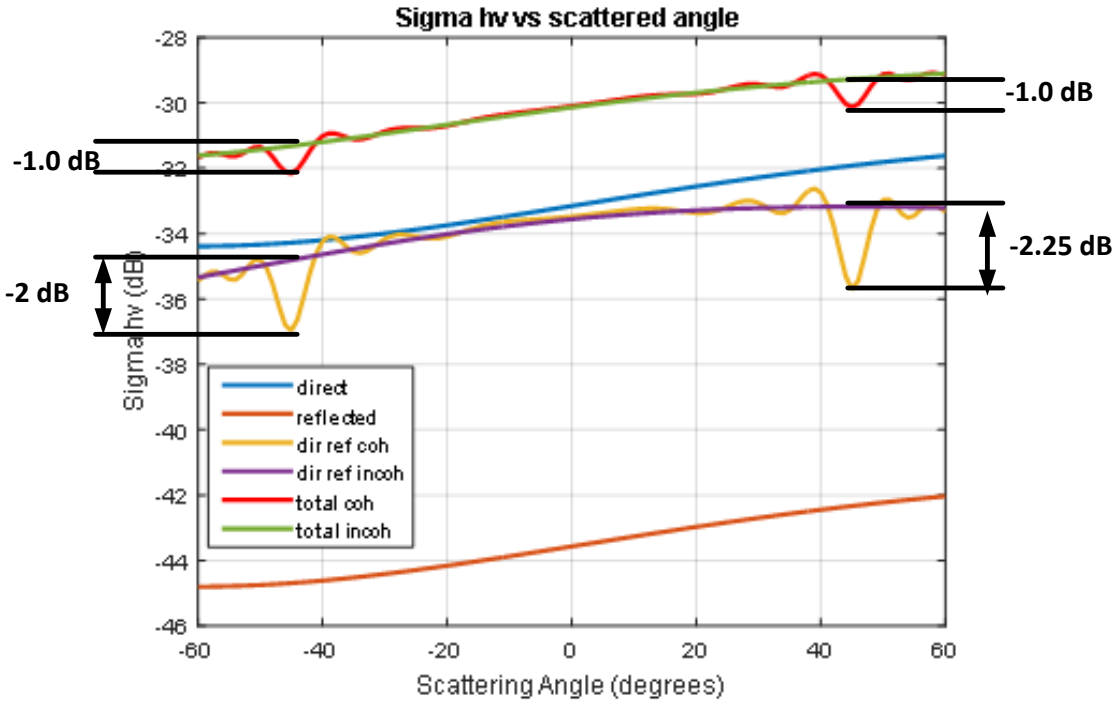

Figure 4.7 SigmaHV bistatic scatter from a circular layer of discs over a dielectric half-space

4.4 Enhancement reduction

In the previous section, the enhancement was seen to be reduced when other scattering terms are introduced. In this section, two notable conditions that reduce the enhancement effects will be explored in more detail, such as surface roughness and antenna beamwidth.

4.4.1 Surface Scatter

The derivations for the scattering coefficients in Chapter 2 modeled the dielectric interface as a flat, smooth surface. In this section, surface roughness at the interface of the half-space dielectric will be introduced. The roughness will introduce an additional

scattering term and a reduction in the reflection coefficient, both of which can reduce the enhancement effect.

As shown in Figure 4.8, the roughness profile consists of a fluctuating component over an average (flat) surface. This roughness is characterized by the surface height standard deviation, σ, correlation length, L, and the surface roughness spectrum (or correlation function).

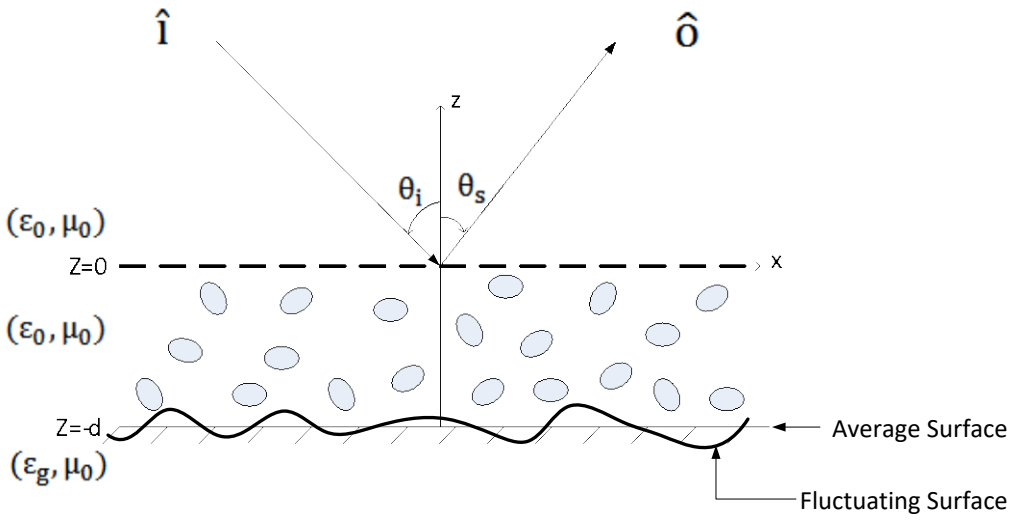

Figure 4.8 Random medium over a dielectric half-space with a rough surface interface

A flat surface has only a specular reflection. As roughness is introduced, the specular component reduces and diffuse components increase. The reduction in the specular reflection coefficient from a rough surface characterized by a Gaussian height distribution with a standard deviation, σ, about the average surface is given as,

$$\Gamma_r = \left|\Gamma_q\right|^2 e^{-(2k_0\sigma\cos\theta_i)^2} \tag{4.14}$$

The exponential term is called the roughness factor and Γ_q is the Fresnel reflection coefficient from a smooth surface, given by Equation 4.14 and 4.15. A few observations can be made about the addition of the roughness to a surface:

- the reflection coefficient will always decrease as the surface roughness increases
- surface roughness effects are more pronounced for higher frequency waves
- surface roughness effects are more pronounced at normal incidence than at grazing

For purposes of this dissertation, only small scale surface roughness will be considered, which is characterized by the product of the wavenumber, k_0 and the standard deviation of the surface height, σ being less than 0.3. Under this constraint, the surface backscatter can be calculated by the Small Perturbation Method (SPM) [Rice, 1951], and given by,

$$\sigma_{hh}^{o} = 4k^4\sigma^2L^2\cos^4\theta_i\left|\frac{\cos\theta_i-\sqrt{\varepsilon_g-\sin^2\theta_i}}{\cos\theta_i+\sqrt{\varepsilon_g-\sin^2\theta_i}}\right|^2\left[1+2\left(k_0L\sin\theta_i\right)^2\right]^{-\frac{3}{2}}\left[e^{-2\mathrm{Im}\left(K_{z_q}\right)d}\right] \quad (4.15)$$

$$\sigma_{vv}^{o} = 4k^4\sigma^2L^2\cos^4\theta_i\left|\left(\varepsilon_g-1\right)\frac{\sin^2\theta_i-\varepsilon_g\left(1+\sin^2\theta_i\right)}{\varepsilon_g\cos\theta_i+\sqrt{\varepsilon_g-\sin^2\theta_i}}\right|^2\left[1+2\left(k_0L\sin\theta_i\right)^2\right]^{-\frac{3}{2}}\left[e^{-2\mathrm{Im}\left(K_{z_q}\right)d}\right] \quad (4.16)$$

Note that these equations are based on a first-order solution, assuming $\sigma_{hv}^{o}=0$. Also, the exponential term accounts for the two-way attenuation through the layer.

As discussed in Section 4.2.1, the direct-reflected coherent scatter in conjunction with a reflecting surface is the source of enhancement. Since surface roughness reduces the

specular reflection coefficient, the contribution from the direct-reflected terms will be reduced, which leads to a reduction in enhancement [Sharma and Lang, 2017].

4.4.2 Antenna beamwidth

As shown in the previous section, the enhancement factor is characterized by its magnitude and its angular width. The relationship of the angular width to the antenna beamwidth is important in detecting the enhanced backscatter. This section will explore this relationship in more detail.

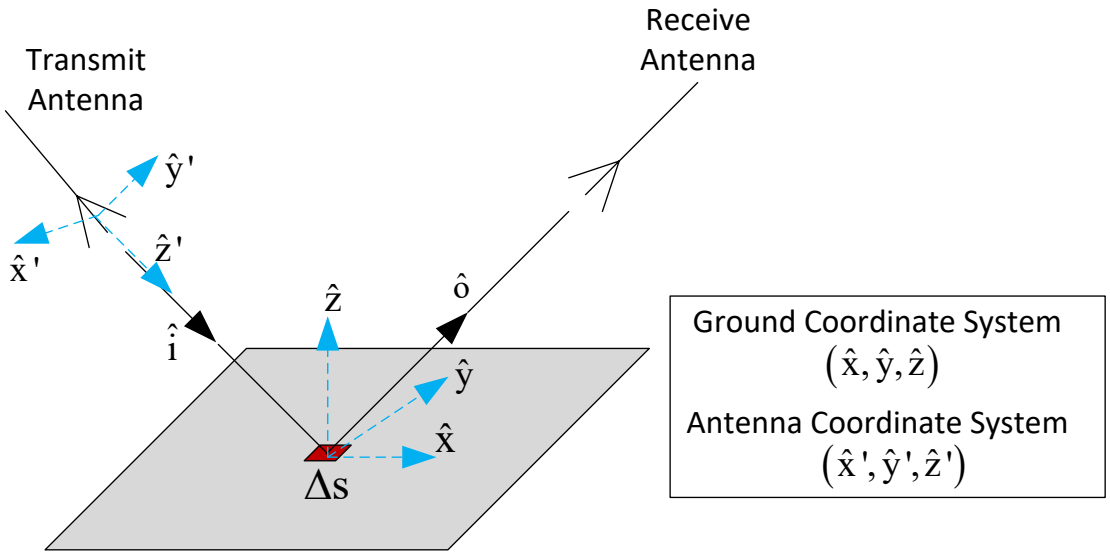

Figure 4.9 Radar antenna geometry

First, a derivation of the received power P_t given a transmit power, P_t, and antenna gain, G_t, the incident power density transmitted in the $\hat{i}$ direction is,

$$S_{i_q}\left(\hat{i}\right) = P_t G_{t_q}\left(\hat{i}\right)\left(\frac{1}{4\pi R^2\left(\hat{i}\right)}\right) \tag{4.17}$$

where $R\left(\hat{i}\right)$ is the distance from the antenna to the surface element Δs, along the $\hat{i}$ direction, and $q \in \{h, v\}$

The scattered power in the $\hat{o}$ direction from an excitation from the $\hat{i}$ direction is described by the scattering coefficient, $\sigma^{o}_{pq}\left(\hat{o}, \hat{i}\right)$. The scattered power density in the $\hat{o}$ direction is,

$$\Delta S_{o_{pq}}\left(\hat{o}\right) = \sigma^{o}_{pq}\left(\hat{o}, \hat{i}\right) S_{i_q}\left(\hat{i}\right)\left(\frac{1}{4\pi R_r^2\left(\hat{o}\right)}\right)\Delta s \tag{4.18}$$

Now, the received power, ΔPr from the surface element Δs can be expressed as,

$$\Delta Pr = A_{r_p}\left(\hat{o}\right)\Delta S_{o_{pq}}\left(\hat{o}\right) = \frac{\lambda^2}{4\pi} G_{r_p}\left(\hat{o}\right)\Delta S_{o_{pq}}\left(\hat{o}\right) \tag{4.19}$$

Summing over all illuminated Δs elements and taking the limit as Δs approaches zero, results in the bistatic radar equation,

$$\frac{P_{r_{pq}}}{P_t} = \frac{\lambda^2}{(4\pi)^3}\int_{Area} d\underline{s}_t \frac{G_{t_q}\left(\hat{i}\right) G_{r_p}\left(\hat{o}\right)\sigma^{o}_{pq}\left(\hat{o}, \hat{i}\right)}{R_t^2\left(\hat{i}\right) R_r^2\left(\hat{o}\right)} \tag{4.20}$$

Setting $\hat{o} = -\hat{i}$, $G_{t_q}\left(\hat{i}\right) = G_{r_p}\left(\hat{o}\right)$ and , will $R_t^2\left(\hat{i}\right) = R_r^2\left(\hat{o}\right)$, will result in the monostatic radar equation,

$$\frac{P_{r_{pq}}}{P_t} = \frac{\lambda^2}{(4\pi)^3}\int_{Area} d\underline{s}_t \frac{G_{t_q}^2\left(\hat{i}\right)\sigma^{o}_{pq}\left(-\hat{i}, \hat{i}\right)}{R_t^4\left(\hat{i}\right)} \tag{4.21}$$

The common assumption when using Equation 4.24 is to assume that the gain, scattering coefficient and the range are all constant. However, the antenna patterns are not always narrow pencil beams and as Figure 4.5 and Figure 4.6 show, the scattering coefficients may not be constant over the beamwidth of the antenna due to the enhancement effect.

Assuming an antenna oriented in the +z-axis, having a Gaussian antenna pattern of the form,

$$G_{t_q}^2\left(\hat{i}\right) = G_{t_q}^2\left(\theta,\phi\right) = G_o^2 e^{-\left(\frac{\theta,\phi}{\theta_{BW}}\right)^2} \tag{4.22}$$

where θ_{BW} is the antenna beamwidth.

To place the antenna in the scatterer's reference plane $\left(\theta',\phi'\right)$, first rotate the antenna about the x-axis by 180°, rotate the new y-axis by θ_i and finally rotate the new z-axis by ϕ_i. This can be described using the following rotation matrix manipulations,

$$\begin{bmatrix} x \\ y \\ z \end{bmatrix} = \begin{bmatrix} \cos\phi_o & -\sin\phi_o & 0 \\ \sin\phi_o & \cos\phi_o & 0 \\ 0 & 0 & 1 \end{bmatrix} \begin{bmatrix} \cos\theta_o & 0 & -\sin\theta_o \\ 0 & 1 & 0 \\ \sin\theta_o & 0 & \cos\theta_o \end{bmatrix} \begin{bmatrix} 1 & 0 & 0 \\ 0 & -1 & 0 \\ 0 & 0 & -1 \end{bmatrix} \begin{bmatrix} x' \\ y' \\ z' \end{bmatrix}$$

Carrying through the matrix multiplication results in,

$$x = \cos\phi_o \cos\theta_o x' + \sin\phi_o y' + \cos\phi_o \sin\theta_o z' \tag{4.23}$$

$$y = \sin\phi_o \cos\theta_o x' - \cos\phi_o y' + \sin\phi_o \sin\theta_o z' \tag{4.24}$$

$$z = \sin\theta_o x' - \cos\theta_o z' \tag{4.25}$$

Transforming both antenna (non-primed) and ground (primed) coordinates to spherical,

$$\begin{aligned} x' &= r'\sin\theta'\cos\phi' & x &= r\sin\theta\cos\phi \\ y' &= -r'\sin\theta'\sin\phi' & y &= -r\sin\theta\sin\phi \\ z' &= r'\cos\theta' & z &= r\cos\theta \end{aligned}$$

Now substitute these expressions into Equations 4.26, 4.27 and 4.28 to get,

$$\begin{aligned} r\sin\theta\cos\phi = {} & \cos\phi_o\cos\theta_o\left(-r\sin\theta'\cos\phi'\right) + \sin\phi_o\left(r\sin\theta'\cos\phi'\right) \\ & + \cos\phi_o\sin\theta_o\left(r\cos\theta'\right) \end{aligned} \tag{4.26}$$

$$\begin{aligned} -r\sin\theta\sin\phi = {} & \sin\phi_o\cos\theta_o\left(-r\sin\theta'\cos\phi'\right) - \cos\phi_o\left(r\sin\theta'\cos\phi'\right) \\ & + \sin\phi_o\sin\theta_o\left(r\cos\theta'\right) \end{aligned} \tag{4.27}$$

$$r\cos\theta = \sin\theta_o\left(-r\sin\theta'\cos\phi'\right) - \cos\theta_o\left(r\sin\theta'\cos\phi'\right) \tag{4.28}$$

Using Equation 4.29 and noting that $r' = r$, an expression for θ can be found to be,

$$\theta = \cos^{-1}\left[\sin\theta_o\sin\theta'\cos\phi' + \cos\theta_o\cos\theta'\right] \tag{4.29}$$

To solve for ϕ, divide Equation 4.29 by 4.28 and solve for ϕ,

$$\phi = \cos^{-1}\left[\frac{\sin\theta\cos\phi'\cos\theta_o - \cos\theta'\sin\theta_o}{1-\left(\sin\theta'\cos\phi'\sin\theta_o + \cos\theta'\cos\theta_o\right)^{\frac{1}{2}}}\right] \tag{4.30}$$

An expression for the antenna pattern in terms of the ground coordinates can be expressed by substituting Equation 4.32 and 4.33 into Equation 4.25,

$$\frac{P_{r_{pq}}}{P_t} = \frac{G_o^2 \lambda^2}{(4\pi)^3} \int_{Area} \tan\theta d\theta d\phi \frac{e^{-\left(\frac{[\sin\theta_o \sin\theta\cos\phi + \cos\theta_o \cos\theta]}{\theta_{BW}}\right)^2} \sigma_{pq}^o\left(-\hat{i}, \hat{i}\right)}{R_t^2\left(\hat{i}\right)} \tag{4.31}$$

And noting that $ds = R_t^2\left(\hat{i}\right)\tan\theta d\theta d\phi$

Using Equation 4.26, the enhancement versus antenna beamwidth will be investigated. First, we will compute the scattering coefficient for a general layer of dielectric cylinders over a lossy ground plane. The parameters for this model are shown in Table 4.3. The scattering coefficients are plotted for both HH-pol and HV-pol in Figure 4.10. The enhancement is around +3 dB and -8.6 dB for HH-pol and HV-pol, respectively. Both have an angular width (null-to-null) of 10.5°.

Parameter	Value
Frequency	1500 MHz
Incident Angle	45°

Layer Depth	1 m
Cylinder Distribution	U[0, 5°]
Cylinder Density	50 cylinders/m^2
Cylinder Dielectric Constant	17.0+i5.55
Ground Dielectric Constant	23+i14.1
Cylinder Radius	0.5 cm
Disc Thickness	0.2 mm

Table 4.3 Layer parameters for dielectric cylinders over a ground plane

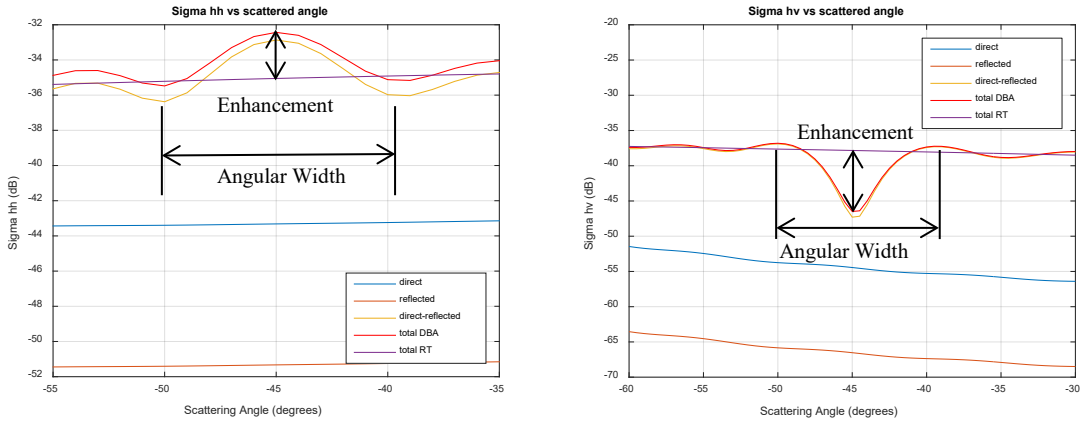

(a) (b)

Fig. 4.10 (a) HH-pol bistatic scattering coefficient, incident angle of -45° (b) HV-pol bistatic scattering coefficient, incident angle of -45°

Next the enhancement is computed for various antenna beamwidths. The antenna pattern assumed is a Gaussian. The results are plotted in Figure 4.11. For antenna beamwidths much smaller than the angular width, the full enhancement is detected. When the antenna beamwidth equals the angular width, a decrease in enhancement for

HH-pol from 3 dB to 1.8 dB is seen. For HV-pol, the enhancement increases from -8.6 dB to -2.3 dB.

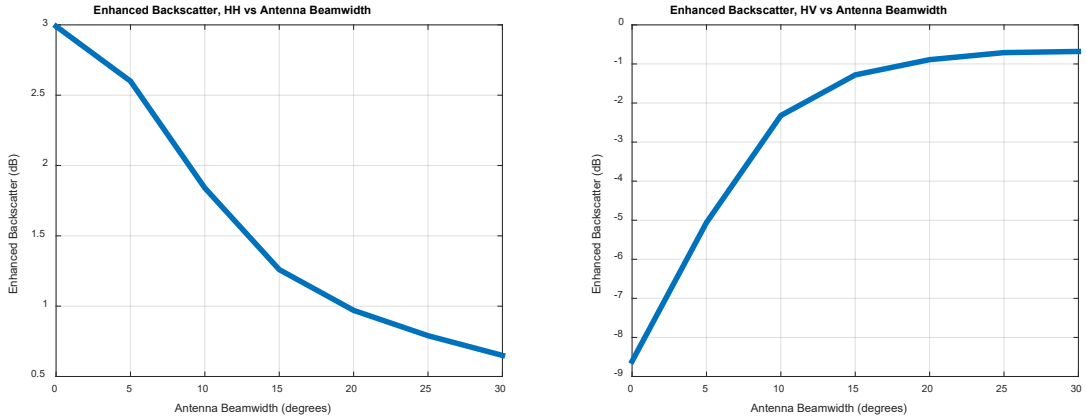

(a) (b)

Fig. 4.11 (a) HH-pol enhanced backscatter versus antenna beamwidth (b) HV-pol enhanced backscatter versus antenna beamwidth

Chapter 5 Radar Model of Corn Canopy over the full growing season

In this chapter, the modeling of a corn canopy over the full growing season is undertaken. Modeling over a full season is an ambitious task due to the complex dynamics in the canopy and underlying soil. These long and short term dynamics will be a good test for the robustness of the model. Model parameters such as plant architecture, dielectric constant, density, and soil moisture are taken from an actual field, located in Beltsville, MD. These measurements are used in the scattering model to predict backscatter at both like-polarizations (HH-pol and VV-pol). Concurrent to the field measurements, backscatter measurements were taken with a truck mounted L-Band radar. A detailed comparison between the modeled (both coherent and incoherent) and measured data will be the highlight of this chapter.

5.1 Radar experiment

The Optimizing Production Inputs for Economic and Environmental Enhancement (OPE^3) site is maintained by the United States Department of Agriculture – Agricultural Research Service (USDA-ARS) [Gish et al., 2003]. The site, located in Beltsville, MD, has a corn canopy equipped with several sensors used to monitor atmospheric, surface and sub-surface parameters. Concurrently, backscatter and in-situ field measurements were taken over the growing season. The backscatter measurements were taken from a truck-mounted L-Band radar system, known as the Combined Radar/Radiometer, or ComRAD [O'Neill et al., 2006], pictured in Figure 5.1. The ComRAD system was built and operated by The George Washington University (GW) and NASA Goddard Space Flight Center (GSFC).

Figure 5.1 ComRad system at OPE3 corn canopy site in Beltsville, MD

The system is a SMAP [Entekhabi et al., 2010] satellite simulator, containing both an L-Band radar and radiometer mounted on a 19 m high boom. The system can illuminate a scene with an incident elevation angle ranging from 0° to 175° and azimuthally from 0° to 300°. The antenna used is a parabolic dish antenna with a Cassegrain-like feed. The feed is implemented with a circular waveguide with two orthogonally placed wire probes, one to support horizontal polarization (HH-pol) and the second to support vertical polarization (VV-pol). The system is fully automated, via GPIB and custom software, allowing for continuous and remote data capture. For this study, the radar is operated at 1.25 GHz, with a fixed incident elevation angle of 40°. A total of 60 independent measurements are made as the boom is swept 120° in azimuth across the canopy. This was done several times over the course of a full day in order to see any relationship between backscatter and measurement time.

5.2 In-situ field measurements:

Detailed in-situ field measurements of the corn plant's constituents, namely the leaves, stalks and cobs are taken approximately weekly over the growing season. The plants are randomly sampled from an area outside of the radar footprint. The majority of measurements were typically taken while the plant was standing. In some cases, the plant was removed and measured stand-alone against a gridded-board, as shown in Figure 5.2.

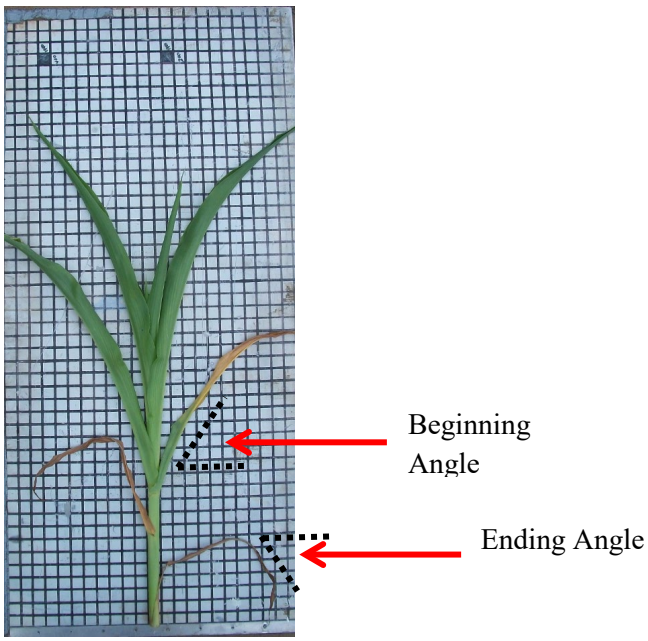

Figure 5.2 Sample corn plant used for measurement

5.2.1 Leaves:

For the leaves, the length, maximum width, thickness, density and location along the stalk were measured. The averages from three randomly sampled plants, taken approximately weekly, are listed in Table 5.1.

DoY	Leaf Major Radius (cm)	Leaf Minor Radius (cm)	Leaf Thickness (mm)	Leaf Density (leaves/m^2)
157	7.43	0.96	0.37	44.7
167	20.23	2.66	0.28	53.6
171	24.87	2.68	0.23	55.8
174	30.36	3.29	0.22	51.4
185	38.40	3.77	0.25	73.7
192	37.63	3.52	0.25	60.3
199	43.00	4.51	0.25	69.3
213	41.50	4.70	0.25	73.8
216	40.40	4.53	0.25	85
221	36.80	4.34	0.25	91.7
228	37.00	4.26	0.25	82.8
236	38.00	4.38	0.12	85
243	38.10	4.40	0.25	85
258	27.60	3.00	0.25	85
263	33.50	3.50	0.07	82.8
269	29.50	3.50	0.16	69.3

Table 5.1 Averaged measured leaf parameters

The density (leaves per m^3) is derived by counting the leaves in a 1 m^2 area and dividing by the canopy height. Another key measurement made is the leaf angular orientation, which is characterized by a beginning angle and an ending angle, illustrated in Figure 5.2. The beginning and ending angles denote the leaf orientation near the stalk and away from the stalk, respectively. An angle of +90° corresponds to a leaf that is oriented vertically in the +z-direction, and an angle of 0° corresponds to a leaf that is oriented parallel to the ground and an angle of -90° corresponds to a leaf that is oriented vertically in the –z-direction. The data collected are used to generate orientation statistics for the leaves, shown in Figure 5.3. The data shows that the beginning angle of the leaves tend to be more vertical in the beginning of the season, having an approximate uniform distribution over 45° to 90°, and tend to a more uniform distribution towards the end of the season. The azimuthal angle is assumed to have a uniform distribution over 0° to 360°. For the ending angle, a uniform distribution over various elevation angle ranges can be used.

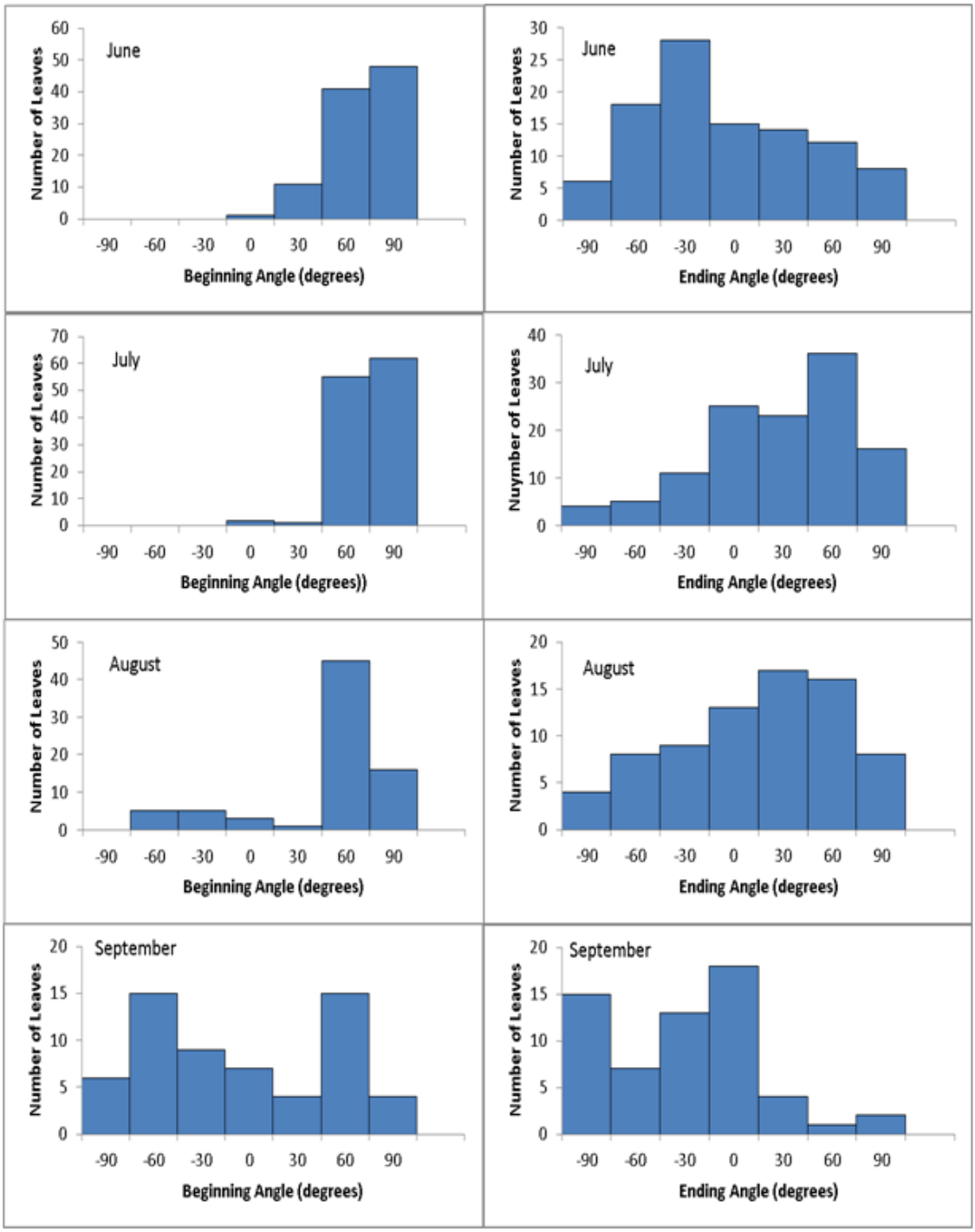

Figure 5.3 Monthly leaf orientation histograms

The dielectric constant of the corn leaves are measured at five different times during the season. A stack of leaves was held between two wooden planks, as shown in Figure 5.4a.

An open coaxial probe in conjunction with a vector network analyzer measures the reflected power from the leaf samples, from which the dielectric constant can be determined [Xu et al., 1991]. The stack of leaves was thick enough such that the coaxial probe sees a half-space of dielectric material at the measurement frequency. A plot of the measured dielectric constant over the growing season is shown in Figure 5.4b. Note that both the real and imaginary parts of the measured dielectric constant are highest at the beginning of the growing season and tend to decrease as the season progresses. The largest decrease in dielectric constant is seen at the onset of senescence after DoY 235, as the leaves begin to dry out.

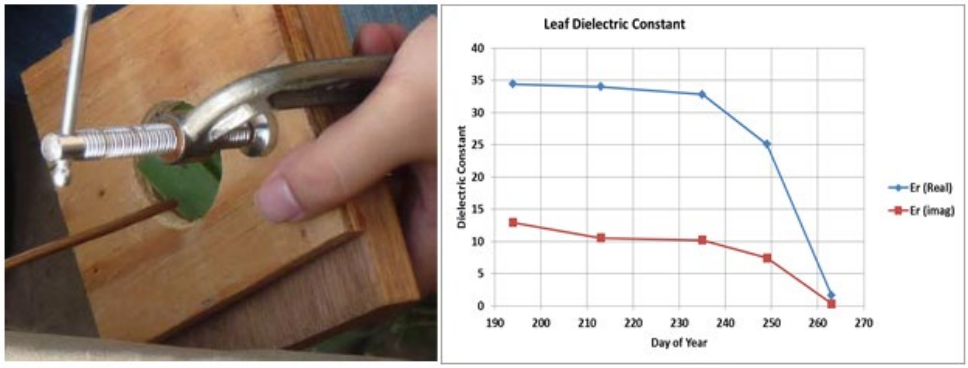

Figure 5.4 (a) Leaf dielectric constant measurement (b) Measured leaf dielectric constant over growing season

5.2.2 Stalks

For the stalks, the height is measured from right under the brace roots to the top node of the plant and the radius is measured at two locations on the stalk, to provide the most representative radius. The first measurement is made between the bottom two nodes and the second measurement is made between the top two nodes. The measurements are averaged and are summarized in Table 5.2. Note that the radius of the stalk at the bottom

node can be significantly higher than at the top node. Since the stalk is modeled as a cylinder, an equivalent radius is used such that the volume of the cylinder is equal to the volume of the conical stalk. The stalk density is fixed over the growing season at 6.7 stalks/m^2.

DoY	Stalk Height (cm)	Bottom Node (mm)	Top Node (mm)	Equivalent Radius (mm)
157	7.7	4.0	3.0	3.5
167	18.0	8.1	6.0	7.1
171	23.0	9.3	7.4	8.4
174	29.3	9.7	6.5	8.2
185	58.0	9.9	6.2	8.1
192	55.3	10.8	8.0	9.4
195	79.0	9.9	7.7	8.8
199	87.0	8.9	4.7	6.9
213	140.0	10.7	3.3	7.3
216	131.7	9.4	3.0	6.4
221	117.3	8.7	2.0	5.7
228	132.0	10.4	3.4	7.2
236	115.7	7.8	1.3	4.9
243	112.0	8.0	1.5	5.1
258	116.7	7.5	2.0	5.0
263	115.0	7.1	1.7	4.7
269	78.3	7.6	3.4	5.6

Table 5.2 Averaged measured stalk parameters

The stalk's anatomy is more complicated than the leaf and comprises a series of longer sections, called internodes, separated by shorter sections called nodes. The nodes are identified by where the leaves are attached to the stalk. The leaf emanates from one node and wraps around the internode, forming a sheath, to just below the next higher node before branching out [Bowman, 1911]. The dielectric constant of the stalk is also measured using an open coaxial probe technique. The stalk is cut into samples containing nodes and internodes and the dielectric constant is measured at a few locations within the cross-section, by inserting the coaxial probe perpendicular to the cut, as shown in Figure 5.5. Note that the nodes on the stalk can be identified by where a leaf begin to grow away from

the stalk. The nodes appear to be more yellow in hue, whereas the internode samples have white regions. A plot of the measured dielectric constants for the nodes and inter-nodes taken on DOY 213 is shown in Figure 5.6. The permittivity at the node is consistently higher than at the internode.

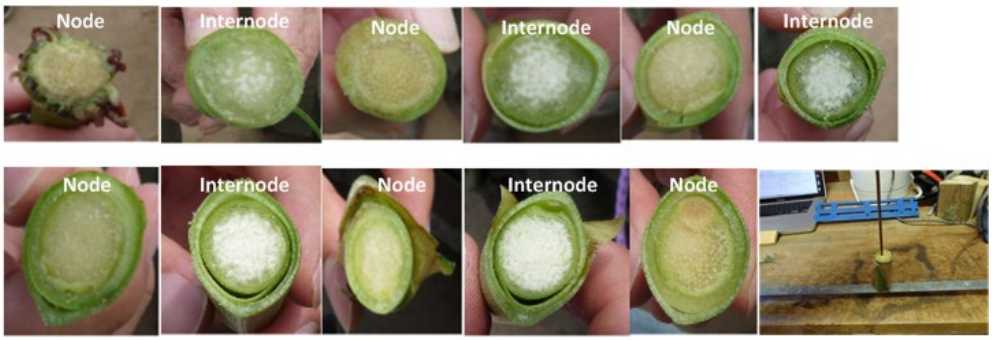

Figure 5.5 Cross-section of stalk nodes and internodes

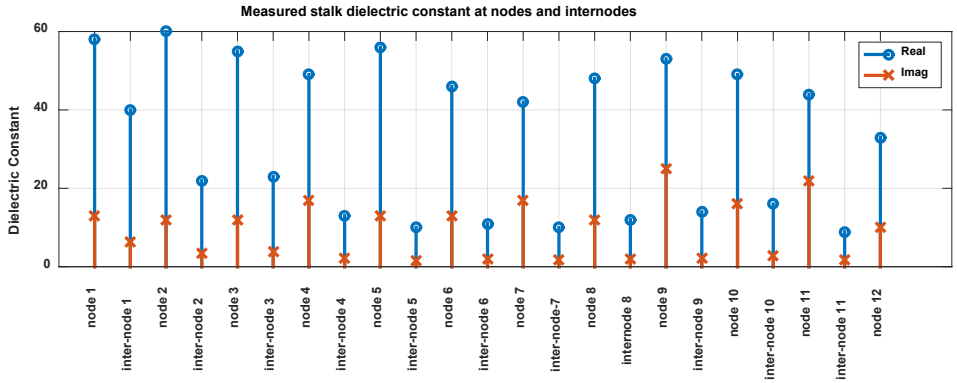

Figure 5.6 Measured dielectric constant of stalk nodes and internodes taken on DoY 213

As mentioned in Chapter 3, a periodic stalk can be approximated with a homogeneous dielectric constant via a simple dielectric mixing model (see Eq. 3.39). Using Eq. 3.39, a uniform homogenous dielectric constant is computed over the whole growing season and plotted in Fig. 5.7.

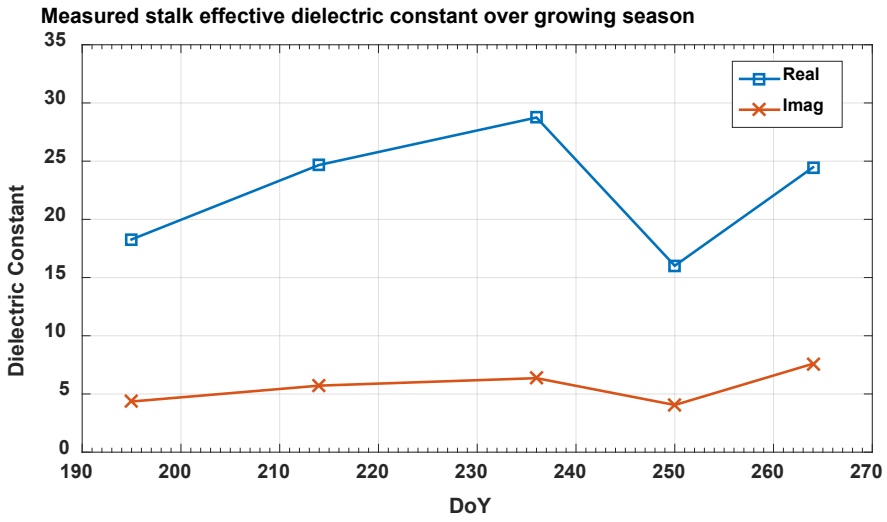

Figure 5.7 Effective dielectric constant for stalk over growing season

5.2.3 Cobs

The measurements of the dimensions of the corn cobs start on DoY 212. The cob's maximum radius and length are measured from random sampling of cobs outside of the radar footprint. The average of the measurements is shown in Table 5.3.

DoY	Cob Radius (mm)	Cob Length (cm)
213	19.2	28
228	22.15	25
236	22.6	20
243	22.4	17
258	22	21
263	30	16
269	25	20

Table 5.3 Averaged measured cob parameters

Similar to the stalk, the dielectric constant varies significantly over the cob. Measurements are made at three locations, the outer leafy layer, the middle layer consisting

of the kernels, and the center layer, as shown in Figure 5.8. For the outer layer, similar to the leaves, a thick stack is formed and measured with the coaxial probe. For the other two layers, the coaxial probe is inserted perpendicular to the cross-section. The measured dielectric constant over the growing season is shown in Figure 5.9.

Figure 5.8 Cross-section of a corn cob

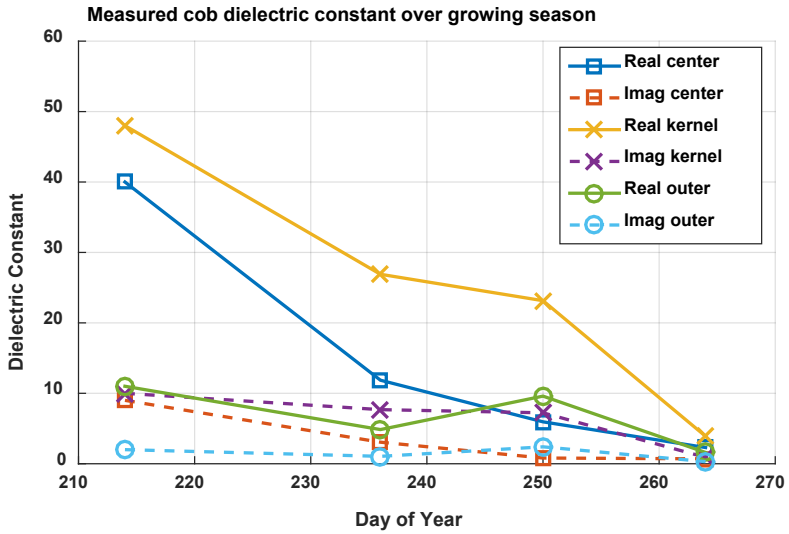

Figure 5.9 Measured dielectric constant of the cob over the growing season

5.2.4 Soil Characteristics

In addition to measurements of the corn plant's constituents, the underlying soil has a significant influence on radar backscatter. The test site has a soil texture that is

characterized as sandy loam, 23.5% silt, 60.3% sand and 16.1% clay, with a bulk density of 1.25 $g \cdot cm^{-3}$. Using an empirical model from [Dobson, 1985], the complex dielectric constant of the soil is computed. The inputs to the Dobson model are the percentage of sand and clay, bulk density, volumetric water content, and soil temperature. The data was taken using a gravimetric sampling technique and Delta-T theta probes. Several location on the edges of the radar footprint was sampled, with the probe inserted 6 cm into the surface, giving a reasonable estimate of the soil moisture in the first 5 cm.

The surface roughness of the soil was measured by using digital images of the surface profile against a known grid. The horizontal surface heights were measured in 1 cm increments. These data are then processed to determine the rms surface height and the correlation length. Note that the initial surface roughness undergoes rapid changes in the beginning of the growing season but tends to a settle to a constant value (and fairly flat, with respect to L-Band frequencies), due to rain and wind effects. A typical measurement which will be used in the models for the surface height for the mature canopy averages to 3.5 mm with a correlation length of 113 mm. This measurement is taken parallel to the row, at a quarter of the distance between adjacent rows.

5.2.5 Biomass

The biomass was measured by cutting three sample plants and separating into stem, leaf and cob components. Each component was placed into its own individual paper bag, which is then placed into air-tight bags and taken to the lab to be weighed. The bags are then oven-dried to constant weight for three days at 70°C and weighed again. From this process, the leaf, stem, cob and total water content is then computed in terms of gm/plant and then converted to g/m^2 using the plant density measurements, and plotted in Figure 5.10.

The peak biomass occurs on DoY 213 and rapidly decreases throughout the rest of the growing season. Both the stalk and leaf biomass tend to decrease rapidly towards the end of the growing season, unlike the stalk, which continues to hold moisture. This can be seen easier in Figure 5.11, which has the %-biomass plotted over DoY. In this plot, the stalk holds upwards of 70% of the total biomass at the end of the growing season.

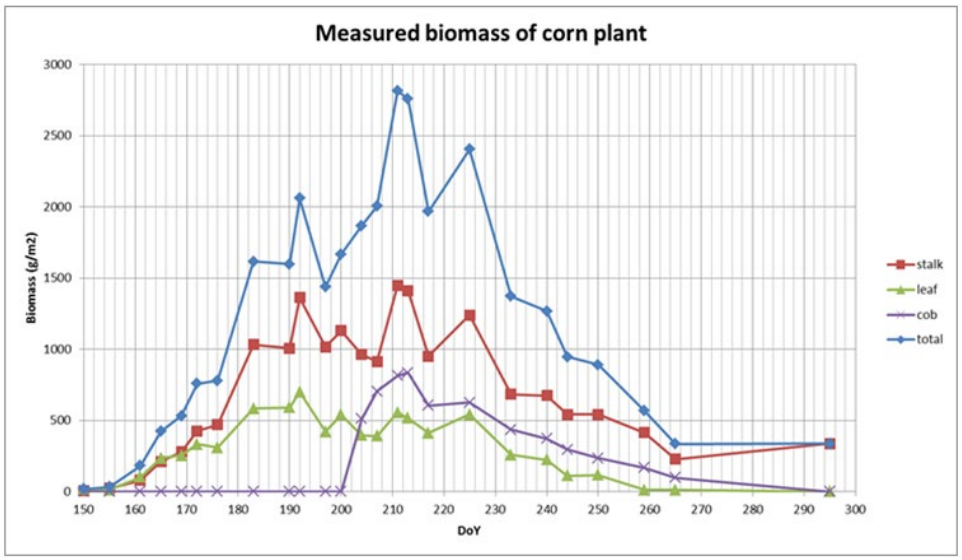

Figure 5.10 Measured biomass of stalk, leaf, cob and total

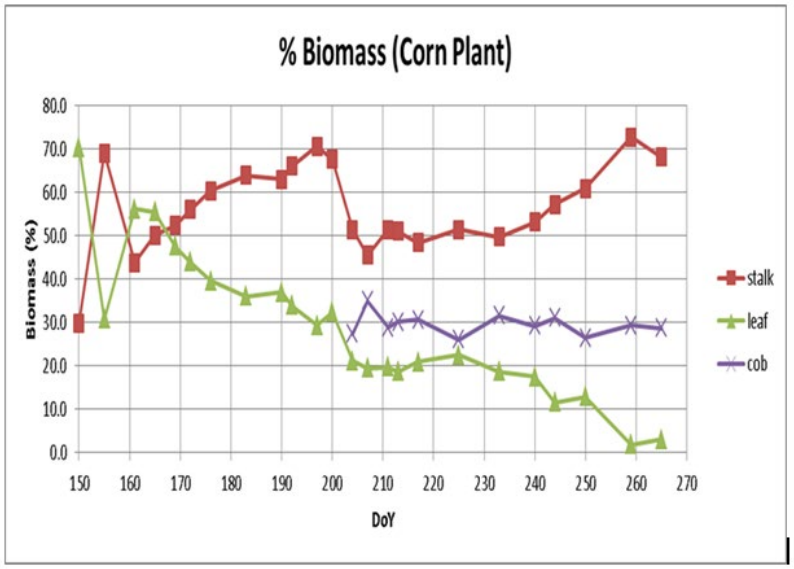

Figure 5.11 Measured %-biomass of corn plant's constituents

5.3 Radar Measurements

In this section, the measured radar backscatter data will be presented along with ground truth such as soil moisture and biomass. As shown in Figure 5.12, HH-pol, VV-pol and soil moisture are plotted over the growing season. The dataset recorded has sufficient samples during the various stages of the growing season, such as early growth, peak growth and senescence.

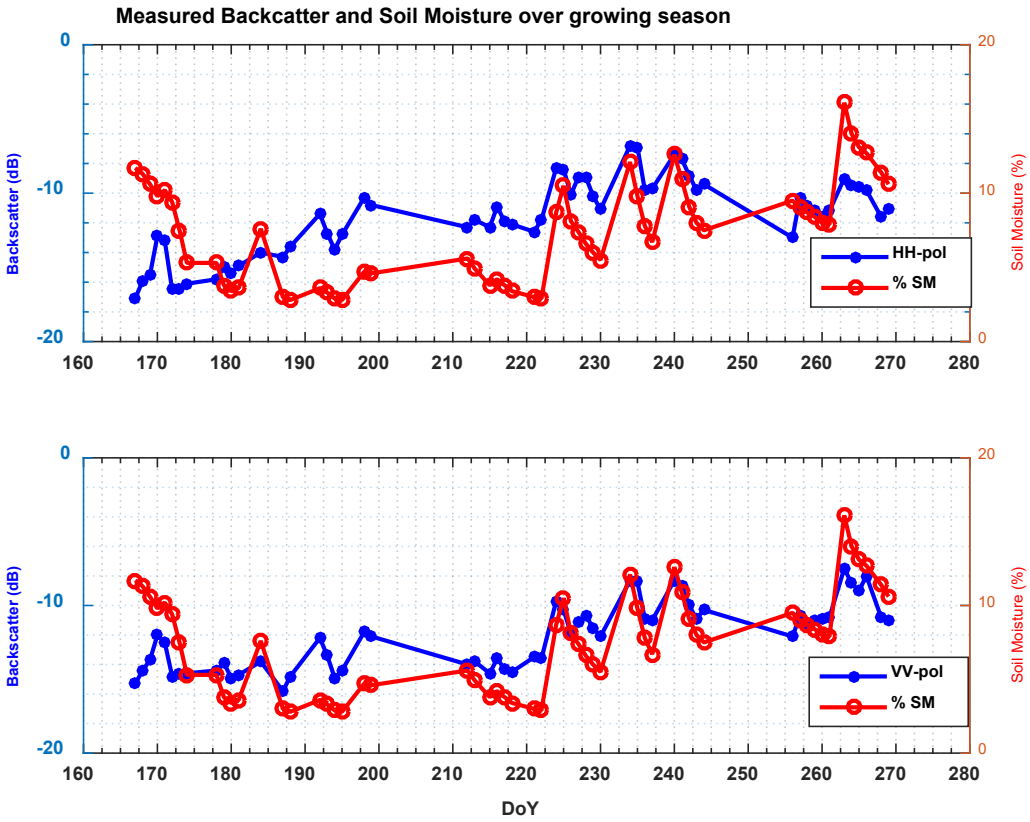

Figure 5.12 Measured HH-pol and VV-pol over the growing season

5.3.1 Radar return versus soil moisture

The measured soil moisture data shows that the season was in general quite dry, with less than 10% soil moisture for over 70% of the growing season. There are five peaks in the soil moisture curve with corresponding peaks in both HH-pol and VV-pol, occurring on DoY 183, 224, 233, 239 and 262.

Figure 5.12 also shows significant changes in both HH-pol and VV-pol from day-to-day measurements, where a negligible change in both soil moisture and plant architecture is seen. For example, from DoY 169 to DoY 170, HH-pol changes by 2.1 dB and VV-pol changes by 1.1 dB. During this time period, the soil moisture changes from 10.5% to 9.8%. Such a small change in soil moisture should not cause such a large change in backscatter. Also, interesting to note that there is an inverse relationship between the soil moisture and backscatter for this case (ie: the soil moisture decreased, but the backscatter increased). Since DoY 169 measurements were taken in the afternoon and DoY 170 measurements were taken in the morning, it is postulated that the AM measurements exhibit increased backscatter because of the presence of dew [Hornbuckle, 2007, 2010; Cosh et al. 2009].

Dew sensors were installed in the field during the month of August. These sensors detect either the presence or absence of dew. A scatterplot of both HH-pol and VV-pol backscatter versus soil moisture is shown in Figure 5.13. From this plot, that data corresponding to the presence of dew is higher on average than the trendline for both HH-pol and VV-pol. Similarly, data corresponding to the absence of dew is lower on average than the trendline. Computing the average increase in backscatter due to the presence of dew is about 1.5 dB for HH-pol and 1 dB for VV-pol. This shows that dew does have a significant effect on backscatter at L-Band.

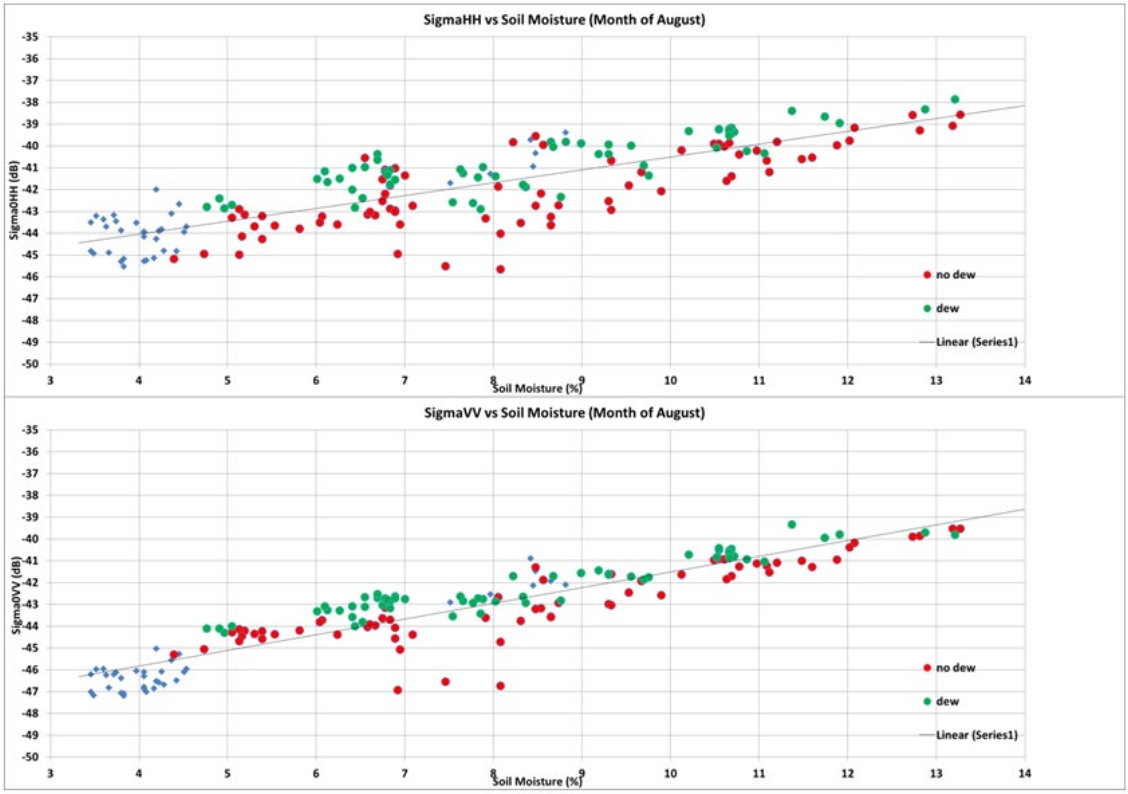

Figure 5.13 HH-pol and VV-pol versus soil moisture with dew sensor data

5.3.2 Radar Return versus biomass

Finally, in Figure 5.14, HH-pol and VV-pol are overlaid with the total measured biomass. In general, both HH-pol and VV-pol tracked the increasing biomass from DoY 156 through 198, with σ^0_{HH} having a stronger correlation with biomass changes. Peak biomass occured at DoY 211 and decreased after DoY 225. During the DoY 211 through the end of the growing season, there isn't a strong correlation between backscatter and biomass. This will be investigated further in the next section dealing with the scattering model for the corn canopy.

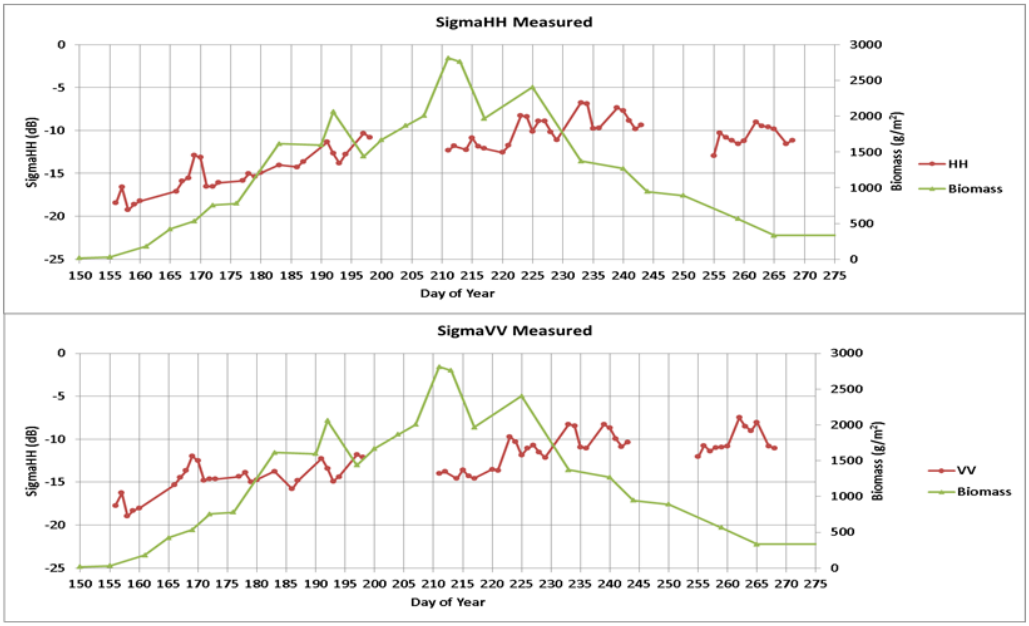

Figure 5.14 $\boldsymbol{\sigma^0_{HH}}$ and $\boldsymbol{\sigma^0_{VV}}$ versus total biomass

5.4 Radar Model and Simulations

In this section, the theory described in Chapter 2 and 3, along with the detailed field measurements from a corn canopy given in this chapter are used to simulate HH-pol and VV-pol backscatter. In addition to backscatter, some other important parameters such as two-way attenuation, individual backscatter contributions (direct, direct-reflected and surface) and enhanced backscatter was also simulated over the growing season. These parameters give physical insight into understanding the relationship between backscatter and canopy parameters. Finally, a comparison between the simulated HH-pol and VV-pol backscatter with concurrent radar backscatter measurements will show the validity of the modeling methods, the importance of enhancement effects and accuracy of the GW scattering model.

5.4.1 Scattering model for corn canopy

A corn plant consists of a stalk, leaves and typically one cob. The stalk is modeled by a dielectric cylinder having a uniform dielectric constant. From the measurements in Section 5.2, the stalk dielectric constant was seen to be non-uniform, having a periodic profile. Using a simple dielectric mixing model, described in Ch. 3, the periodic dielectric constant profile can be replaced with a uniform dielectric constant. The leaves are modeled as thin dielectric discs. The cob is modeled by a dielectric cylinder. Similar to the stalk, a simple dielectric mixing model was used to find a uniform dielectric constant. The orientation statistics were also measured and detailed in Section 5.2 and used in the model.

The ground is modeled having a rms height and correlation function, which are measured parameters. The backscatter due to the rough surface was predicted using the Small Perturbation Method [Fung, 2009]. More complicated methods, such as the Integral Equation Method [Fung 2009] was used, but showed little to no difference. This was because the roughness measured was relative small [Sharma and Lang, 2017].

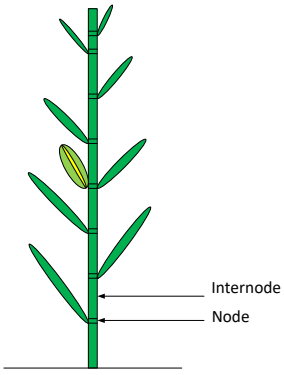

Figure 5.15 Corn plant model

5.4.2 Two-way canopy attenuation

The two-way canopy attenuation, $10\log_{10}\left(e^{-2\,\mathrm{Im}(\kappa_s)d}\right)$ is plotted in Fig 5.16. The plot is as expected, with the canopy having low attenuation during the early part of the season, increasing in the middle of the season and becoming low again towards the end of the season as the plants dry out and leaves shed. The attenuation is about 2 dB higher for VV-pol than HH-pol during the middle part of the season. This is because the stalks are physically the largest constituent of the plants and is dominantly vertically oriented.

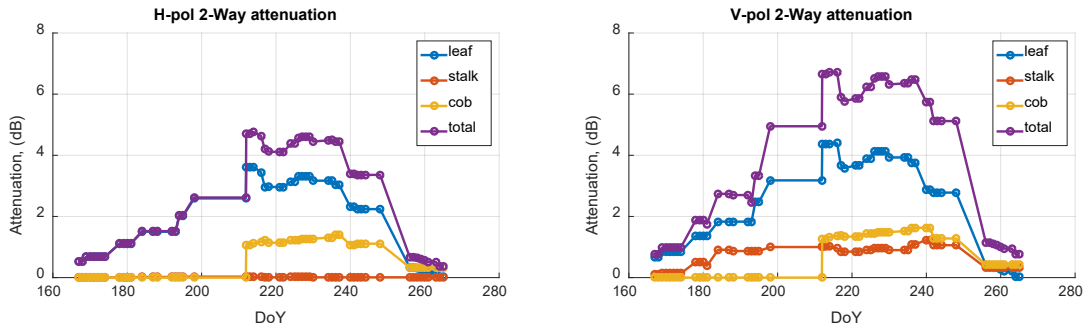

Figure 5.16 Simulated Two-way canopy attenuation

5.4.3 Leaf, Stalk and cob scatter

The direct, direct-reflected (both coherent and incoherent) and surface scatter is plotted in Figure 5.17 for both HH-pol and VV-pol cases over the growing season. For HH-pol, the leaf scatter is dominant during the early and middle stages, and decrease rapidly during senescence. This follows a similar trend in dielectric constant as seen back in Fig. 5.4. For VV-pol the stalk is the dominant scatterer throughout the entire growing season. It is interesting to see that unlike the leaf scatter, which decreases towards the end of the season, the stalk scatter remains high. This can be explained by the stalks' ability to retain moisture, as shown in the measured biomass in Fig. 5.10 and Fig. 5.11, where the stalk accounts for 70% of the corn plant moisture towards the end of the season.

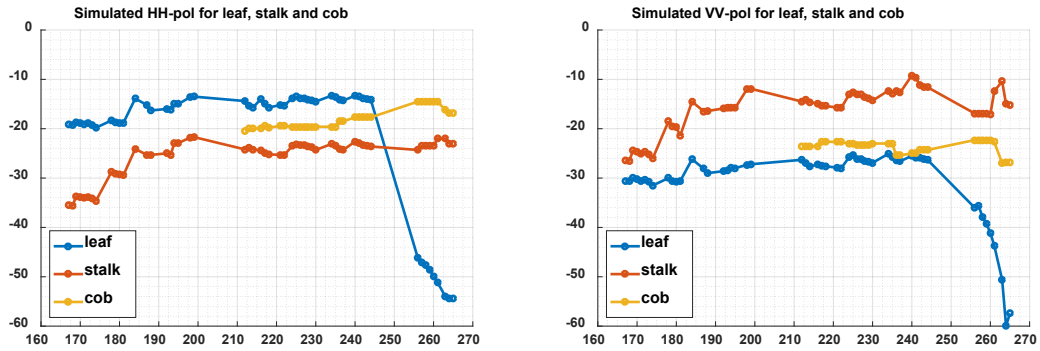

Figure 5.17 Simulated σ^0_{HH} and σ^0_{VV} for individual scattering components of leaf, stalk and cob

5.4.4 Direct, Direct-Reflected and Surface Scatter

The dominant individual scattering contributors, namely direct, direct-reflected and surface scatter is plotted in Fig. 5.18. During the early season, the surface scatter for VV-pol is dominant during the first part of the early season. Whereas for HH-pol, the direct-reflected scatter is greater the surface scatter. Direct scatter is negligible for both HH-pol and VV-pol cases. As the season progresses, the direct-scatter increases and surface scatter decreases, primarily due to the increased canopy attenuation. Direct-reflected scatter continues to be dominant. Finally, in the late part of the season, the direct scatter begins to decrease as the plants begin to dry out and shed leaves. The surface scatter begins to increase since the canopy attenuation decreases. Direct-reflected scatter remains the dominant scattering term. For VV-pol it is worth pointing out that the increase in the direct-reflected scatter during the late season is due to a rain event.

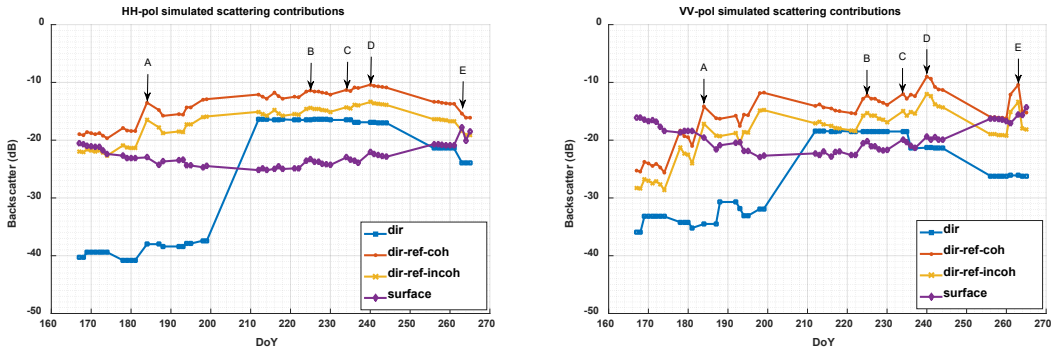

Figure 5.18 Simulated σ^0_{HH} and σ^0_{VV} for individual scattering components direct, direct-reflected (coherent and incoherent) and surface.

5.4.5 Enhanced backscatter

Next, a plot of the simulated enhancement at backscatter for both HH-pol and VV-pol is shown in Fig. 5.19. During the early part of the season, the enhanced backscatter is higher for HH-pol than for VV-pol. This is primarily due to the high amount of surface scatter for VV-pol, which swamps out the coherent effect caused by the direct-reflected scatter. Towards the later part of the early the season the enhanced backscatter approaches 2.6 dB (close to the theoretical 3 dB). In the middle of the season, both HH-pol and VV-pol have on average 2 dB of enhanced backscatter. In the late season, HH-pol enhancement continues to remain high, whereas VV-pol enhancement decreases, expect for a rain event causing a spike. Again, the reason for HH-pol enhancement remaining high is due to direct-reflected scatter being higher than the direct and surface scatter. As opposed to the VV-pol case, where again, the surface scatter is the highest scatter contributor, as seen in Fig. 5.18.

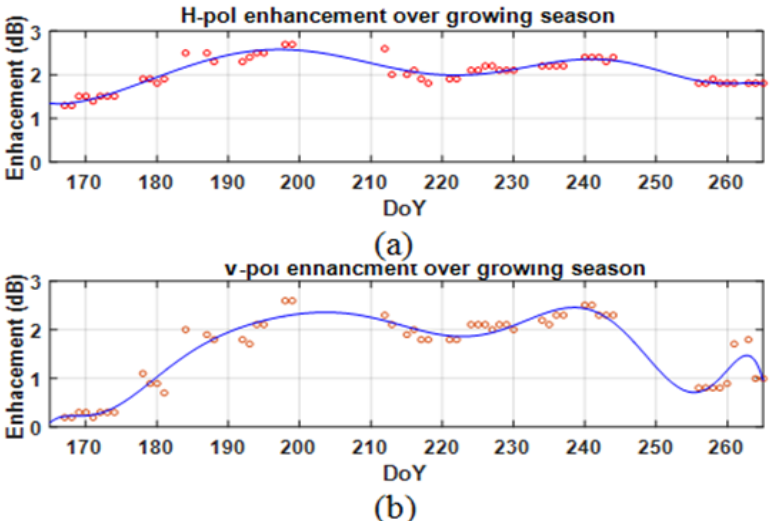

Figure 5.19. Enhanced backscatter for HH-pol and VV-pol over the growing season

5.5 Measured vs simulated total backscatter

Finally, this section will compare the simulated and measured backscatter over the growing season. The total simulated coherent and incoherent backscatter, $\sigma^0_{HH}$and σ^0_{VV}, is plotted in Figure 5.20, along with the measured backscatter.

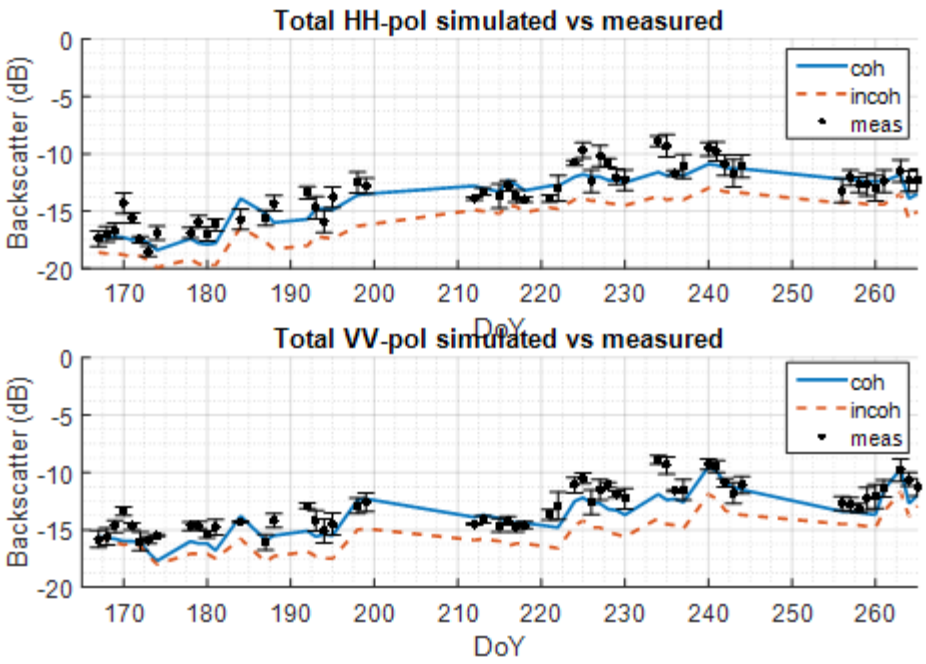

Figure 5.20 Measured versus modeled (continuous curves) σ^0_{HH} and σ^0_{VV} over the growing season

In general, both the incoherent and coherent model compared well with the measured backscatter. This is primarily due to the extensive amount of field measurements taken, in particular the detailed dielectric constant measurements taken over the season. However, the coherent model matched the data better, with a RMSD (root mean square error in dB) varying from 0.9 to 1.1 dB for HH-pol and 0.8 to 1.1 dB for VV-pol over the entire growing season. The most comparable study with this research was done by [Monsivais-Huertero et. al, 2018] with their results of 0.55 dB to 2.42 dB RMSD for HH-pol and a 1.78 dB to 2.22 dB for VV-pol. A final comparison uses a well-known open source incoherent scattering model, MIMICS, from the University of Michigan to model the corn canopy. The model uses gravimetric water content and an empirical model [Ulaby and El-Rayes, 1987] to compute the dielectric constant. The final results from the MIMICS simulation

showed that the RMSD for HH-pol varied from 1.7 to 2.5 dB and 1.3 to 1.6 dB for VV-pol.

Based on the comparisons of other scattering models and other similar research, the GW coherent model clearly is the most accurate, and confirms that coherent scattering is an important effect to model in a corn canopy at microwave frequencies, such as L-Band.

Chapter 6 Conclusions and Future Work

In Chapter 2, a careful derivation of the bistatic scattering coefficients for a model consisting of a layer of random medium over a lossy dielectric half-space was presented. The total bistatic scattering coefficients was shown to the sum of direct (or volume) scatter, direct-reflected (or double-bounce) scatter and intuitive graphical depictions are used to provide physical insight into a complex scattering problem. The remaining scattering terms are shown to not contribute.

In Chapter 3, techniques to compute the scattering amplitude of scatterers useful in the modeling of vegetation were developed. The first method uses the polarizability dyadic accurate for electrically small (or Raleigh) scatterers. The second technique uses an electrostatic approximation for the fields inside of a scatterer. It was shown that the results from this method converge to the first method for small scatterers. Finally, for non-canonical shapes with inhomegenous dielectric constant profiles, a brief introduction to the use of commercial numerical EM solvers, such as FEKO was presented.

In Chapter 4, a careful analysis of coherent scattering effects is undertaken. It was shown that for like-polarization the maximum enhancement is +3dB, whereas for cross-polarization, the enhancements can be negative, zero or positive, depending on the relationship of the incident angle to the Brewster angle. Also, small-scale surface roughness was introduced and shown to reduce the enhancement by lowering the contribution of the double-bounce terms. Finally, when using the radar equation, the antenna beamwidth should be considered, since the bistatic scattering coefficient is not constant over the antenna illumination area due to coherent effects.

In Chapter 5, all the concepts from the previous chapters were used to model a corn canopy over its entire growing season. Concurrent field and radar measurements were made, allowing for a good comparison between model and measured backscatter. For the model, both the Distorted Born Approximation, which accounts for coherent scattering effects and the Radiative Transfer (the incoherent model) was used. It was shown that the coherent model yielded about 1 dB RMSD against the measured data for both HH-pol and VV-pol, which is better than previous and current published research. The main contributors to this accuracy were the leaf orientation statistics, the periodic stalk model and the cob model. Also, a simple dielectric mixing formulism was used to simplify the complicated dielectric constant inhomogeneity in the stalk and the cob to a uniform effective dielectric constant. Numerical electromagnetic simulations were used to show equivalence of the simplified dielectric mixing model.

Even with the accurate performance of the scattering model, there are two main areas for further research. The first is modeling of the dew effect which can increase backscatter by up to 1.5 dB. Second, the effect of the plant row periodicity could be taken into account. Finally, an experiment measuring enhanced backscatter for cross-polarization would be important to the research community in this field.

References

H.L. Bertoni, L.S. Cheo and T. TAmir, “Frequency-selective reflection and transmission by a periodic dielectric layer,” IEEE Transactions on Antennas and Propagation, vol. 37, no.1, pp. 78-83, Jan. 1989.

Born M. and E. Wolf (1980), *Principle of Optics*, Sixth Edition, Pergamon Press, New York.

M.L. Bowman and B.W. Crossley, *Corn Growing, Judging, Breeding, Feeding and Marketing*, Waterloo, IA, Waterloo Publishing Co., 1911.5

Chandrasekhar, S. (1960), *Radiative Transfer*, Dover, NY.

N. S. Chauhan, R. H. Lang and K. J. Ranson, "Radar modeling of a boreal forest," IEEE Transactions on Geoscience and Remote Sensing, vol. 29, no. 4, pp. 627-638, Jul 1991.

N. S. Chauhan, D. M. Le Vine and R. H. Lang, "Discrete scatter model for microwave radar and radiometer response to corn: comparison of theory and data," in IEEE Transactions on Geoscience and Remote Sensing, vol. 32, no. 2, pp. 416-426, Mar 1994.

Chukhlantsev, A.A., *Microwave radiometry of vegetation canopies*, Springer, 2006.

Collin, R., F. Zucker (1969), *Antenna Theory*, Part I, McGraw Hill, New York.

M.H. Cosh, E.D. Kabela, B. Hornbuckle, M.L. Gleason, T.J. Jackson, J. Prueger, “Observations of dew amount using in situ and satellite measurements in an agricultural landscape,” in Agric. Meteorol., 149 (2009), pp. 1082-1086.

Dobson, M.C., F. T. Ulaby, H. Hallikainen, and M. A. El-Rayes, “Microwave dielectric behavior of wet soil-Part 11: Four components dielectric mixing models,” IEEE Trans. Geosci. Remote Sensing, vol. 23, pp. 35-46, 1985.

A. Della-Vecchia, P. Ferrazzoli, L. Guerriero, L. Ninivaggi, T. Strozzi and U. Wegmuller, "Observing and Modeling Multifrequency Scattering of Maize During the

Whole Growth Cycle," in IEEE Transactions on Geoscience and Remote Sensing, vol. 46, no. 11, pp. 3709-3718, Nov. 2008.

C. Elachi, J.J. van Zyl, *Introduction To The Physics and Techniques of Remote Sensing*, John Wiley & Sons, Inc., 2006.

D. Entekhabi, E.G. Njoku, P.E. O'Neill, K.H. Kellogg, W.T. Crow, W.N. Edelstein, J.K. Entin, S.D. Goodman, T.J. Jackson, J. Johnson, J. Kimball, J.R. Piepmeier, R.D. Koster, N. Martin, K.C. McDonald, M. Moghaddam, S. Moran, R. Reichle, J. C. Shi, M.W. Spencer, S.W. Thurman, L.Tsang, and J. Van Zyl, "The soil moisture active passive (SMAP) mission," Proc. IEEE, vol. 98, no. 5, pp. 704–716, May 2010.

Foldy, L.L. (1945), The multiple scattering of waves, *Phy. Rev*., **67**, 107-119.

Fung, A.K. and F.T. Ulaby (1978), A scatter model for leafy vegetation, *IEEE Trans. Geosci. Electron.*, **GE-16**, 281-285.

Fung, A.K. (1979), Scattering from a vegetation layer, IEEE Trans. Geoscience. Electron., **GE-17**, 1-6.

Fung, A.K. and F.T. Ulaby (1978), A scatter model for leafy vegetation, IEEE Trans. Geosci. Electron., **GE-16**, 281-285.

A.K. Fung, K.S. Chen, *Microwave scatter and emission models for users*., Arctech House, 2009.

T.J. Gish, C. L Walthall, C.S. T. Daughtry, W.P. Dulaney, and G. W. McCarty, "Watershed-scale sensing of subsurface flow pathways at OPE3 site," in Proc. 1st Interagency Conf. Res. Watersheds, Benson, AZ, Oct. 27-30, 2003, pp. 192-197.

B. K. Hornbuckle, A. W. England, M. C. Anderson, "The effect of intercepted precipitation on the microwave emission of maize at 1.4 GHz", IEEE Trans. Geosci. Remote Sens., vol. 45, no. 7, pp. 1988-1995, 2007.

B. K. Hornbuckle, T. Rowlandson, E. Russell, A. Kruger and T. Sauer, "Water residing on plants alters the L-band brightness of senescing corn," 2010 11th Specialist Meeting on Microwave Radiometry and Remote Sensing of the Environment, Washington, DC, 2010, pp. 76-80.

Ishimaru, A., Electromagnetic Wave Propagation, Radiation and Scattering, Prentice-Hall (1991), New Jersey.

Ishimaru, A. (1978), Wave Propagation and Scattering in Random Media, **1** and **2**, Academic Press, New York.

A. T. Joseph, R. van der Velde, P. E. O'Neill, R. H. Lang and T. Gish, "Soil Moisture Retrieval During a Corn Growth Cycle Using L-Band (1.6 GHz) Radar Observations," in IEEE Transactions on Geoscience and Remote Sensing, vol. 46, no. 8, pp. 2365-2374, Aug. 2008.

Karam, M.A. and A.K. Fung (1983), Scattering from a randomly oriented circular discs with applications to vegetation, *Radio Science*, **18**, 557-565.

Keller, J.B. (1962), Wave propagation in random media, Proc. Symp. Appl. Math, **13**, 145-170.

Kuga, Y. and A. Ishimaru (1984), Retroreflectance from a distribution of spherical particles, J. Opt. Soc. AM., A, **1**, 831-835.

Lang, R.H. (1981), Electromagnetic backscattering from a sparse distribution of lossy dielectric scatterers, Radio Science. Vol 16, Issue 1.

Lang, R.H, "Microwave modeling of vegetation: A historical prospective," 2016 IEEE International Geoscience and Remote Sensing Symposium (IGARSS), Beijing, 2016, pp. 1878-1880.

Lang, R. H., A. Sharma and M. Cosh, "Scattering from a layer of vegetation: Enhancement effects," 2017 IEEE International Geoscience and Remote Sensing Symposium (IGARSS), Fort Worth, TX, 2017, pp. 1419-1421.

Lang, R. H., N. Chauhan, C. Utku and D. M. Le Vine, "L-Band Active and Passive Sensing of Soil Moisture through Forests," 2006 IEEE MicroRad, SanJuan, 2006, pp. 193-196.

Lang, R. H. (2004) Scattering from a layer of discrete random medium over a random interface: application to microwave backscattering from forests, Waves in Random Media, 14:2, S359-S391

R.H. Lang N. Khadr "Effects of backscattering enhancement of soil moisture sensitivity" Proc. IGARSS pp. 916-919 1992.

Lang, R. H., S. Seker, Y. Yuan, M. Kurum, M. Ogut, P.E. O'Neill, M. Cosh, "Use of periodic stalks to model L band returns from corn," 2014 XXXIth URSI General Assembly and Scientific Symposium (URSI GASS), Beijing, 2014, pp. 1-1.

Lang, R., S. Seker, Q. Zhao, M. Kurum, M. Ogut, P. O'Neill, and M. Cosh, "L-Band Radar Backscattering from a Mature Corn Canopy: Effect of Cobs," National Radio Science Meeting, USNC/URSI, Boulder, CO, January 8-11, 2014, doi: 10.1109/USNC-URSI-NRSM.2014.6928036.

D. Le Vine, A. Schneider, Roger Lang and H. Carter, "Scattering from thin dielectric disks," in IEEE Transactions on Antennas and Propagation, vol. 33, no. 12, pp. 1410-1413, December 1985.

Lobell, D. B., Burke, M. B., Tebaldi, C., Mastrandrea, M. D., Falcon, W. P. & Naylor, R. L. (2008). Prioritizing climate change adaptation needs for food security in 2030. Science 319, 607–610.

A. Monsivais-Huertero and J. Judge, "Comparison of Backscattering Models at L-Band for Growing Corn," in IEEE Geoscience and Remote Sensing Letters, vol. 8, no. 1, pp. 24-28, Jan. 2011.

Alejandro Monsivais-Huertero, Pang-Wei Liu, Jasmeet Judge, "Phenology-Based Backscattering Model for Corn at L-Band", *Geoscience and Remote Sensing IEEE Transactions on*, vol. 56, no. 9, pp. 4989-5005, 2018.

P. E. O'Neill, R. H. Lang, M. Kurum, C. Utku and K. R. Carver, "Multi-Sensor Microwave Soil Moisture Remote Sensing: NASA's Combined Radar/Radiometer (ComRAD) System," 2006 IEEE MicroRad, SanJuan, 2006, pp. 50-54.

J. F. Paris, "Radar Backscattering Properties of Corn And Soybeans at Frequencies of 1.6, 4.75, And 13.3 GHz," in IEEE Transactions on Geoscience and Remote Sensing, vol. GE-21, no. 3, pp. 392-400, July 1983.

Rice, S. O., “Reflection of electromagnetic waves from slightly rough surfaces,” Commun. Pure Appl. Math, vol. 4, pp. 361-378, 1951.

S. S. Seker and A. Schneider, “Electromagnetic scattering from a dielectric cylinder of finite length,’’ IEEE Trans. Antennas Prop.,vol. 36, no. 2, pp. 303-307, 1988.

A. Sharma and R. H. Lang, "Antenna beamwidth effect in detecting microwave enhanced backscatter in a layer of vegetation," 2017 United States National Committee of URSI National Radio Science Meeting (USNC-URSI NRSM), Boulder, CO, 2017, pp. 1-2..

A. Sharma and R. H. Lang, "Small scale surface roughness effects on enhanced backscatter from a layer of vegetation," 2017 USNC-URSI Radio Science Meeting (Joint with AP-S Symposium), San Diego, CA, 2017, pp. 59-60.

S. C. Steele-Dunne, H. McNairn, A. Monsivais-Huertero, J. Judge, P. W. Liu and K. Papathanassiou, "Radar Remote Sensing of Agricultural Canopies: A Review," in IEEE Journal of Selected Topics in Applied Earth Observations and Remote Sensing, vol. 10, no. 5, pp. 2249-2273, May 2017.

Tsang, L. and A. Ishimaru (1984), Backscattering enhancement of random discrete scatterers, *J. Opt. Soc. Am.* A, **1**, 836-839.

Tsang, L. and J.A. Kong (1983), Scattering of electromagnetic waves from a half space of densely distributed dielectric scatterers, *Radio Science*, 18, 1260-1272.

Mandt, Tsang, Ishimaru, Copolarized and depolarized backscattering enhancement of random discrete scatterers of large size based on second order ladder and cyclical theory, *J. Opt. Soc. Am.* A, **7**, 585-592.

Tsang, L. and J.A. Kong (1980), Multiple scattering of electromagnetic waves by random distribution of discreet scatterers with coherent potential and quantum mechanical formulation, *J. Appl. Phys*. **15**, 3465-3485.

Tsang, L., J.A. Kong, and R.T. Shin, Theory of Microwave

F. Ulaby and T. Bush, "Corn growth as monitored by radar," in IEEE Transactions on Antennas and Propagation, vol. 24, no. 6, pp. 819-828, November 1976.

F. T. Ulaby and M. A. El-Rayes, "Microwave Dielectric Spectrum of Vegetation - Part II: Dual-Dispersion Model," in IEEE Transactions on Geoscience and Remote Sensing, vol. GE-25, no. 5, pp. 550-557, Sept. 1987.

Y. Xu, R. G. Bosisio and T. K. Bose, "Some calculation methods and universal diagrams for measurement of dielectric constants using open-ended coaxial probes," in IEE Proc H Microw, Antennas and Propag UK, vol. 138, no. 4, pp. 356-360, Aug. 1991.

M. Zribi , O. Taconet , V. Ciarletti & D. Vidal-Madjar (2002) Effect of row structures on radar microwave measurements over soil surface, International Journal of Remote Sensing, 23:24, 5211-5224, DOI: 10.1080/01431160110115762.

Appendix A

A.1 Derivation of propagation constant in mean medium

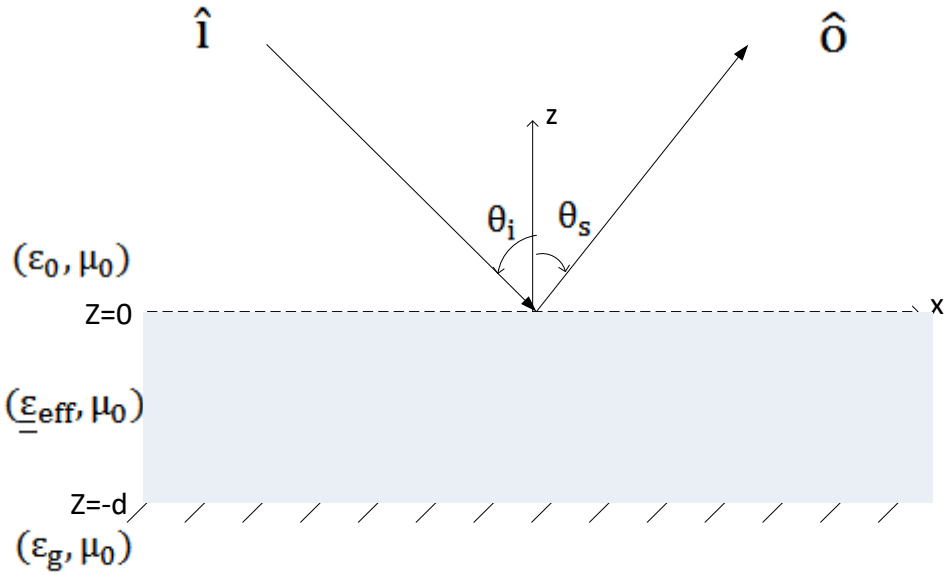

Figure A.1

From Chapter 2, Equation 2.18 is a vector integro-differential equation described the scattered field within the random medium layer shown in Figure A.1.

$$\nabla\times\nabla\times\left\langle \underline{E}(\underline{x}')\right\rangle - k_o^2\left\langle \underline{E}(\underline{x}')\right\rangle - \delta\iint d\underline{s}\,d\underline{x}'\left[\rho(\delta\underline{s})\,\underline{\underline{t}}(\underline{x}'-\underline{s},\underline{x}''-\underline{s})\cdot\left\langle \underline{E}(\underline{x}'')\right\rangle\right] = g(\underline{x}') \quad (A.1)$$

Applying the following to Equation A.1,

- $g(\underline{x}')$ can be set to zero since there are no sources within the medium.
- $\rho(\delta\underline{s}) \to \rho$

$$\nabla\times\nabla\times\left\langle \underline{E}(\underline{x}')\right\rangle - k_o^2\left\langle \underline{E}(\underline{x}')\right\rangle - \rho\delta\iint d\underline{s}\,d\underline{x}'\left[\underline{\underline{t}}(\underline{x}'-\underline{s},\underline{x}''-\underline{s})\cdot\left\langle \underline{E}(\underline{x}'')\right\rangle\right] = 0 \quad (A.2)$$

Assuming a plane wave solution of the form,

$$\left\langle \underline{E}(\underline{x})\right\rangle = \underline{E}_o e^{+i\underline{\kappa}\cdot\underline{x}}$$

where

$$\underline{\kappa} = \hat{i}\kappa$$

And substituting into Equation A.2 and carrying through the ∇ operation,

$$\underline{\kappa}\times\left(\underline{\kappa}\times\underline{E}_o e^{+i\underline{\kappa}\cdot\underline{x}}\right)+k_o^2\underline{E}_o e^{+i\underline{\kappa}\cdot\underline{x}}+\rho\delta\iint d\underline{s}\,d\underline{x}'\left[\underline{\underline{t}}\left(\underline{x}'-\underline{s},\underline{x}''-\underline{s}\right)\cdot\underline{E}_o e^{+i\underline{\kappa}\cdot\underline{x}'}\right]=0$$

Dividing through by $e^{+i\underline{\kappa}\cdot\underline{x}}$,

$$\underline{\kappa}\times\left(\underline{\kappa}\times\underline{E}_o\right)+k_o^2\underline{E}_o+\rho\delta\iint d\underline{s}\,d\underline{x}'\left[\underline{\underline{t}}\left(\underline{x}'-\underline{s},\underline{x}''-\underline{s}\right)\cdot\underline{E}_o e^{+i\underline{\kappa}\cdot\left(\underline{x}'-\underline{x}\right)}\right]=0$$

Applying the following change of variables,

$$\begin{array}{llll}\underline{x}'-\underline{s}=\overline{\underline{x}}' & d\underline{x}'=d\overline{\underline{x}}' & \underline{x}'=\overline{\underline{x}}'+\underline{s}\\ \underline{x}-\underline{s}=\overline{\underline{x}} & -d\underline{s}=d\overline{\underline{x}} & \underline{x}=\overline{\underline{x}}+\underline{s}\end{array}$$

$$\underline{\kappa}\times\left(\underline{\kappa}\times\underline{E}_o\right)+k_o^2\underline{E}_o+\rho\delta\iint d\overline{\underline{x}}\,d\overline{\underline{x}}'\left[\underline{\underline{t}}\left(\overline{\underline{x}},\overline{\underline{x}}'\right)\cdot\underline{E}_o e^{+i\underline{\kappa}\cdot\left(\underline{x}'-\underline{x}\right)}\right]=0$$

Recognizing that the double integral is a the Fourier Transform of the transition operator,

$$\underline{\kappa}\times\left(\underline{\kappa}\times\underline{E}_o\right)+k_o^2\underline{E}_o+\left(2\pi\right)^3\rho\delta\underline{\underline{\tilde{t}}}\left(\underline{\kappa},\underline{\kappa}\right)\cdot\underline{E}_o=0 \qquad \text{(A.3)}$$

Using the following vector identity, $\underline{A}\times\underline{B}\times\underline{C}=\underline{B}\left(\underline{A}\cdot\underline{C}\right)-\underline{C}\left(\underline{A}\cdot\underline{B}\right)$, Equation A.3 can be recast as,

$$\left(\underline{\kappa}\cdot\underline{E}_o\right)\underline{\kappa}-\left(\underline{\kappa}\cdot\underline{\kappa}\right)\underline{E}_o+k_o^2\underline{E}_o+\left(2\pi\right)^3\rho\delta\underline{\underline{\tilde{t}}}\left(\underline{\kappa},\underline{\kappa}\right)\cdot\underline{E}_o=0$$

Explicitly writing out $\underline{\kappa}$,

$$\left(\kappa\hat{i}\cdot\underline{E}_o\right)\kappa\hat{i}-\left(\kappa\hat{i}\cdot\kappa\hat{i}\right)\underline{E}_o+k_o^2\underline{E}_o+\left(2\pi\right)^3\rho\delta\underline{\underline{\tilde{t}}}\left(\kappa\hat{i},\kappa\hat{i}\right)\cdot\underline{E}_o=0$$

This simplifies to,

$$\left(k_o^2-\kappa^2\right)\underline{E}_o+\kappa^2\left(\hat{i}\cdot\underline{E}_o\right)\hat{i}+\left(2\pi\right)^3\rho\delta\underline{\underline{\tilde{t}}}\left(\kappa\hat{i},\kappa\hat{i}\right)\cdot\underline{E}_o=0 \qquad \text{(A.4)}$$

Expanding $\underline{E}_o$ and κ in a power series in δ,

$$\kappa=\kappa_0+\delta\kappa_1 \qquad \text{(A.5)}$$

$$\underline{E}_o = \underline{E}_o^{(0)} + \delta \underline{E}_o^{(1)} \tag{A.6}$$

To solve for the δ^0 (zeroth order solution), substitute Equation A.5 and A.6 into Equation A.4,

$$\left(k_o^2 - \kappa_0^2\right)\underline{E}_o^{(0)} + \kappa_0^2\left(\hat{i}\cdot\underline{E}_o^{(0)}\right)\hat{i} + (2\pi)^3 \rho\delta\underline{\underline{\tilde{t}}}\left(\kappa_0^2\hat{i}, \kappa_0^2\hat{i}\right)\cdot\underline{E}_0^{(1)} = 0$$

Collecting only the δ^0 terms,

$$\left(k_o^2 - \kappa_0^2\right)\underline{E}_o^{(0)} + \kappa_0^2\left(\hat{i}\cdot\underline{E}_o^{(0)}\right)\hat{i} = 0 \tag{A.7}$$

Dotting by $\hat{i}$, Equation A.7 reduces to, $\underline{E}_o^{(0)}\cdot\hat{i} = 0$. Substituting this into Equation A.7 gives the following relationship for κ_0 to zeroth order,

$$\kappa_0 = k_o \tag{A.8}$$

To solve for κ_1, start with Equation A.4,

$$\left(k_o^2 - \kappa^2\right)\underline{E}_o + \kappa^2\left(\hat{i}\cdot\underline{E}_o\right)\hat{i} + (2\pi)^3 \rho\delta\underline{\underline{\tilde{t}}}\left(\kappa\hat{i}, \kappa\hat{i}\right)\cdot\underline{E}_o = 0$$

Substituting Equation A.5 and A.6,

$$\left(k_o^2 - \left(\kappa_0 + \delta\kappa_1\right)^2\right)\left(\underline{E}_o^{(0)} + \delta\underline{E}_o^{(1)}\right) + \left(\kappa_0 + \delta\kappa_1\right)^2\left(\hat{i}\cdot\left(\underline{E}_o^{(0)} + \delta\underline{E}_o^{(1)}\right)\right)\hat{i}$$
$$+ (2\pi)^3 \rho\delta\underline{\underline{\tilde{t}}}\left(\left(\kappa_0 + \delta\kappa_1\right)\hat{i}, \left(\kappa_0 + \delta\kappa_1\right)\hat{i}\right)\cdot\underline{E}_o = 0$$

Collecting δ^1 and $\underline{E}_o^{(0)}$ terms:

$$-2\kappa_0\kappa_1\underline{E}_o^{(0)} + 2\kappa_0\kappa_1\left(\hat{i}\cdot\underline{E}_o^{(0)}\right)\hat{i} + (2\pi)^3 \rho\underline{\underline{\tilde{t}}}\left(\kappa_0\hat{i}, \kappa_0\hat{i}\right)\cdot\underline{E}_o^{(0)} = 0 \tag{A.9}$$

Define two polarization unit vectors, $\hat{\alpha}$ and $\hat{\beta}$, both orthogonal to the direction of propagation, $\hat{i}$. Rewriting $\underline{E}_o^{(0)} = \underline{E}_{\alpha_o}^{(0)}\hat{\alpha} + \underline{E}_{\beta_o}^{(0)}\hat{\beta}$ into Equation A.9, a dot from the left by $\hat{\alpha}$

Repeat except dot from the left by $\hat{\beta}$. This results in the following two equations,

$$\hat{\alpha}\cdot\left[-2\kappa_0\kappa_1\left(\underline{E}^{(0)}_{\alpha_o}\hat{\alpha}+\underline{E}^{(0)}_{\beta_o}\hat{\beta}\right)+2\kappa_0\kappa_1\left(\hat{i}\cdot\left(\underline{E}^{(0)}_{\alpha_o}\hat{\alpha}+\underline{E}^{(0)}_{\beta_o}\hat{\beta}\right)\right)\hat{i}+(2\pi)^3\rho\underline{\underline{\tilde{t}}}\left(\kappa_0\hat{i},\kappa_0\hat{i}\right)\cdot\left(\underline{E}^{(0)}_{\alpha_o}\hat{\alpha}+\underline{E}^{(0)}_{\beta_o}\hat{\beta}\right)\right]=0$$

$$\hat{\beta}\cdot\left[-2\kappa_0\kappa_1\left(\underline{E}^{(0)}_{\alpha_o}\hat{\alpha}+\underline{E}^{(0)}_{\beta_o}\hat{\beta}\right)+2\kappa_0\kappa_1\left(\hat{i}\cdot\left(\underline{E}^{(0)}_{\alpha_o}\hat{\alpha}+\underline{E}^{(0)}_{\beta_o}\hat{\beta}\right)\right)\hat{i}+(2\pi)^3\rho\underline{\underline{\tilde{t}}}\left(\kappa_0\hat{i},\kappa_0\hat{i}\right)\cdot\left(\underline{E}^{(0)}_{\alpha_o}\hat{\alpha}+\underline{E}^{(0)}_{\beta_o}\hat{\beta}\right)\right]=0$$

These two expressions reduce to,

$$\begin{aligned}&\left[-2\kappa_0\kappa_1\underline{E}^{(0)}_{\alpha_o}+(2\pi)^3\rho\hat{\alpha}\cdot\underline{\underline{\tilde{t}}}\left(\kappa_0\hat{i},\kappa_0\hat{i}\right)\cdot\underline{E}^{(0)}_{\alpha_o}\right]=0\\&\left[-2\kappa_0\kappa_1\underline{E}^{(0)}_{\beta_o}+(2\pi)^3\rho\hat{\beta}\cdot\underline{\underline{\tilde{t}}}\left(\kappa_0\hat{i},\kappa_0\hat{i}\right)\cdot\underline{E}^{(0)}_{\beta_o}\right]=0\end{aligned}\qquad\text{(A.10)}$$

Note that the dyadic transition operator when expanded out, contains nine terms,

$$\underline{\underline{\tilde{t}}}\left(\kappa_0\hat{i},\kappa_0\hat{i}\right)=\underline{\underline{\tilde{t}}}_{\alpha\alpha}\hat{\alpha}\hat{\alpha}+\underline{\underline{\tilde{t}}}_{\alpha\beta}\hat{\alpha}\hat{\beta}+\underline{\underline{\tilde{t}}}_{\alpha i}\hat{\alpha}\hat{i}+\underline{\underline{\tilde{t}}}_{\beta\alpha}\hat{\beta}\hat{\alpha}+\underline{\underline{\tilde{t}}}_{\beta\beta}\hat{\beta}\hat{\beta}+\underline{\underline{\tilde{t}}}_{\beta i}\hat{\beta}\hat{i}+\underline{\underline{\tilde{t}}}_{i\alpha}\hat{i}\hat{\alpha}+\underline{\underline{\tilde{t}}}_{i\beta}\hat{i}\hat{\beta}+\underline{\underline{\tilde{t}}}_{ii}\hat{i}\hat{i}$$

Carrying out the dot product operation in Equation A.10,

$$\begin{aligned}&\left[-2\kappa_0\kappa_1\underline{E}^{(0)}_{\alpha_o}+(2\pi)^3\rho\left[\underline{\underline{\tilde{t}}}_{\alpha\alpha}\underline{E}^{(0)}_{\alpha_o}+\underline{\underline{\tilde{t}}}_{\alpha\beta}\underline{E}^{(0)}_{\beta_o}\right]\right]=0\\&\left[-2\kappa_0\kappa_1\underline{E}^{(0)}_{\beta_o}+(2\pi)^3\rho\left[\underline{\underline{\tilde{t}}}_{\beta\alpha}\underline{E}^{(0)}_{\alpha_o}+\underline{\underline{\tilde{t}}}_{\beta\beta}\underline{E}^{(0)}_{\beta_o}\right]\right]=0\end{aligned}$$

Or in matrix form,

$$\begin{bmatrix}-2\kappa_0\kappa_1+(2\pi)^3\rho\underline{\underline{\tilde{t}}}_{\alpha\alpha} & (2\pi)^3\rho\underline{\underline{\tilde{t}}}_{\alpha\beta}\\(2\pi)^3\rho\underline{\underline{\tilde{t}}}_{\beta\alpha} & -2\kappa_0\kappa_1+(2\pi)^3\rho\underline{\underline{\tilde{t}}}_{\beta\beta}\end{bmatrix}\begin{bmatrix}\underline{E}^{(0)}_{\alpha_o}\\\underline{E}^{(0)}_{\beta_o}\end{bmatrix}=\begin{bmatrix}0\\0\end{bmatrix}\qquad\text{(A.11)}$$

Using the relationship between the transition operator and the scattering amplitude, given in Appendix B,

$$\underline{\underline{f}}\left(\hat{i},\hat{i}\right)=2\pi^2\left(\underline{\underline{I}}-\hat{i}\hat{i}\right)\cdot\underline{\underline{\tilde{t}}}\left(\kappa_o\hat{i},\kappa_o\hat{i}\right)\cdot\left(\underline{\underline{I}}-\hat{i}\hat{i}\right)$$

Note that

$$\underline{\underline{I}}=\hat{\alpha}\hat{\alpha}+\hat{\beta}\hat{\beta}+\hat{i}\hat{i}$$

$$\underline{\underline{I}}-\hat{i}\hat{i}=\hat{\alpha}\hat{\alpha}+\hat{\beta}\hat{\beta}$$

Equation A.11 becomes,

$$\begin{bmatrix} -2\kappa_0\kappa_1 + 4\pi\rho\bar{f}_{\alpha\alpha} & 4\pi\rho\bar{f}_{\alpha\beta} \\ 4\pi\rho\bar{f}_{\beta\alpha} & -2\kappa_0\kappa_1 + 4\pi\rho\bar{f}_{\beta\beta} \end{bmatrix} \begin{bmatrix} \underline{E}_{\alpha_o}^{(0)} \\ \underline{E}_{\beta_o}^{(0)} \end{bmatrix} = \begin{bmatrix} 0 \\ 0 \end{bmatrix} \tag{A.12}$$

For a non-trivial solution to matrix equation A.12, its determinant must be zero.

$$\begin{vmatrix} -2\kappa_0\kappa_1 + 4\pi\rho\bar{f}_{\alpha\alpha} & 4\pi\rho\bar{f}_{\alpha\beta} \\ 4\pi\rho\bar{f}_{\beta\alpha} & -2\kappa_0\kappa_1 + 4\pi\rho\bar{f}_{\beta\beta} \end{vmatrix} = 0$$

Carrying out the determinant operation results in the following equation,

$$\kappa_1^2 - \frac{2\pi\rho}{\kappa_0}\left(\bar{f}_{\alpha\alpha} + \bar{f}_{\beta\beta}\right)\kappa_1 + \left(\frac{2\pi\rho}{\kappa_0}\right)^2\left(\bar{f}_{\alpha\alpha}\bar{f}_{\beta\beta} - \bar{f}_{\alpha\beta}\bar{f}_{\beta\alpha}\right) = 0$$

This equation can be solved for κ_1 using the quadratic formula,

$$\kappa_1 = \frac{2\pi\rho}{2\kappa_0}\left(\bar{f}_{\alpha\alpha} + \bar{f}_{\beta\beta}\right) \pm \sqrt{\frac{1}{4}\left(\frac{2\pi\rho}{\kappa_0}\left(\bar{f}_{\alpha\alpha} + \bar{f}_{\beta\beta}\right)\right)^2 - \frac{4}{4}\left(\frac{2\pi\rho}{\kappa_0}\right)^2\left(\bar{f}_{\alpha\alpha}\bar{f}_{\beta\beta} - \bar{f}_{\alpha\beta}\bar{f}_{\beta\alpha}\right)}$$

$$= \frac{\pi\rho}{\kappa_0}\left(\bar{f}_{\alpha\alpha} + \bar{f}_{\beta\beta}\right) \pm \sqrt{\left(\frac{\pi\rho}{\kappa_0}\right)^2\left(\bar{f}_{\alpha\alpha} + \bar{f}_{\beta\beta}\right)^2 - 4\left(\frac{\pi\rho}{\kappa_0}\right)^2\left(\bar{f}_{\alpha\alpha}\bar{f}_{\beta\beta} - \bar{f}_{\alpha\beta}\bar{f}_{\beta\alpha}\right)}$$

$$= \frac{\pi\rho}{\kappa_0}\left(\bar{f}_{\alpha\alpha} + \bar{f}_{\beta\beta}\right) \pm \frac{\pi\rho}{\kappa_0}\sqrt{\left(\bar{f}_{\alpha\alpha} + \bar{f}_{\beta\beta}\right)^2 - 4\left(\bar{f}_{\alpha\alpha}\bar{f}_{\beta\beta} - \bar{f}_{\alpha\beta}\bar{f}_{\beta\alpha}\right)}$$

Finally, an expression for κ_1 is given by,

$$\kappa_1 = \frac{\pi\rho}{\kappa_0}\left[\bar{f}_{\alpha\alpha} + \bar{f}_{\beta\beta} \pm \sqrt{\left(\bar{f}_{\alpha\alpha} - \bar{f}_{\beta\beta}\right)^2 - 4\bar{f}_{\alpha\beta}\bar{f}_{\beta\alpha}}\right] \tag{A.13}$$

If the average depolarization is zero, then $\bar{f}_{\alpha\beta} = \bar{f}_{\beta\alpha} = 0$, which is valid when the scatterers in the mean medium have azimuthal symmetry, and Equation A.13 reduces to,

$$\kappa_1 = \frac{\pi\rho}{\kappa_0}\left[\bar{f}_{\alpha\alpha} + \bar{f}_{\beta\beta} \pm \bar{f}_{\alpha\alpha} - \bar{f}_{\beta\beta}\right]$$

$$\kappa_1^+ = \frac{2\pi\rho}{\kappa_0}\bar{f}_{\alpha\alpha} \tag{A.14}$$

$$\kappa_1^- = \frac{2\pi\rho}{\kappa_0}\bar{f}_{\beta\beta} \tag{A.15}$$

Therefore, κ to first order, can be expressed by using Equations A.8, A.14 and A.15 in Equation A.5,

$$\kappa^+ = \kappa_0 + \delta\kappa_1^+ = k_o + \delta\frac{2\pi\rho}{k_o}\bar{f}_{\alpha\alpha} \tag{A.16}$$

$$\kappa^- = \kappa_0 + \delta\kappa_1^- = k_o + \delta\frac{2\pi\rho}{k_o}\bar{f}_{\beta\beta} \tag{A.17}$$

Introducing more common nomenclature for polarization, let $\alpha = h$ and $\beta = v$, and the expressions for κ to first order, including polarization can be expressed as,

$$\kappa^+ = \kappa_h = k_o + \delta\frac{2\pi\rho}{k_o}\bar{f}_{hh}$$

$$\kappa^- = \kappa_v = k_o + \delta\frac{2\pi\rho}{k_o}\bar{f}_{vv}$$

This can be written more compactly as,

$$\kappa_q = k_o + \delta\frac{2\pi\rho}{k_o}\bar{f}_{qq}\left(\hat{i},\hat{i}\right) \tag{A.18}$$
$$q \in \{h, v\}$$

A.2 Stationary phase integral

The solution to Equation 2.26 is accomplished by using the Method of Stationary Phase since this integral has a slowly varying function $f(k_x, k_y)$ multiplying a fast varying exponential phase function. This type of integral can be readily approximated via the Method of Stationary Phase [Colin and Zucker, 1969],

$$\iint dk_x dk_y F\left(k_x, k_y\right) e^{+iPq\left(k_x, k_y\right)} \approx F\left(k_{x_s}, k_{y_s}\right) e^{+iPq\left(k_{x_s}, k_{y_s}\right)} \frac{2\pi}{P\sqrt{\left|ab - c^2\right|}} e^{+i\frac{\pi}{4}\left[\text{sign}(\lambda_1)+\text{sign}(\lambda_2)\right]} \quad \text{(A.19)}$$

Recasting Equation 2.26 as and solve for the stationary points.

$$G_p\left(\underline{x}, \underline{x}'\right) = \frac{1}{\left(2\pi\right)^2} \int_{-\infty}^{\infty} dk_x dk_y f(k_x, k_y) e^{+i\left(k_x x + k_y y + k_z z\right)} \quad \text{(A.20)}$$

where

$$f(k_x, k_y) = \left[\frac{e^{-i\kappa_{z_p} z'} + \Gamma_p e^{+i\kappa_{z_p} z'}}{i2\kappa_{z_p}}\right] e^{-i\underline{k}_t \cdot \underline{x}'_t}$$

Where the stationary points, k_{x_s} and k_{y_s} can be found by solving:

$$\frac{\partial q}{\partial k_x} = 0$$

$$\frac{\partial q}{\partial k_y} = 0$$

And the coefficients a, b and c are various derivatives of $q\left(k_x, k_y\right)$ evaluated at the stationary points, k_{x_s} and k_{y_s}.

$$a = \frac{\partial q^2}{\partial k_x^2}$$

$$b = \frac{\partial q^2}{\partial k_y^2}$$

$$c = \frac{\partial q}{\partial k_x \partial k_y}$$

And

$$\lambda_{1,2} = \frac{(a+b) \pm \sqrt{(a+b)^2 + 4c^2}}{2}$$

At the stationary points, the integral's contribution is greatest and away from the stationary points, the integral's contribution is negligible. Comparing Equation A.19to Equation A.20, the relevant terms are identified, in order to find the solution to the integral. First, q is found, since the derivatives of q are needed to find the stationary points.

$$q\left(k_x, k_y\right) = k_x x + k_y y + k_z z$$

where

$$k_z = \sqrt{k_0^2 - k_x^2 - k_y^2}$$

Carrying through the derivative operations for $a = \frac{\partial q^2}{\partial k_{x_s}^2}$ and solving for k_x evaluated at the stationary point,

$$q = \frac{\partial q}{\partial k_x} = \frac{\partial}{\partial x}\left[k_x x + k_y y + k_z z\right] = \frac{\partial}{\partial x}\left[k_x x + k_y y + \sqrt{k_0^2 - k_x^2 - k_y^2} z\right] = 0$$

$$k_{x_s} = \frac{k_z x}{z} \tag{A.21}$$

Next, carry through the derivative operations for $b = \frac{\partial q^2}{\partial k_{y_s}^2}$ and solve for k_y evaluated at the stationary point,

$$q = \frac{\partial q}{\partial k_y} = \frac{\partial}{\partial y}\left[k_x x + k_y y + k_z z\right] = \frac{\partial}{\partial x}\left[k_x x + k_y y + \sqrt{k_0^2 - k_x^2 - k_y^2}\, z\right] = 0$$

$$k_{y_s} = \frac{k_z y}{z} \tag{A.22}$$

To get an explicit expression for k_{x_s}, divide Equation A.21 by Equation A.22 to get expressions for k_x and k_y without a dependence on the z-variable.

$$k_{x_s} = k_{y_s}\frac{x}{y} \tag{A.23}$$

$$k_{y_s} = k_{x_s}\frac{y}{x} \tag{A.24}$$

Squaring Equation A.21, and substituting Equations A.24,

$$x^2 k_z^2 = k_{x_s}^2 z^2$$
$$x^2\left(k_0^2 - k_{x_s}^2 - k_{y_s}^2\right) = k_{x_s}^2 z^2$$
$$x^2\left(k_0^2 - k_{x_s}^2 - k_{x_s}^2\frac{y^2}{x^2}\right) = k_{x_s}^2 z^2$$

Solving for k_{x_s},

$$k_{x_s} = \frac{k_0 x}{\sqrt{x^2 + y^2 + z^2}} = \frac{k_0 x}{r} \tag{A.25}$$

Similarly, the other stationary point, k_{y_s} is found to be

$$k_{y_s} = \frac{k_0 y}{\sqrt{x^2 + y^2 + z^2}} = \frac{k_0 y}{r} \tag{A.26}$$

Substituting, Equations A.25 and A.26 into the expression for k_{z_s}

$$k_{z_s} = \sqrt{k_0^2 - k_x^2 - k_y^2} = \sqrt{k_0^2 - \frac{k_0^2 x^2}{r^2} - \frac{k_0^2 y^2}{r^2}} = \frac{k_0}{r}\sqrt{r^2 - x^2 - y^2}$$

$$= \frac{k_0}{r} z \tag{A.27}$$

Now an expression for $q\left(k_{x_s}, k_{y_s}\right)$ can be found by substituting the expressions for k_{x_s}, k_{y_s} and k_{z_s} (Equations A.25, A.26, A.27) into the expression for $q\left(k_x, k_y\right)$:

$$
\begin{aligned}
&q\left(k_{x_s}, k_{y_s}\right) = k_{x_s} x + k_{y_s} y + k_{z_s} z \\
&= \frac{k_0 x}{r} x + \frac{k_0 y}{r} y + \sqrt{k_0^2 - k_x^2 - k_y^2}\, z \\
&= \frac{k_0 x^2}{r} + \frac{k_0 y^2}{r} + \sqrt{k_0^2 - \frac{k_0^2 x^2}{r^2} - \frac{k_0^2 y^2}{r^2}}\, z \\
&= \frac{k_0 x^2}{r} + \frac{k_0 y^2}{r} + \frac{k_0}{r}\sqrt{r^2 - x^2 - y^2}\, z \\
&= \frac{k_0 x^2}{r} + \frac{k_0 y^2}{r} + \frac{k_0}{r} z^2 \\
&= \frac{k_0}{r}\left(x^2 + y^2 + z^2\right) = \frac{k_0}{r} r
\end{aligned}
$$

$$
q\left(k_{x_s}, k_{y_s}\right) = k_0 r \tag{A.28}
$$

Next, the following derivative are computed and evaluated at the stationary points,

$$
a = \frac{\partial^2 q}{\partial k_x^2} = -z\left[\frac{k_0^2 - k_y^2}{k_z^3}\right] \tag{A.29}
$$

$$
b = \frac{\partial^2 q}{\partial k_y^2} = -z\left[\frac{k_0^2 - k_x^2}{k_z^3}\right] \tag{A.30}
$$

$$
c = \frac{\partial q}{\partial k_x \partial k_y} = \frac{k_x k_y z}{k_z^3} \tag{A.31}
$$

Substituting Equations A.26 and A.27 into Equation A.29 will result in the expression for ‘a’ evaluated at the stationary points.

$$a = -z\frac{\left[k_0^2 - k_{y_s}^2\right]}{k_{z_s}^3} = -z\frac{\left[k_0^2 - \frac{k_0^2 y^2}{r^2}\right]}{\left(k_0^2 - k_{x_s}^2 - k_{y_s}^2\right)^{\frac{3}{2}}}$$

$$= -z\frac{\frac{\left[k_0^2 r^2 - k_0^2 y^2\right]}{r^2}}{\left(\frac{k_0^2 r^2 - k_0^2 x^2 - k_0^2 y^2}{r^2}\right)^{\frac{3}{2}}} = -z\frac{\frac{\left[k_0^2\left(x^2 + y^2 + z^2\right) - k_0^2 y^2\right]}{r^2}}{\left(\frac{k_0^2 r^2 - k_0^2 x^2 - k_0^2 y^2}{r^2}\right)^{\frac{3}{2}}} \cdot$$

$$= -z\frac{\frac{\left[k_0^2 x^2 + k_0^2 z^2\right]}{r^2}}{\left(\frac{k_0^2 z^2}{r^2}\right)^{\frac{3}{2}}} = -z\frac{\frac{\left[k_0^2 x^2 + k_0^2 z^2\right]}{r^2}}{\left(\frac{k_0^3 z^3}{r^2}\right)}$$

$$a = \frac{\left(x^2 + z^2\right)r}{k_0 z^2} \tag{A.32}$$

Similarly, ‘b’ evaluated at the stationary points can be expressed as,

$$b = \frac{\left(y^2 + z^2\right)r}{k_0 z^2} \tag{A.33}$$

And ‘c’ evaluated at the stationary points can be found as follows,

$$c = \frac{k_{x_s} k_{y_s} z}{k_{z_x}^3} = \frac{\frac{k_0 x}{r}\frac{k_0 x}{r} z}{\frac{k_0^3 z^3}{r^3}} = \frac{xyr}{k_0 z^2} \tag{A.34}$$

Now the final term to be evaluated is $\sqrt{\left|ab - c^2\right|}$:

$$= \sqrt{\left|\frac{\left(x^2 + z^2\right)r}{k_0 z^4}\frac{\left(y^2 + z^2\right)r}{k_0 z^4} - \left(\frac{xyr}{k_0 z^2}\right)^2\right|} = \sqrt{\left|\frac{r^2\left(x^2 + z^2\right)\left(y^2 + z^2\right) - x^2 y^2 r^2}{k_0 z^4}\right|}$$

$$= \sqrt{\left|\frac{r^2 z^2\left(x^2 + y^2 + z^2\right)}{k_0 z^4}\right|} = \sqrt{\frac{r^4 z^2}{k_0^2 z^4}}$$

$$\sqrt{\left|ab-c^2\right|}=\frac{r^2}{k_0 z} \tag{A.35}$$

Now substitute in the above derived terms into the right-hand side of Equation A.19 to get asymptotic expression for the integral. Note that $\text{sign}(\lambda_1)$ and $\text{sign}(\lambda_2)$ are both equal to 1. Finally, we get,

$$= F\left(k_{x_s}, k_{y_s}\right) e^{iPq\left(k_{x_s}, k_{y_s}\right)} \frac{2\pi}{P\sqrt{\left|ab-c^2\right|}} e^{+i\frac{\pi}{4}\left[\text{sign}(\lambda_1)+\text{sign}(\lambda_2)\right]}$$

$$= \frac{1}{(2\pi)^2}\left[\frac{e^{-i\kappa_{z_p} z'}+\Gamma_p e^{+i\kappa_{z_p} z'}}{i2k_{z_s}}\right] e^{-i\underline{k}_t\cdot\underline{x}'_t} e^{ik_0 r} \frac{2\pi}{\frac{r^2}{k_0 z}} e^{+i\frac{\pi}{2}}$$

$$= \frac{1}{(2\pi)^2} i2\pi \frac{e^{ik_0 r}}{r} k_{z_s}\left[\frac{e^{-i\kappa_{z_p} z'}+\Gamma_p e^{+i\kappa_{z_p} z'}}{i2k_{z_s}}\right] e^{-i\underline{k}_t\cdot\underline{x}'_t}$$

$$= \frac{1}{4\pi}\frac{e^{ik_0 r}}{r}\left[e^{-i\kappa_{z_p} z'}+\Gamma_p e^{+i\kappa_{z_p} z'}\right] e^{-i\underline{k}_t\cdot\underline{x}'_t}$$

A.3 Derivation of the z-component of the propagation constant

The z-component of Equation A.18 is also used in Chapter 2 denoted as κ_{z_q} and can be derived as follows,

$$\begin{aligned}
\kappa_{z_q} &= \sqrt{\kappa_q^2 - \left|k_{t_i}\right|^2} \\
&= \sqrt{\left(k_o + \delta \frac{2\pi\rho}{k_o} \bar{f}_{qq}\left(\hat{i}, \hat{i}\right)\right)^2 - \left|k_{t_i}\right|^2} \\
&= \sqrt{k_o^2 + \delta \frac{4\pi\rho}{k_o} \bar{f}_{qq}\left(\hat{i}, \hat{i}\right) + O(\delta^2) - \left|k_{t_i}\right|^2} \\
&= \sqrt{k_{z_i}^2 + \delta \frac{4\pi\rho}{k_o} \bar{f}_{qq}\left(\hat{i}, \hat{i}\right) + O(\delta^2)}
\end{aligned}$$

Using the binomial approximation, a final expression for the z-component of the propagation constant in the mean medium is,

$$\kappa_{z_q} = k_{z_i} + \delta \frac{2\pi\rho}{k_{z_i}} \bar{f}_{qq}\left(\hat{i}, \hat{i}\right) \tag{A.19}$$

A.4 Correlation of scattered field integrals

From Chapter 2, the following expression for the bistatic scattering coefficient was introduced.

$$\sigma^{0}_{pqp'q'} = \lim_{A\to\infty}\lim_{|\underline{x}|\to\infty}\frac{4\pi|\underline{x}|^2}{A}\left\{\delta\rho\int_{A} d\underline{s}_t\int ds_z\sum_{i=1}^{4}\sum_{j=1}^{4}\left\langle E^{(i)}_{s_{pq}}(\underline{x},\underline{s})E^{*(j)}_{s_{p'q'}}(\underline{x},\underline{s})\right\rangle\right\}$$

Note that of the sixteen integrals of $E^{(i)}_{s_{pq}}(\underline{x},\underline{s})E^{*(j)}_{s_{p'q'}}(\underline{x},\underline{s})$ term integrated over s_z will be of the form,

$$\delta\int_{-d}^{0} ds_z e^{i(a+\delta b)s_z}$$

where either a=0 or a≠0. When a≠0, the integral is of $O(\delta^1)$ as shown below.

$$\delta\int_{-d}^{0} ds\, e^{i(a+\delta b)s} = \delta\left[\frac{1-e^{-i(a+\delta b)d}}{i(a+\delta b)}\right] = \delta\left[\frac{1-(1-i(a+\delta b)d}{i(a+\delta b)}\right] = \delta d = O(\delta^1)$$

When a=0, the integral becomes $O(\delta^0)$ as shown below.

$$\delta\int_{-d}^{0} ds\, e^{i(\delta b)s} = \delta\left[\frac{1-e^{-i(\delta b)d}}{i(\delta b)}\right] = \delta\left[\frac{1}{i(\delta b)}\right] = \frac{1}{ib} = O(\delta^0)$$

The sixteen expressions for $E^{(i)}_{s_{pq}}(\underline{x},\underline{s})E^{*(j)}_{s_{p'q'}}(\underline{x},\underline{s})$ are listed below. On inspection, the expressions that are $O(\delta^0)$ occur for the following:

i=j=1 1=j=2 i=j=3 i=j=4 i=2, j=3 i=3, j=2

$$
\begin{aligned}
&E^{(1)}_{s_{pq}}\left(\underline{x},\underline{s}\right)E^{*(1)}_{s_{p'q'}}\left(\underline{x},\underline{s}\right)\\
&=\left[\frac{e^{+ik_0 r}}{r}e^{-i\underline{\underline{\kappa}}_s s_z}\cdot\underline{\underline{f}}\left(\hat{o}^+,\hat{i}^-\right)\cdot e^{-i\underline{\underline{\kappa}}_i s_z}e^{+ik_0\left(-\hat{o}^+ +\hat{i}^-\right)\cdot\underline{s}}\right]\left[\frac{e^{-ik_0 r}}{r}e^{+i\underline{\underline{\kappa}}^*_s s_z}\cdot\underline{\underline{f}}^*\left(\hat{o}^+,\hat{i}^-\right)\cdot e^{+i\underline{\underline{\kappa}}^*_i s_z}e^{-ik_0\left(-\hat{o}^+ +\hat{i}^-\right)\cdot\underline{s}}\right]\\
&=\underline{\underline{f}}\left(\hat{o}^+,\hat{i}^-\right)\underline{\underline{f}}^*\left(\hat{o}^+,\hat{i}^-\right)\left[e^{-i\underline{\underline{\kappa}}_s s_z}e^{-i\underline{\underline{\kappa}}_i s_z}e^{+i\underline{\underline{\kappa}}^*_s s_z}e^{+i\underline{\underline{\kappa}}^*_i s_z}\right]\\
&=\underline{\underline{f}}\left(\hat{o}^+,\hat{i}^-\right)\underline{\underline{f}}^*\left(\hat{o}^+,\hat{i}^-\right)\left[e^{+i\left(-\underline{\underline{\kappa}}_s-\underline{\underline{\kappa}}_i+\underline{\underline{\kappa}}^*_s+\underline{\underline{\kappa}}^*_i\right)s_z}\right]
\end{aligned}
$$

$$
\begin{aligned}
&E^{(1)}_{s_{pq}}\left(\underline{x},\underline{s}\right)E^{*(2)}_{s_{p'q'}}\left(\underline{x},\underline{s}\right)\\
&=\left[\frac{e^{+ik_0 r}}{r}e^{-i\underline{\underline{\kappa}}_s s_z}\cdot\underline{\underline{f}}\left(\hat{o}^+,\hat{i}^-\right)\cdot e^{-i\underline{\underline{\kappa}}_i s_z}e^{+ik_0\left(-\hat{o}^+ +\hat{i}^-\right)\cdot\underline{s}}\right]\left[\frac{e^{-ik_0 r}}{r}e^{+i\underline{\underline{\kappa}}^*_s s_z}\cdot\underline{\underline{f}}^*\left(\hat{o}^+,\hat{i}^+\right)\cdot\underline{\Gamma}^*_q e^{-i\underline{\underline{\kappa}}^*_i s_z}e^{-ik_0\left(-\hat{o}^+ +\hat{i}^+\right)\cdot\underline{s}}\right]\\
&=\underline{\underline{f}}\left(\hat{o}^+,\hat{i}^-\right)\cdot\underline{\underline{f}}^*\left(\hat{o}^+,\hat{i}^+\right)\underline{\Gamma}^*_q\left[e^{-i\underline{\underline{\kappa}}_s s_z}e^{+i\underline{\underline{\kappa}}^*_s s_z}e^{-i\underline{\underline{\kappa}}_i s_z}e^{-i\underline{\underline{\kappa}}^*_i s_z}e^{+ik_0\left(-\hat{o}^+ +\hat{i}^-\right)\cdot\underline{s}}e^{-ik_0\left(-\hat{o}^+ +\hat{i}^+\right)\cdot\underline{s}}\right]\\
&=\underline{\underline{f}}\left(\hat{o}^+,\hat{i}^-\right)\cdot\underline{\underline{f}}^*\left(\hat{o}^+,\hat{i}^+\right)\underline{\Gamma}^*_q\left[e^{+ik_0\left(\hat{i}^- -\hat{i}^+\right)\cdot\underline{s}}e^{+i\left(-\underline{\underline{\kappa}}_s+\underline{\underline{\kappa}}_s{}^*-\underline{\underline{\kappa}}_i-\underline{\underline{\kappa}}^*_i\right)s_z}\right]
\end{aligned}
$$

$$
\begin{aligned}
&E^{(1)}_{s_{pq}}\left(\underline{x},\underline{s}\right)E^{*(3)}_{s_{p'q'}}\left(\underline{x},\underline{s}\right)\\
&=\left[\frac{e^{+ik_0 r}}{r}e^{-i\underline{\underline{\kappa}}_s s_z}\cdot\underline{\underline{f}}\left(\hat{o}^+,\hat{i}^-\right)\cdot e^{-i\underline{\underline{\kappa}}_i s_z}e^{+ik_0\left(-\hat{o}^+ +\hat{i}^-\right)\cdot\underline{s}}\right]\left[\frac{e^{-ik_0 r}}{r}\underline{\Gamma}^*_p e^{-i\underline{\underline{\kappa}}^*_s s_z}\cdot\underline{\underline{f}}^*\left(\hat{o}^-,\hat{i}^-\right)\cdot e^{+i\underline{\underline{\kappa}}^*_i s_z}e^{+ik_0\left(\hat{o}^- +\hat{i}^-\right)\cdot\underline{s}}\right]\\
&=\underline{\underline{f}}\left(\hat{o}^+,\hat{i}^-\right)\underline{\underline{f}}^*\left(\hat{o}^-,\hat{i}^-\right)\underline{\Gamma}^*_p\left[e^{-i\underline{\underline{\kappa}}_s s_z}e^{-i\underline{\underline{\kappa}}_i s_z}e^{-i\underline{\underline{\kappa}}^*_s s_z}e^{+i\underline{\underline{\kappa}}^*_i s_z}e^{+ik_0\left(-\hat{o}^+ +\hat{i}^-\right)\cdot\underline{s}}e^{+ik_0\left(\hat{o}^- +\hat{i}^-\right)\cdot\underline{s}}\right]\\
&=\underline{\underline{f}}\left(\hat{o}^+,\hat{i}^-\right)\underline{\underline{f}}^*\left(\hat{o}^-,\hat{i}^-\right)\underline{\Gamma}^*_p\left[e^{+ik_0\left(-\hat{o}^+ +\hat{o}^- +\hat{i}^- +\hat{i}^-\right)\cdot\underline{s}}e^{+i\left(\underline{\underline{\kappa}}_s-i\underline{\underline{\kappa}}_i-i\underline{\underline{\kappa}}^*_s+i\underline{\underline{\kappa}}_i{}^*\right)s_z}\right]
\end{aligned}
$$

$$
\begin{aligned}
&E^{(1)}_{s_{pq}}\left(\underline{x},\underline{s}\right)E^{*(4)}_{s_{p'q'}}\left(\underline{x},\underline{s}\right)\\
&=\left[\frac{e^{+ik_0 r}}{r}e^{-i\underline{\underline{\kappa}}_s s_z}\cdot\underline{\underline{f}}\left(\hat{o}^+,\hat{i}^-\right)\cdot e^{-i\underline{\underline{\kappa}}_i s_z}e^{+ik_0\left(-\hat{o}^+ +\hat{i}^-\right)\cdot\underline{s}}\right]\left[\frac{e^{-ik_0 r}}{r}\underline{\Gamma}^*_p e^{-i\underline{\underline{\kappa}}^*_s s_z}\cdot\underline{\underline{f}}^*\left(\hat{o}^-,\hat{i}^+\right)\cdot\underline{\Gamma}^*_q e^{-i\underline{\underline{\kappa}}^*_i s_z}e^{+ik_0\left(\hat{o}^- -\hat{i}^+\right)\cdot\underline{s}}\right]\\
&=\underline{\underline{f}}\left(\hat{o}^+,\hat{i}^-\right)\underline{\underline{f}}^*\left(\hat{o}^-,\hat{i}^+\right)\underline{\Gamma}^*_p\underline{\Gamma}^*_q\left[e^{-i\underline{\underline{\kappa}}_s s_z}e^{-i\underline{\underline{\kappa}}_i s_z}e^{-i\underline{\underline{\kappa}}^*_s s_z}e^{-i\underline{\underline{\kappa}}^*_i s_z}e^{+ik_0\left(-\hat{o}^+ +\hat{i}^-\right)\cdot\underline{s}}e^{+ik_0\left(\hat{o}^- -\hat{i}^+\right)\cdot\underline{s}}\right]\\
&=\underline{\underline{f}}\left(\hat{o}^+,\hat{i}^-\right)\underline{\underline{f}}^*\left(\hat{o}^-,\hat{i}^+\right)\underline{\Gamma}^*_p\underline{\Gamma}^*_q\left[e^{+ik_0\left(-\hat{o}^+ +\hat{i}^- +\hat{o}^- -\hat{i}^+\right)\cdot\underline{s}}e^{+i\left(-\underline{\underline{\kappa}}_s-\underline{\underline{\kappa}}_i-\underline{\underline{\kappa}}_s{}^*-\underline{\underline{\kappa}}^*_i\right)s_z}\right]
\end{aligned}
$$

$$
\begin{aligned}
&E^{(2)}_{s_{pq}}\left(\underline{x},\underline{s}\right)E^{*(1)}_{s_{p'q'}}\left(\underline{x},\underline{s}\right)\\
&=\left[\frac{e^{+ik_0 r}}{r}e^{-i\underline{\underline{\kappa}}_s s_z}\cdot\underline{\underline{f}}\left(\hat{o}^+,\hat{i}^+\right)\cdot\underline{\Gamma}_q e^{+i\underline{\underline{\kappa}}_i s_z}e^{+ik_0\left(-\hat{o}^+ +\hat{i}^+\right)\cdot\underline{s}}\right]\left[\frac{e^{-ik_0 r}}{r}e^{+i\underline{\underline{\kappa}}^*_s s_z}\cdot\underline{\underline{f}}^*\left(\hat{o}^+,\hat{i}^-\right)\cdot e^{+i\underline{\underline{\kappa}}^*_i s_z}e^{-ik_0\left(-\hat{o}^+ +\hat{i}^-\right)\cdot\underline{s}}\right]\\
&=\underline{\underline{f}}\left(\hat{o}^+,\hat{i}^+\right)\cdot\underline{\underline{f}}^*\left(\hat{o}^+,\hat{i}^-\right)\underline{\Gamma}_q\left[e^{-i\underline{\underline{\kappa}}_s s_z}e^{+i\underline{\underline{\kappa}}_i s_z}e^{+i\underline{\underline{\kappa}}^*_s s_z}e^{+i\underline{\underline{\kappa}}^*_i s_z}e^{+ik_0\left(-\hat{o}^+ +\hat{i}^+\right)\cdot\underline{s}}e^{+ik_0\left(-\hat{o}^+ +\hat{i}^+\right)\cdot\underline{s}}\right]\\
&=\underline{\underline{f}}\left(\hat{o}^+,\hat{i}^+\right)\cdot\underline{\underline{f}}^*\left(\hat{o}^+,\hat{i}^-\right)\underline{\Gamma}_q\left[e^{+ik_0\left(-\hat{o}^+ +\hat{i}^+ -\hat{o}^+ +\hat{i}^+\right)\cdot\underline{s}}e^{+i\left(-\underline{\underline{\kappa}}_s+\underline{\underline{\kappa}}_i+\underline{\underline{\kappa}}^*_s+\underline{\underline{\kappa}}^*_i\right)}\right]
\end{aligned}
$$

$$
\begin{aligned}
&E^{(2)}_{s_{pq}}\left(\underline{x},\underline{s}\right)E^{*(2)}_{s_{p'q'}}\left(\underline{x},\underline{s}\right)\\
&=\left[\frac{e^{+ik_0 r}}{r}e^{-i\underline{\underline{\kappa}}_s s_z}\cdot\underline{\underline{f}}\left(\hat{o}^+,\hat{i}^+\right)\cdot\underline{\Gamma}_q e^{+i\underline{\underline{\kappa}}_i s_z}e^{+ik_0\left(-\hat{o}^+ +\hat{i}^+\right)\cdot\underline{s}}\right]\left[\frac{e^{-ik_0 r}}{r}e^{+i\underline{\underline{\kappa}}^*_s s_z}\cdot\underline{\underline{f}}^*\left(\hat{o}^+,\hat{i}^+\right)\cdot\underline{\Gamma}^*_q e^{-i\underline{\underline{\kappa}}^*_i s_z}e^{-ik_0\left(-\hat{o}^+ +\hat{i}^+\right)\cdot\underline{s}}\right]\\
&=\underline{\underline{f}}\left(\hat{o}^+,\hat{i}^+\right)\cdot\underline{\underline{f}}^*\left(\hat{o}^+,\hat{i}^+\right)\cdot\underline{\Gamma}_q\cdot\underline{\Gamma}^*_q\left[e^{-i\underline{\underline{\kappa}}_s s_z}e^{+i\underline{\underline{\kappa}}_i s_z}e^{+i\underline{\underline{\kappa}}^*_s s_z}e^{-i\underline{\underline{\kappa}}^*_i s_z}e^{+ik_0\left(-\hat{o}^+ +\hat{i}^+ +\hat{o}^+ -\hat{i}^+\right)\cdot\underline{s}}\right]\\
&=\underline{\underline{f}}\left(\hat{o}^+,\hat{i}^+\right)\cdot\underline{\underline{f}}^*\left(\hat{o}^+,\hat{i}^+\right)\cdot\underline{\Gamma}_q\cdot\underline{\Gamma}^*_q\left[e^{+i\left(-\underline{\underline{\kappa}}_s+\underline{\underline{\kappa}}_i+\underline{\underline{\kappa}}^*_s-\underline{\underline{\kappa}}^*_i\right)s_z}\right]
\end{aligned}
$$

$$
\begin{aligned}
&E^{(2)}_{s_{pq}}\left(\underline{x},\underline{s}\right)E^{*(3)}_{s_{p'q'}}\left(\underline{x},\underline{s}\right)\\
&=\left[\frac{e^{+ik_0 r}}{r}e^{-i\underline{\underline{\kappa}}_s s_z}\cdot\underline{\underline{f}}\left(\hat{o}^+,\hat{i}^+\right)\cdot\underline{\Gamma}_q e^{+i\underline{\underline{\kappa}}_i s_z}e^{+ik_0\left(-\hat{o}^+ +\hat{i}^+\right)\cdot\underline{s}}\right]\left[\frac{e^{-ik_0 r}}{r}\underline{\Gamma}^*_p e^{-i\underline{\underline{\kappa}}^*_s s_z}\cdot\underline{\underline{f}}^*\left(\hat{o}^-,\hat{i}^-\right)\cdot e^{+i\underline{\underline{\kappa}}^*_i s_z}e^{+ik_0\left(\hat{o}^- +\hat{i}^-\right)\cdot\underline{s}}\right]\\
&=\underline{\underline{f}}\left(\hat{o}^+,\hat{i}^+\right)\cdot\underline{\underline{f}}^*\left(\hat{o}^-,\hat{i}^-\right)\cdot\underline{\Gamma}_q\cdot\underline{\Gamma}_p{}^*\left[e^{-i\underline{\underline{\kappa}}_s s_z}\cdot e^{+i\underline{\underline{\kappa}}_i s_z}e^{-i\underline{\underline{\kappa}}^*_s s_z}e^{+i\underline{\underline{\kappa}}^*_i s_z}e^{+ik_0\left(-\hat{o}^+ +\hat{i}^+ +\hat{o}^- +\hat{i}^-\right)\cdot\underline{s}}\right]\\
&=\underline{\underline{f}}\left(\hat{o}^+,\hat{i}^+\right)\cdot\underline{\underline{f}}^*\left(\hat{o}^-,\hat{i}^-\right)\cdot\underline{\Gamma}_q\cdot\underline{\Gamma}_p{}^*\left[e^{+ik_0\left(-\hat{o}^+ +\hat{i}^+ +\hat{o}^- +\hat{i}^-\right)\cdot\underline{s}}e^{+i\left(-\underline{\underline{\kappa}}_s+\underline{\underline{\kappa}}_i-\underline{\underline{\kappa}}^*_s+\underline{\underline{\kappa}}^*_i\right)s_z}\right]
\end{aligned}
$$

$$
\begin{aligned}
&E^{(2)}_{s_{pq}}\left(\underline{x},\underline{s}\right)E^{*(4)}_{s_{p'q'}}\left(\underline{x},\underline{s}\right)\\
&=\left[\frac{e^{+ik_0 r}}{r}e^{-i\underline{\underline{\kappa}}_s s_z}\cdot\underline{\underline{f}}\left(\hat{o}^+,\hat{i}^+\right)\cdot\underline{\Gamma}_q e^{+i\underline{\underline{\kappa}}_i s_z}e^{+ik_0\left(-\hat{o}^+ +\hat{i}^+\right)\cdot\underline{s}}\right]\left[\frac{e^{-ik_0 r}}{r}\underline{\Gamma}^*_p e^{-i\underline{\underline{\kappa}}^*_s s_z}\cdot\underline{\underline{f}}^*\left(\hat{o}^-,\hat{i}^+\right)\cdot\underline{\Gamma}^*_q e^{-i\underline{\underline{\kappa}}^*_i s_z}e^{+ik_0\left(\hat{o}^- -\hat{i}^+\right)\cdot\underline{s}}\right]\\
&=\underline{\underline{f}}\left(\hat{o}^+,\hat{i}^+\right)\cdot\underline{\underline{f}}^*\left(\hat{o}^-,\hat{i}^+\right)\underline{\Gamma}_q\underline{\Gamma}^*_p\left[e^{-i\underline{\underline{\kappa}}_s s_z}e^{+i\underline{\underline{\kappa}}_i s_z}e^{-i\underline{\underline{\kappa}}^*_s s_z}e^{-i\underline{\underline{\kappa}}^*_i s_z}e^{+ik_0\left(-\hat{o}^+ +\hat{i}^+ +\hat{o}^- -\hat{i}^+\right)\cdot\underline{s}}\right]\\
&=\underline{\underline{f}}\left(\hat{o}^+,\hat{i}^+\right)\cdot\underline{\underline{f}}^*\left(\hat{o}^-,\hat{i}^+\right)\underline{\Gamma}_q\underline{\Gamma}^*_q\underline{\Gamma}^*_p\left[e^{+ik_0\left(-\hat{o}^+ +\hat{i}^+ +\hat{o}^- -\hat{i}^+\right)\cdot\underline{s}}e^{+i\left(-\underline{\underline{\kappa}}_s+\underline{\underline{\kappa}}_i-\underline{\underline{\kappa}}^*_s-\underline{\underline{\kappa}}^*_i\right)}\right]
\end{aligned}
$$

$$
\begin{aligned}
&E^{(3)}_{s_{pq}}\left(\underline{x},\underline{s}\right)E^{*(1)}_{s_{p'q'}}\left(\underline{x},\underline{s}\right)\\
&=\left[\frac{e^{+ik_0 r}}{r}\underline{\Gamma}_p e^{+i\underline{\underline{\kappa}}_s s_z}\cdot\underline{\underline{f}}\left(\hat{o}^-,\hat{i}^-\right)\cdot e^{-i\underline{\underline{\kappa}}_i s_z}e^{-ik_0\left(\hat{o}^-+\hat{i}^-\right)\cdot\underline{s}}\right]\left[\frac{e^{-ik_0 r}}{r}e^{+i\underline{\underline{\kappa}}^*_s s_z}\cdot\overline{\underline{\underline{f}}}^*\left(\hat{o}^+,\hat{i}^-\right)\cdot e^{+i\underline{\underline{\kappa}}^*_i s_z}e^{-ik_0\left(-\hat{o}^++\hat{i}^-\right)\cdot\underline{s}}\right]\\
&=\underline{\underline{f}}\left(\hat{o}^-,\hat{i}^-\right)\cdot\overline{\underline{\underline{f}}}^*\left(\hat{o}^+,\hat{i}^-\right)\underline{\Gamma}_p\left[e^{-ik_0\left(\hat{o}^-+\hat{i}^-+\hat{o}^+-\hat{i}^-\right)\cdot\underline{s}}e^{+i\underline{\underline{\kappa}}_s s_z}e^{-i\underline{\underline{\kappa}}_i s_z}e^{+i\underline{\underline{\kappa}}^*_s s_z}e^{+i\underline{\underline{\kappa}}^*_i s_z}\right]
\end{aligned}
$$

$$
\begin{aligned}
&E^{(3)}_{s_{pq}}\left(\underline{x},\underline{s}\right)E^{*(2)}_{s_{p'q'}}\left(\underline{x},\underline{s}\right)\\
&=\left[\frac{e^{+ik_0 r}}{r}\underline{\Gamma}_p e^{+i\underline{\underline{\kappa}}_s s_z}\cdot\underline{\underline{f}}\left(\hat{o}^-,\hat{i}^-\right)\cdot e^{-i\underline{\underline{\kappa}}_i s_z}e^{-ik_0\left(\hat{o}^-+\hat{i}^-\right)\cdot\underline{s}}\right]\left[\frac{e^{-ik_0 r}}{r}e^{+i\underline{\underline{\kappa}}^*_s s_z}\cdot\overline{\underline{\underline{f}}}^*\left(\hat{o}^+,\hat{i}^+\right)\cdot\underline{\Gamma}^*_q e^{-i\underline{\underline{\kappa}}^*_i s_z}e^{-ik_0\left(-\hat{o}^++\hat{i}^+\right)\cdot\underline{s}}\right]\\
&=\underline{\underline{f}}\left(\hat{o}^-,\hat{i}^-\right)\cdot\overline{\underline{\underline{f}}}^*\left(\hat{o}^+,\hat{i}^+\right)\underline{\Gamma}_p\underline{\Gamma}^*_q\left[e^{-ik_0\left(\hat{o}^-+\hat{i}^-+\hat{o}^+-\hat{i}^+\right)\cdot\underline{s}}e^{+i\underline{\kappa}_s s_z}\cdot e^{-i\underline{\kappa}_i s_z}e^{+i\underline{\underline{\kappa}}^*_s s_z}e^{-i\underline{\kappa}^*_i s_z}\right]
\end{aligned}
$$

$$
\begin{aligned}
&E^{(3)}_{s_{pq}}\left(\underline{x},\underline{s}\right)E^{*(3)}_{s_{p'q'}}\left(\underline{x},\underline{s}\right)\\
&=\left[\frac{e^{+ik_0 r}}{r}\underline{\Gamma}_p e^{+i\underline{\underline{\kappa}}_s s_z}\cdot\underline{\underline{f}}\left(\hat{o}^-,\hat{i}^-\right)\cdot e^{-i\underline{\underline{\kappa}}_i s_z}e^{-ik_0\left(\hat{o}^-+\hat{i}^-\right)\cdot\underline{s}}\right]\left[\frac{e^{-ik_0 r}}{r}\underline{\Gamma}^*_p e^{-i\underline{\underline{\kappa}}^*_s s_z}\cdot\overline{\underline{\underline{f}}}^*\left(\hat{o}^-,\hat{i}^-\right)\cdot e^{+i\underline{\underline{\kappa}}^*_i s_z}e^{+ik_0\left(\hat{o}^-+\hat{i}^-\right)\cdot\underline{s}}\right]\\
&=\underline{\underline{f}}\left(\hat{o}^-,\hat{i}^-\right)\cdot\overline{\underline{\underline{f}}}^*\left(\hat{o}^-,\hat{i}^-\right)\underline{\Gamma}_p\underline{\Gamma}_p{}^*\left[e^{+i\underline{\underline{\kappa}}_s s_z}e^{-i\underline{\underline{\kappa}}_i s_z}e^{-i\underline{\underline{\kappa}}^*_s s_z}e^{+i\underline{\underline{\kappa}}^*_i s_z}\right]
\end{aligned}
$$

$$
\begin{aligned}
&E^{(3)}_{s_{pq}}\left(\underline{x},\underline{s}\right)E^{*(4)}_{s_{p'q'}}\left(\underline{x},\underline{s}\right)\\
&=\left[\frac{e^{+ik_0 r}}{r}\underline{\Gamma}_p e^{+i\underline{\underline{\kappa}}_s s_z}\cdot\underline{\underline{f}}\left(\hat{o}^-,\hat{i}^-\right)\cdot e^{-i\underline{\underline{\kappa}}_i s_z}e^{-ik_0\left(\hat{o}^-+\hat{i}^-\right)\cdot\underline{s}}\right]\left[\frac{e^{-ik_0 r}}{r}\underline{\Gamma}^*_p e^{-i\underline{\underline{\kappa}}^*_s s_z}\cdot\overline{\underline{\underline{f}}}^*\left(\hat{o}^-,\hat{i}^+\right)\cdot\underline{\Gamma}^*_q e^{-i\underline{\underline{\kappa}}^*_i s_z}e^{+ik_0\left(\hat{o}^--\hat{i}^+\right)\cdot\underline{s}}\right]\\
&=\underline{\underline{f}}\left(\hat{o}^-,\hat{i}^-\right)\cdot\overline{\underline{\underline{f}}}^*\left(\hat{o}^-,\hat{i}^+\right)\underline{\Gamma}_p\underline{\Gamma}^*_p\underline{\Gamma}_q{}^*\left[e^{-ik_0\left(\hat{o}^-+\hat{i}^-+\hat{o}^--\hat{i}^+\right)\cdot\underline{s}}e^{+i\left(\underline{\underline{\kappa}}_s-\underline{\kappa}_i-\underline{\underline{\kappa}}^*_s-\underline{\kappa}^*_i\right)}\right]
\end{aligned}
$$

$$
\begin{aligned}
&E^{(4)}_{s_{pq}}\left(\underline{x},\underline{s}\right)E^{*(1)}_{s_{p'q'}}\left(\underline{x},\underline{s}\right)\\
&=\left[\frac{e^{+ik_0 r}}{r}\underline{\Gamma}_p e^{+i\underline{\underline{\kappa}}_s s_z}\cdot\underline{\underline{f}}\left(\hat{o}^-,\hat{i}^+\right)\cdot\underline{\Gamma}_q e^{+i\underline{\kappa}_i s_z}e^{-ik_0\left(\hat{o}^--\hat{i}^+\right)\cdot\underline{s}}\right]\left[\frac{e^{-ik_0 r}}{r}e^{+i\underline{\underline{\kappa}}^*_s s_z}\cdot\overline{\underline{\underline{f}}}^*\left(\hat{o}^+,\hat{i}^-\right)\cdot e^{+i\underline{\underline{\kappa}}^*_i s_z}e^{-ik_0\left(-\hat{o}^++\hat{i}^-\right)\cdot\underline{s}}\right]\\
&=\underline{\underline{f}}\left(\hat{o}^-,\hat{i}^+\right)\cdot\overline{\underline{\underline{f}}}^*\left(\hat{o}^+,\hat{i}^-\right)\underline{\Gamma}_p\underline{\Gamma}_q\left[e^{+i\underline{\underline{\kappa}}_s s_z}\cdot e^{+i\underline{\underline{\kappa}}_i s_z}e^{+i\underline{\underline{\kappa}}^*_s s_z}e^{+i\underline{\underline{\kappa}}^*_i s_z}e^{-ik_0\left(\hat{o}^--\hat{i}^++\hat{o}^+-\hat{i}^-\right)\cdot\underline{s}}\right]\\
&=\underline{\underline{f}}\left(\hat{o}^-,\hat{i}^+\right)\cdot\overline{\underline{\underline{f}}}^*\left(\hat{o}^+,\hat{i}^-\right)\underline{\Gamma}_p\underline{\Gamma}_q\left[e^{+i\left(\underline{\underline{\kappa}}_s+\underline{\kappa}_i+\underline{\kappa}^*_s+i\underline{\underline{\kappa}}^*_i\right)}e^{-ik_0\left(\hat{o}^--\hat{i}^++\hat{o}^+-\hat{i}^-\right)\cdot\underline{s}}\right]
\end{aligned}
$$

$$
\begin{aligned}
&E^{(4)}_{s_{pq}}\left(\underline{x},\underline{s}\right)E^{*(2)}_{s_{p'q'}}\left(\underline{x},\underline{s}\right)\\
&=\left[\frac{e^{+ik_0 r}}{r}\underline{\Gamma}_p e^{+i\underline{\underline{\kappa}}_s s_z}\cdot\underline{\underline{f}}\left(\hat{o}^-,\hat{i}^+\right)\cdot\underline{\Gamma}_q e^{+i\underline{\underline{\kappa}}_i s_z}e^{-ik_0\left(\hat{o}^- -\hat{i}^+\right)\cdot\underline{s}}\right]\left[\frac{e^{-ik_0 r}}{r}e^{+i\underline{\underline{\kappa}}^*_s s_z}\cdot\underline{\underline{f}}^*\left(\hat{o}^+,\hat{i}^+\right)\cdot\underline{\Gamma}^*_q e^{-i\underline{\underline{\kappa}}^*_i s_z}e^{-ik_0\left(-\hat{o}^+ +\hat{i}^+\right)\cdot\underline{s}}\right]\\
&=\underline{\underline{f}}\left(\hat{o}^-,\hat{i}^+\right)\cdot\underline{\underline{f}}^*\left(\hat{o}^+,\hat{i}^-\right)\underline{\Gamma}_p\underline{\Gamma}_q\left[e^{+i\underline{\underline{\kappa}}_s s_z}\cdot e^{+i\underline{\underline{\kappa}}_i s_z}e^{+i\underline{\underline{\kappa}}^*_s s_z}e^{+i\underline{\underline{\kappa}}^*_i s_z}e^{-ik_0\left(\hat{o}^- -\hat{i}^+ +\hat{o}^+ -\hat{i}^-\right)\cdot\underline{s}}\right]\\
&=\underline{\underline{f}}\left(\hat{o}^-,\hat{i}^+\right)\cdot\underline{\underline{f}}^*\left(\hat{o}^+,\hat{i}^-\right)\underline{\Gamma}_p\underline{\Gamma}_q\left[e^{+i\left(\underline{\underline{\kappa}}_s+\underline{\underline{\kappa}}_i+\underline{\underline{\kappa}}^*_s+i\underline{\underline{\kappa}}^*_i\right)s_z}e^{-ik_0\left(\hat{o}^- -\hat{i}^+ +\hat{o}^+ -\hat{i}^-\right)\cdot\underline{s}}\right]
\end{aligned}
$$

$$
\begin{aligned}
&E^{(4)}_{s_{pq}}\left(\underline{x},\underline{s}\right)E^{*(3)}_{s_{p'q'}}\left(\underline{x},\underline{s}\right)\\
&=\left[\frac{e^{+ik_0 r}}{r}\underline{\Gamma}_p e^{+i\underline{\underline{\kappa}}_s s_z}\cdot\underline{\underline{f}}\left(\hat{o}^-,\hat{i}^+\right)\cdot\underline{\Gamma}_q e^{+i\underline{\underline{\kappa}}_i s_z}e^{-ik_0\left(\hat{o}^- -\hat{i}^+\right)\cdot\underline{s}}\right]\left[\frac{e^{-ik_0 r}}{r}\underline{\Gamma}^*_p e^{-i\underline{\underline{\kappa}}^*_s s_z}\cdot\underline{\underline{f}}^*\left(\hat{o}^-,\hat{i}^-\right)\cdot e^{+i\underline{\underline{\kappa}}^*_i s_z}e^{+ik_0\left(\hat{o}^- +\hat{i}^-\right)\cdot\underline{s}}\right]\\
&=\underline{\underline{f}}\left(\hat{o}^-,\hat{i}^+\right)\cdot\underline{\underline{f}}^*\left(\hat{o}^-,\hat{i}^-\right)\underline{\Gamma}_p\underline{\Gamma}^*_p\underline{\Gamma}_q\left[e^{-ik_0\left(\hat{o}^- -\hat{i}^+ +\hat{o}^- +\hat{i}^-\right)\cdot\underline{s}}e^{+i\left(\underline{\kappa}_s+\underline{\kappa}_i-\underline{\kappa}^*_s+\underline{\kappa}^*_i\right)s_z}\right]
\end{aligned}
$$

$$
\begin{aligned}
&E^{(4)}_{s_{pq}}\left(\underline{x},\underline{s}\right)E^{*(4)}_{s_{p'q'}}\left(\underline{x},\underline{s}\right)\\
&=\left[\frac{e^{+ik_0 r}}{r}\underline{\Gamma}_p e^{+i\underline{\underline{\kappa}}_s s_z}\cdot\underline{\underline{f}}\left(\hat{o}^-,\hat{i}^+\right)\cdot\underline{\Gamma}_q e^{+i\underline{\underline{\kappa}}_i s_z}e^{-ik_0\left(\hat{o}^- -\hat{i}^+\right)\cdot\underline{s}}\right]\left[\frac{e^{-ik_0 r}}{r}\underline{\Gamma}^*_p e^{-i\underline{\underline{\kappa}}^*_s s_z}\cdot\underline{\underline{f}}^*\left(\hat{o}^-,\hat{i}^+\right)\cdot\underline{\Gamma}^*_q e^{-i\underline{\underline{\kappa}}^*_i s_z}e^{+ik_0\left(\hat{o}^- -\hat{i}^+\right)\cdot\underline{s}}\right]\\
&=\underline{\underline{f}}\left(\hat{o}^-,\hat{i}^+\right)\cdot\underline{\underline{f}}^*\left(\hat{o}^-,\hat{i}^+\right)\underline{\Gamma}_p\underline{\Gamma}^*_p\underline{\Gamma}_q\underline{\Gamma}^*_q\left[e^{+i\left(\underline{\kappa}_s+\underline{\kappa}_i-\underline{\kappa}^*_s-\underline{\kappa}^*_i\right)s_z}\right]
\end{aligned}
$$

Appendix B

Relationship between the dyadic transition operator and the dyadic scattering amplitude

A dyadic incident plane wave can be expressed as:

$$\underline{E}_i\left(\underline{x},\hat{i}\right)=\left(\underline{\underline{I}}-\hat{i}\hat{i}\right)e^{+ik_o\cdot\underline{x}} \tag{B.1}$$

A dyadic scattered wave can be expressed as as:

$$\underline{E}_s\left(\underline{x},\hat{i}\right)=\underline{\underline{f}}\left(\hat{o},\hat{i}\right)\frac{e^{+ik_o\cdot|\underline{x}|}}{|\underline{x}|} \tag{B.2}$$

From Chapter 2, the scattered field can be written in terms of a dyadic Green's function, a dyadic transition operator and the incident field.

$$\underline{E}_s\left(\underline{x},\hat{i}\right)=\int d\underline{x}'G\left(\underline{x},\underline{x}'\right)\int d\underline{x}''\,\underline{\underline{t}}\left(\underline{x}',\underline{x}''\right)\cdot\underline{E}_i\left(\underline{x}'',\hat{i}\right) \tag{B.3}$$

The free space Dyadic Green's Function, given in Insert Reference:

$$\underline{\underline{G}}\left(\underline{x},\underline{x}'\right)=\left(\underline{\underline{I}}+\frac{\nabla\nabla}{k_o^2}\right)\frac{e^{+ik_0|\underline{x}-\underline{x}'|}}{4\pi|\underline{x}-\underline{x}'|} \tag{B.4}$$

In the far-field, B.4 can be asymptotically expressed as,

$$\underline{\underline{G}}\left(\underline{x},\underline{x}'\right)\square\left(\underline{\underline{I}}-\hat{o}\hat{o}\right)\frac{e^{-ik_0\hat{o}\cdot\underline{x}'}}{4\pi|\underline{x}|}e^{ik_o|\underline{x}|} \tag{B.5}$$

Substituting B.1 and B.5 into B.3,

$$\underline{\underline{E}}_s\left(\underline{x},\hat{i}\right)=\int d\underline{x}'\left(\underline{\underline{I}}-\hat{o}\hat{o}\right)\frac{e^{-ik_0\hat{o}\cdot x'}}{4\pi|\underline{x}|}e^{ik_o|\underline{x}|}\int d\underline{x}''\,\underline{\underline{t}}\left(\underline{x}',\underline{x}''\right)\cdot\left(\underline{\underline{I}}-\hat{i}\hat{i}\right)e^{+ik_o\cdot\underline{x}}$$

$$=\frac{(2\pi)^3}{4\pi}\left(\underline{\underline{I}}-\hat{o}\hat{o}\right)\int d\underline{x}'d\underline{x}''\,\underline{\underline{t}}\left(\underline{x}',\underline{x}''\right)e^{-ik_o\hat{o}\cdot\underline{x}'}e^{+ik_o\hat{i}\cdot\underline{x}''}\left(\underline{\underline{I}}-\hat{i}\hat{i}\right)\frac{e^{ik_o|\underline{x}|}}{|\underline{x}|}$$

$$=\frac{(2\pi)^3}{4\pi}\left(\underline{\underline{I}}-\hat{o}\hat{o}\right)\cdot\underline{\underline{\tilde{t}}}\left(k_o\hat{o},k_o\hat{i}\right)\cdot\left(\underline{\underline{I}}-\hat{i}\hat{i}\right)\frac{e^{ik_o|\underline{x}|}}{|\underline{x}|} \tag{B.6}$$

Comparing B.6 with B.2, an explicit relationship between the dyadic scattering amplitude, $\underline{\underline{f}}\left(\hat{o},\hat{i}\right)$ and the dyadic transition operator is seen as,

$$\underline{\underline{f}}\left(\hat{o},\hat{i}\right)=\frac{(2\pi)^3}{4\pi}\left(\underline{\underline{I}}-\hat{o}\hat{o}\right)\cdot\underline{\underline{\tilde{t}}}\left(k_o\hat{o},k_o\hat{i}\right)\cdot\left(\underline{\underline{I}}-\hat{i}\hat{i}\right)$$

$$\underline{\underline{f}}\left(\hat{o},\hat{i}\right)=2\pi^2\left(\underline{\underline{I}}-\hat{o}\hat{o}\right)\cdot\underline{\underline{\tilde{t}}}\left(k_o\hat{o},k_o\hat{i}\right)\cdot\left(\underline{\underline{I}}-\hat{i}\hat{i}\right) \tag{B.7}$$

Note that the tilde above the transition operator denotes the Fourier Transform.